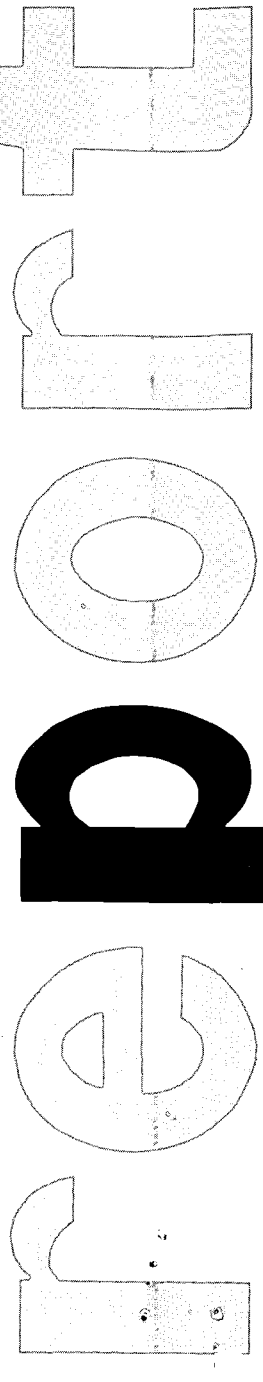

WYLE LABORATORIES

EASTERN OPERATIONS — HUNTSVILLE FACILITY

(NASA-CR-124079) ACOUSTIC FATIGUE AND SOUND TRANSMISSION CHARACTERISTICS OF A RAM COMPOSITE PANEL DESIGN (Wyle Labs., Inc.) 102 p HC $8.00 CSCL 11D

N73-22529

Unclas
G3/18 17044

research

WYLE LABORATORIES - RESEARCH STAFF

TECHNICAL MEMORANDUM 72-3

ACOUSTIC FATIGUE AND SOUND TRANSMISSION CHARACTERISTICS OF A RAM COMPOSITE PANEL DESIGN

By

J. A. Cockburn
K. Y. Chang
G. C. Kao

Work Performed Under Contract NAS8-29146

October 1972

Revised December 1972

WYLE LABORATORIES
EASTERN OPERATIONS, HUNTSVILLE, ALABAMA

COPY NO. 03

FOREWORD

The work reported herein was performed under Contract No. NAS8-29146 for the Advanced Technology Branch, National Aeronautics and Space Administration, Marshall Space Flight Center, Huntsville, Alabama, under the direction of Mr. J. B. Herring.

SUMMARY

An experimental study to determine the acoustic fatigue characteristics of a flat multi-layered structural panel is described. The test panel represented a proposed design for the outer skin of a Research Application Module (RAM) to be housed within the Space Shuttle Orbiter Vehicle. The test specimen was mounted in one wall of the Wyle 100,000 ft^3 reverberation room and exposed to a broadband acoustic environment having an overall level of 145 dB. Instrumentation consisted of strain gauges and accelerometers mounted on the specimen surfaces, and microphones placed within the reverberation room, at the surface of the test specimen, and in the free field outside the reverberation room immediately behind the test specimen. The positioning of the microphones enabled an estimate to be made of the sound transmission characteristics of the test specimen. The test panel was exposed to nine separate applications of the acoustic environment, each application consisting of 250 seconds duration. Upon completion of the ninth test run, the specimen was exposed to a simulated micro-meteoroid impact near the panel center. One additional test run of 250 seconds duration was then performed to complete the overall simulation of 50 flight missions. The experimental results show that no significant fatigue damage occurred until the test specimen was exposed to a simulated micro-meteoroid impact. The intermediate foam layer forming the core of the test specimen suffered considerable damage due to this impact, causing a marked variation in the dynamic characteristics of the overall test panel. During the final application of the acoustic environment, the strain and acceleration response spectra showed considerable variation from those spectra obtained prior to impact of the panel. Fatigue damage from acoustic loading however, was limited to partial de-bonding around the edges of the composite panel.

TABLE OF CONTENTS

LIST OF FIGURES

LIST OF FIGURES (Concluded)

1.0 INTRODUCTION

This report describes an experimental study which was undertaken to determine the acoustic fatigue and sound transmission characteristics of a flat multi-layered structural panel. The test panel represented a simulation of a radiator/meteoroid bumper which forms the outer skin of a proposed cylindrical-shaped research application module (RAM), to be housed within the Space Shuttle Orbiter Vehicle.

Following initial experiments to determine the mode shapes and resonant frequencies of the panel specimen, the test panel was mounted in a fixture placed in the wall of the Wyle 100,000 ft^3 acoustic facility and subjected to a broadband reverberant acoustic environment having an overall level of 145 dB. The test panel was instrumented with six strain gauges and 3 accelerometers. Sound pressure level measurements were taken at the center of the reverberation room, at the panel surface (using a microphone with its active face placed within 0.3 in. of the panel surface), and in the free field outside the reverberation room immediately behind the test panel.

The test panel was subjected to nine separate applications of the acoustic environment; each application consisted of 250 seconds duration. During each test run, the signals from the three microphones were analyzed using a B & K one-third octave band analyzer, and the strain gauge and accelerometer signals were recorded on tape. At the end of each 250 second test run, the panel was inspected visually for damage before proceeding with the next test run. Upon completion of the nine individual test runs the specimen was shipped to NASA-MSFC and subjected to an impact by a simulated micro-meteoroid. The test specimen was then re-installed in the acoustic facility and one additional 250 second duration acoustic test was performed.

A description of the test panel together with its dynamic characteristics is presented in Section 2.0. This is followed by a detailed description of the experimental program in Section 3.0. Finally, the results of the experimental program are discussed in Section 4.0. A method to predict the acoustic fatigue life of structural panels is presented in Appendix B.

2.0 CHARACTERISTICS OF THE TEST PANEL

2.1 Description of the Test Specimen

The test specimen consisted of a composite polyurethane foam-filled panel approximately 40 in. by 40 in. by 4.1 in. thick overall, as shown in Figures 1 and 2. The basic panel consisted of an inner and outer skin, bonded to a one inch layer of polyurethane foam of 2 lb/ft^3 density. The inner and outer skins were manufactured from 2024-T3 aluminum alloy, having thicknesses of 0.01 in. and 0.016 in., respectively. The perimeter of the test panel consisted of aluminum alloy Z-section stiffeners having a thickness of 0.08 in. An additional angle-section stiffener was placed around the perimeter of the inner skin and rivetted to the Z-section stiffener as shown in Figure 2.

The basic composite panel formed by the aluminum sheets and the polyurethane foam represented a simulation of a radiator/meteoroid bumper which has been proposed for the outer skin of a cylindrical-shaped research application module (RAM), housed within the Space Shuttle Orbiter vehicle. The Z-section stiffeners around the perimeter test specimen were chosen merely to provide a simulation of the proper boundary conditions for the composite panel and were not considered to be an integral part of the radiator/meteoroid bumper flight article.

2.2 Modal Characteristics of the Test Specimen

A preliminary analysis was conducted to determine the fundamental resonance of the test specimen; this was followed by a brief experimental study to determine the modal characteristics of the panel, and to determine the optimum locations for accelerometers and strain gauges for the fatigue experiments.

The resonant frequencies of a simply-supported square panel may be determined from the relation;

$$f_{m,n} = \frac{\pi}{2} \left[\frac{m^2 + n^2}{\ell^2} \right] \sqrt{\frac{D}{\mu}} \qquad (1)$$

where m,n = number of half-waves in the vibrating panel

ℓ = length of panel side (inch)

D = flexural rigidity $= EI/(1-\sigma^2)$ (lb in.)

μ = mass per unit area (lb $sec^2/in.^3$)

For a square panel with fixed edges, the fundamental resonance may be computed from the relation (Reference 1);

$$f_{1,1} = \frac{18}{\pi \ell^2} \sqrt{\frac{D}{\mu}} \tag{2}$$

In order to compute the flexural rigidity, D, it is first necessary to determine the neutral axis of the composite panel and then its second moment of area, I. Treating the Z-section stiffeners as the panel boundaries, the position of the neutral axis is given by (see Figure 2);

$$d = \frac{t_1\left(h - t_1/2\right) + t_2^2/2}{t_1 + t_2} \quad \text{in.} \tag{3}$$

Substituting $t_1 = 0.016$ in., $t_2 = 0.01$ in., and $h = 1.0$ in., results in a value of d equal to 0.614 in.

The second moment of area is determined from the relation (see Figure 2):

$$I = t_1\left(h - d - t_1/2\right)^2 + t_2\left(d - t_2/2\right)^2 \quad \text{in.}^4/\text{in.} \tag{4}$$

Substituting for t_1, t_2, h and d yields a value of I equal to 0.006 $in.^4$/inch. Assuming a value of 1.10^7 lb/$in.^2$ for Young's Modulus and a value of 0.3 for Poisson's Ratio gives a value of D equal to $6.6 \cdot 10^4$ lb in.

The total mass per unit area is the sum of the aluminum panel masses and the mass of the polyurethane foam, neglecting the mass of the Z-section stiffeners for the moment. Thus the mass per unit area of the aluminum panels and polyurethane foam is given by;

$$\mu = \frac{0.0016 + 0.001 + 0.00116}{386.4} = 9.725 \cdot 10^{-6} \quad \text{lb sec}^2/\text{in}^3 \qquad (5)$$

A correction to this mass per unit area must be made to account for that portion of the stiffener mass which acts at the edges of the panel, since it cannot be assumed that the basic panel will totally de-couple from the stiffeners. This additional mass consists of two 1.0 in. by 0.08 in. aluminum strips around the perimeter of the panel. Thus the additional mass amounts to approximately 2.3 lb, and if this is simply assumed to be distributed over the entire panel surface, the correction to be added to the above mass per unit area is equal to $4.6 \cdot 10^{-6}$ lb sec^2/in^3.

Thus the effective mass per unit area of the panel is;

$$(9.725 \cdot 10^{-6}) + (4.6 \cdot 10^{-6}) = 1.4325 \cdot 10^{-5} \quad \text{lb sec}^2/\text{in}^3 \qquad (6)$$

Substituting the above properties into Equations (1) and (2) yields fundamental resonant frequencies of 188 Hz for the simply-supported panel and 342 Hz for the fully-fixed panel. An estimate of the free-free resonant mode may be obtained by utilizing the square panel resonant frequency multipliers presented in Reference 2. These results show that the free-free modal frequency is 0.392 times the fully-fixed modal frequency, which for the present case would be 0.392 x 342, i.e., 134 Hz. A summary of the predicted resonant frequencies for the fundamental mode of the test panel is as follows:

- Free-free boundary conditions — 134 Hz
- Simply-supported boundary conditions — 188 Hz
- Fully-fixed boundary conditions — 342 Hz

A modal survey was conducted using a loudspeaker to drive the panel, which was suspended by flexible cords attached to the Z-section stiffeners. Several sinesweeps were performed in order to properly identify the fundamental mode and during resonant dwell tests, sand was sprinkled on the test panel to determine the approximate mode shape. The results of the modal survey are summarized in Figures 3, 4, and 5, which illustrate the vibration mode shapes obtained by sprinkling sand upon the vibrating panel. Figure 3 shows the fundamental free-free panel mode (the 1-1 mode) which was measured at 112 Hz. During this mode the Z-section stiffeners forming the panel boundary were observed to be vibrating. The fundamental simply-supported vibration mode is illustrated in Figure 4; during this mode, which was measured at 198 Hz, very little vibratory motion of the Z-section stiffeners was detected. The mode shape depicted in Figure 5 is most likely the (3-3) mode and this was measured at 268 Hz. Since the panel was excited by essentially plane waves at normal incidence, excitation of even-numbered modes (that is, modes having an even number of elastic half-waves across the panel) would not be anticipated due to cancellation effects. The vibration modes which were observed (at 112 Hz, 198 Hz and 268 Hz) all involved in-phase motion of the inner and outer skins of the composite panel. The measured fundamental modes at 112 Hz and 198 Hz are in fair agreement with the predicted fundamental resonances of 134 Hz and 188 Hz.

3.0 EXPERIMENTAL PROGRAM

3.1 Objectives

The basic objectives of the experimental program were to determine both the acoustic fatigue and the sound transmission characteristics of the multi-layered test panel in a reverberant acoustic environment. The specified acoustic environment is illustrated in the one-third octave band plot shown in Figure 6; the spectrum is observed to be broadband with an overall level of 145 dB. The basic requirement to be met during the fatigue experiments was to simulate 45 flight profiles of the Space Shuttle Orbiter vehicle. The duration of each flight profile has been defined to be 50 seconds, and for the fatigue experiments the acoustic environment was to be applied for 250 seconds at a time, that is, five consecutive flight profiles. Thus the fatigue experiments comprised a total of nine (9) applications of the acoustic environment, each application being of 250 seconds duration. Inspection of the test panel was to be carried out upon completion of each application. After accumulating nine test runs, the test panel was to be shipped to NASA-MSFC for simulation of a micro-meteoroid impact, and then the panel re-installed in the reverberation room for one additional test run. During the acoustic fatigue program, microphone, strain gauge and accelerometer signals were to be monitored continuously and recorded for subsequent detection of any panel degradation.

3.2 Experimental Set-Up

The test panel was mounted in a fixture placed in the wall of the Wyle 100,000 ft^3 reverberation room, as shown in Figures 7 and 8. The reverberation room has four removable concrete blocks in one of the walls, as shown in Figure 7, each block being approximately 7 ft high by 5 ft wide. The upper right-hand concrete block was removed from the facility and replaced by a modified concrete block having a suitable opening to receive the test panel and a cast-in angle section fixture to which the test panel was mounted. An exterior view of the reverberation room with the test panel in position is shown in Figure 9, and details of the panel mounting arrangement are shown in Figure 10.

The panel was instrumented with three accelerometers and six strain gauges. Accelerometers A1 and A2 were located on the outer skin at the panel center and the quarter-chord respectively as shown in Figures 1 and 8; accelerometer A3 was located on the inner skin at the panel center. Strain gauges SG1, SG2 and SG3 were located on the centerline of the outer skin at the edge, quarter-chord, and mid-point of the panel respectively, as shown in Figures 1 and 8. Similarly, strain gauges SG4, SG5 and SG6 were located on the centerline of the inner skin at the edge, quarter-chord, and mid-point of the panel respectively; the positions of these strain gauges can be seen in Figure 9.

Three microphones were used to measure the sound pressure levels during the experiments. Microphone M1 was positioned near the center of the reverberation room about 6 ft from the floor as shown in Figure 7; this microphone was designated as a control microphone and was used for initial spectrum shaping in conjunction with the MSFC one-third octave band sound pressure level specifications. Microphone M2 was mounted within the reverberation room such that its active face was within about 0.3 in. of the test panel surface, as close to the panel center as possible, as shown in Figure 8. Placement of the microphone in this way enables the true surface sound pressure level to be measured provided that the gap between the active face of the microphone and the panel surface is within one-eighth of a wavelength at the highest frequency of interest. Thus for the specified gap of 0.3 in., it was expected that true surface pressures would be measured up to about 5000 Hz. Microphone M3 was positioned outside the reverberation room in the free-field environment behind the test opening as shown in Figure 9. This microphone, which was placed about 1 foot away from the outside wall, was used to measure ambient sound pressure levels prior to and after each test run, and also to derive an estimate of the transmission loss through the test panel.

A block diagram showing the instrumentation utilized during the fatigue experiments is shown in Figure 11.

3.3 Experimental Procedure

Before installing the test fixture and panel in the reverberation room wall, a preliminary calibration was performed in order to shape the acoustic test spectrum to the desired levels. This test was performed with the original concrete blocks in place at the test opening. Ambient sound pressure levels measured by microphone M3 in the free field were recorded prior to start-up of the compressors, during operation of the compressors only, and during operation of the reverberant facility at the specified 145 dB overall level within the room. Sound pressure levels measured by microphones M1 and M2 within the reverberation room were also recorded during the preliminary calibration run at 145 dB overall.

The upper right-hand concrete block (as viewed from within the reverberation room) was then removed, and the modified concrete block together with the fixture and the test specimen were installed. After installation of the test specimen, the locations of microphones M1, M2 and M3 were checked for consistency with the calibration test set-up. A series of low level broadband tests was then performed to checkout the instrumentation and the panel responses.

An individual acoustic fatigue test run consisted of prior recording of the ambient noise levels measured by microphone M3, application of the design acoustic environment of 145 dB overall for a duration of 250 seconds (during which the strain gauge, accelerometer and microphone signals were recorded) and re-recording of the ambient noise levels measured by microphone M3 after shutdown of the facility. The test panel was then visually inspected for damage. This procedure was repeated until a total of nine test runs had been accomplished.

Upon completion of the nine test runs, no major fatigue damage was evident. The test panel was then punctured by a simulated micro-meteoroid impact at NASA-MSFC and re-installed in the reverberant facility. One additional test run of 250 seconds duration was then performed at 145 dB overall according to the procedure outlined above.

4.0 EXPERIMENTAL RESULTS AND DISCUSSION

4.1 Measured Sound Pressure Levels

The ambient sound pressure levels measured within the reverberation room and in the free field before operating the facility are shown in Figure 12. The results of the facility calibration run are presented in Figure 13, which shows the measured sound pressure levels within the reverberation room and in the free field. The MSFC specified one-third octave band levels are also shown in Figure 13, and it can be seen that the acoustic environment within the reverberation room is in good agreement with the specified environment up to about 1250 Hz. Above this frequency, the spectrum rolls off below the specified levels at about 8 dB per octave compared with the specified roll-off of 3 dB per octave. Since the fundamental resonance of the installed test panel was found to occur at approximately 100 Hz, and the acoustic environment was in good agreement with the specified levels up to about 1250 Hz (which is almost four octaves above the fundamental of the panel), it was concluded that the deficiencies in the acoustic environment above 1250 Hz would have a negligible effect on the fatigue characteristics of the test specimen.

The sound pressure levels measured during Test Run Number 1, with the test specimen installed, are shown in Figure 14. Three spectra are shown in this figure, corresponding to microphones M1, M2 and M3, at the center of the reverberation room, at the surface of the test specimen, and in the free field outside the room, respectively. The effect of pressure doubling at the test specimen surface can be clearly seen by comparing the levels measured by microphones M1 and M2; this pressure doubling amounts to about 5 dB over most of the frequency range shown in Figure 14. The acoustic levels measured by microphone M3 exhibit a pronounced peak in the one-third octave band centered at 100 Hz, corresponding to the fundamental mode of the test panel. This result is to be expected, and indicates maximum sound transmission through the test panel.

The effective sound transmission through the test panel is shown in Figure 15. This result, which was obtained by subtracting the calibration free-field levels shown in Figure 13 from the free-field levels shown in Figure 14, represents the observed increase in the free-field sound pressure levels due to the geometry of the test panel alone. Effectively, the result shown in Figure 15

may be considered to be the panel amplification factor with respect to an arbitrary reference level, or an inverted transmission loss curve. In order to estimate the absolute transmission loss of the test specimen, two approaches were adopted. The first method simply consisted of subtracting the free-field sound pressure levels (with the test specimen installed) from the internal sound pressure levels within the reverberation room, i.e., the noise reduction given by M1 minus M3. This result is shown by the lower noise reduction curve in Figure 16. It should be noted that the noise reduction results for frequencies above 1000 Hz are questionable because of the relatively high background noise levels in the higher third octave bands (see Figure 12); this may be verified by comparing the free-field sound pressure levels shown in Figure 14 with the background noise levels shown in Figure 12. This comparison shows free-field levels are only 1-1/2 dB to 2 dB higher than the background noise levels at higher frequencies. The second method of estimating the panel transmission loss consisted of utilizing the effective sound transmission results presented in Figure 15. As stated previously, this curve, if inverted, would represent the shape of the transmission loss curve for the panel specimen since it basically describes the qualitative change in the measured third octave band sound pressure levels caused by insertion of the panel between a given noise source and the measuring point. In order to determine the absolute third octave band levels for this curve, a baseline noise reduction of 5 dB at 100 Hz was assumed. This corresponds to the noise reduction obtained by subtracting the free-field sound pressure level from the sound pressure level within the reverberation room at 100 Hz. At this particular frequency, the free-field sound pressure level is considerably higher than the background noise level and thus the 5 dB noise reduction is considered reasonable. The noise reduction spectrum determined by this latter method is also shown in Figure 16. It is immediately observed that the noise reduction above 1000 Hz is more realistic for this type of structure than that shown by the lower curve.

In order to convert measured Noise Reduction to Transmission Loss, the following relationship must be utilized for sound transmission between two enclosures separated by a common wall (Reference 2)

$$NR = TL - 10 \log_{10} \left[\frac{1}{4} + \frac{S_W}{S} \frac{(1 - \bar{\alpha})}{\bar{\alpha}} \right] \qquad (7)$$

where S_W = Area of the transmitting wall or panel (ft^2)

S = Total Area of absorbing surfaces (ft^2) of the enclosure behind secondary side of panel

$\bar{\alpha}$ = Average Absorption Coefficient for the above surfaces in the relevant frequency bandwidth

NR = $SPL_1 - SPL_2$ dB

Subscripts $_1$ and $_2$ refer to primary and secondary sides of panel.

Ordinarily for the type of experiment described above, where the secondary side of the test panel opens into an outdoor environment, the absorbing term S in the above expression becomes infinite and the Noise Reduction simply reduces to:

$$NR = TL + 6 \quad dB \tag{8}$$

However, the cavity behind the secondary side of the test panel (see Figure 9) was in fact partially reverberant and the free-field microphone was positioned within one foot of this cavity. As a result, the effective Transmission Loss of the panel would be modified accordingly by several dB, and would therefore be greater than the TL given by Equation (8). It is reasonable to assume that the correction would be no greater than 3 dB because of the small size of the cavity, and the fact that the microphone on the secondary side of the test panel was not actually placed within the cavity. Therefore the above relationship between NR and TL would be modified to approximately NR = TL + 3 dB.

The effective Transmission Loss of the test specimen, derived from the approximate relation TL = (NR - 3) dB, is shown in Figure 17. Two curves are again presented, both of which have been derived from the noise reduction curves of Figure 16. Also shown in Figure 17 is the "mass law" field incidence transmission loss derived from the theoretical results presented by Beranek (Reference 3) for limp, mass-controlled panels. This theoretical curve is observed to be in good agreement with the experimental results between the fundamental resonance of the panel at 100 Hz and an upper limit of 2000 Hz. Above this frequency the experimental results are lower than the theoretical mass-law results, due possibly to acoustic coincidence effects.

The change in the panel transmission loss as a result of the simulated micro-meteoroid impact may be deduced from the results presented in Figure 18. This figure shows the sound pressure levels recorded by the free-field microphone, M3, during acoustic test runs 1, 2, 9 and 10. It may be deduced from these results that at low frequencies the transmission loss of the panel is reduced by as much as 10 dB while at high frequencies it is substantially unchanged. In the region of the fundamental mode of the panel at 100 Hz the transmission loss is increased by about 7 dB. This modification to the panel sound transmission behavior was caused by severe degradation of the polyurethane foam sandwich between the inner and outer aluminum alloy layers of the test panel following the simulated impact. As a result, the test panel no longer behaved as a composite panel with each layer vibrating in phase; the inner and outer panel layers were in fact observed to be vibrating independently of each other.

4.2 Measured Panel Responses

The acceleration power spectral densities measured by accelerometers A1, A2 and A3 are shown in Figures 19, 20 and 21 for Test Run Number 3. Accelerometers A1 and A2, which were attached to the panel center on the outer and inner skin respectively exhibit almost identical responses. From these three figures, significant responses associated with individual modes of the panel can be identified at approximately 85 Hz, 150 Hz, 210 Hz, 260 Hz, 310 Hz and 375 Hz. Higher order mode responses may also be identified at approximately 525 Hz and 650 Hz.

Strain power spectral densities measured by strain gauges SG1 through SG6 are shown in Figures 22 through 27, respectively. Strain gauges SG1, SG2 and SG3 were located on the outer skin of the test panel (towards the acoustic environment) while strain gauges SG4, SG5 and SG6 were located on the inner skin of the test panel (the free-field side). In general these results again indicate significant responses associated with the individual panel modes identified above. Maximum rms strains were recorded by strain gauges SG3 and SG6 located at the center of the outer and inner skins, respectively. Strain levels measured by gauges SG1 and SG4 at the edges of the panel were considerably lower than the strain levels away from the panel edges. Examination of the response results for Test Runs 1 through 9 generally show negligible change in acceleration or strain which could be associated with any cumulative damage effects.

However, after the test panel was subjected to a simulated micro-meteoroid impact, the character of the acceleration and strain responses changed significantly. The acceleration power spectral density measured by accelerometer A2 for Run Number 10 is shown in Figure 28. Comparing this result with Figure 20, it can be seen that the peak response shifted downward in frequency to about 30 Hz and the rms level was reduced from 70 g to 48 g. This change in the character of the response was a direct result of the breakdown of the polyurethane foam layer, which caused the inner and outer skin of the composite panel to respond independently. Accelerometers A1 and A3 were de-bonded from the test panel immediately after initial application of the acoustic environment during Run Number 10. This probably resulted from excessive displacements of the inner and outer skin caused by the breakdown of the polyurethane foam. Strain power spectral densities obtained during Run Number 10 are shown in Figures 29 through 34 corresponding to strain gauges SG1 through SG6, respectively. The marked frequency shift observed in the acceleration response data is also evident in the strain spectra. A summary of the rms strain levels recorded during Test Run Number 1 and Test Run Number 10 is presented in the following table.

STRAIN GAUGE	TEST RUN NO. 3	TEST RUN NO. 10
SG1	13.0	280.0
SG2	50.0	75.0
SG3	62.0	70.0
SG4	14.5	80.0
SG5	60.0	60.0
SG6	60.0	75.0

TABLE I. CHANGE IN RMS STRAIN (MICRO-INCHES/INCH) FOLLOWING MICRO-METEOROID IMPACT

The foregoing table shows a general increase in the measured panel strains following a simulated micro-meteoroid impact, particularly for strain gauge SG1 which was located at the edge of the outer skin (facing the acoustic environment). This large increase in the measured strain for SG1 is apparently inconsistent with the observed increase in strain for SG4 which was located at the edge of the inner panel skin. However, this result was checked by examining rms strain versus time records and appears to be a valid result. During the course of the acoustic fatigue testing, progressive de-bonding around the panel edges was observed for both the outer and inner skin. This is illustrated in Figure 35 which shows a view of the test panel from the interior of the reverberation room. The experimental results suggest that this de-bonding was only partial, since the response and sound transmission characteristics were unaffected. Only when the test specimen was subjected to micro-meteoroid impact did the response and sound transmission characteristics show considerable variation.

REFERENCES

1. Den Hartog, J.P., Mechanical Vibrations, McGraw-Hill Book Co., Inc., 1956.

2. Beranek, L.L., Acoustics, Chapter 10, McGraw-Hill Book Co., Inc., 1954.

3. Beranek, L.L., Noise Reduction, Chapter 13, McGraw-Hill Book Co., Inc., 1960.

FIGURES

16

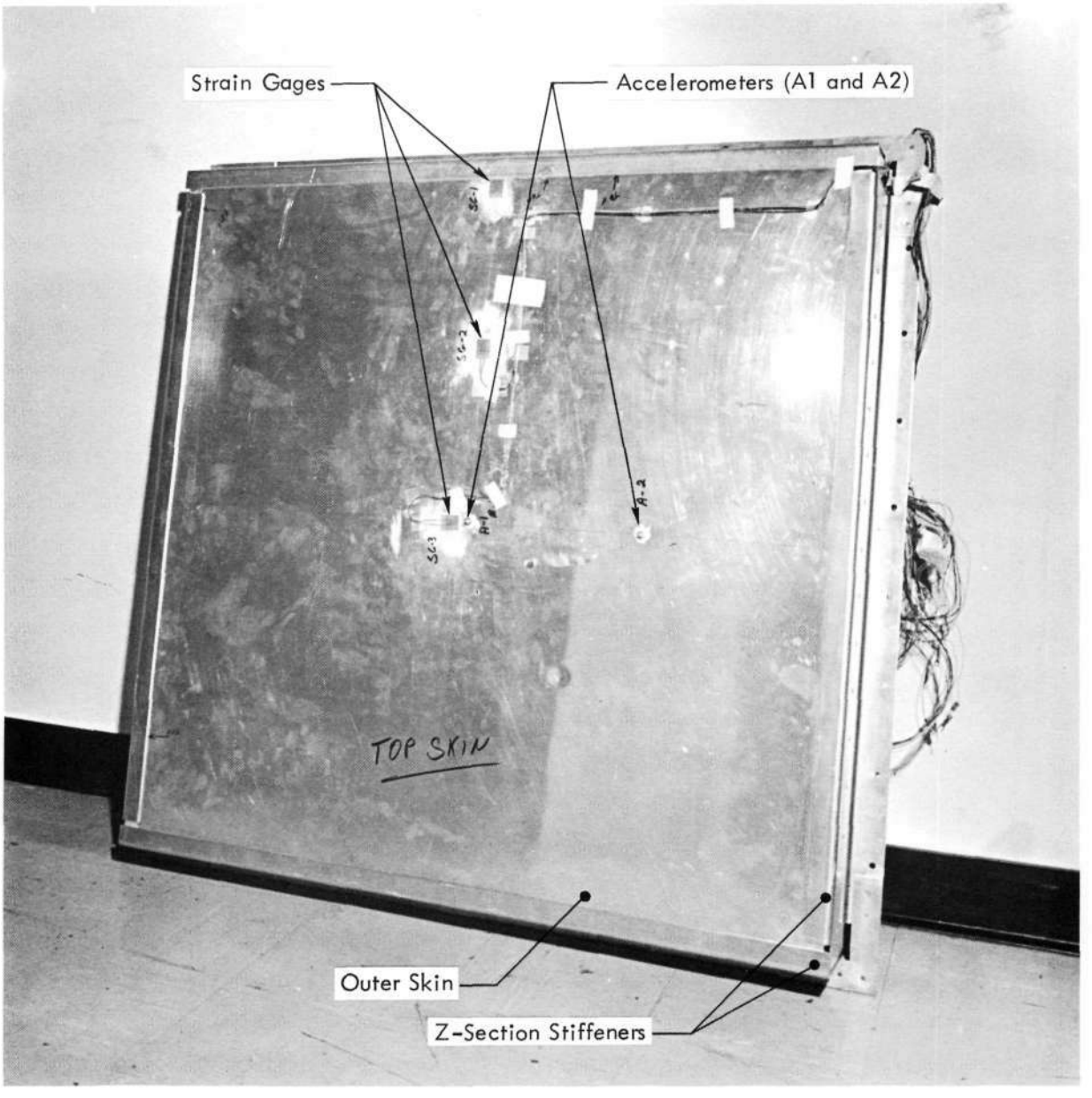

Figure 1. Photograph of the Multi-Layered RAM Structural Panel

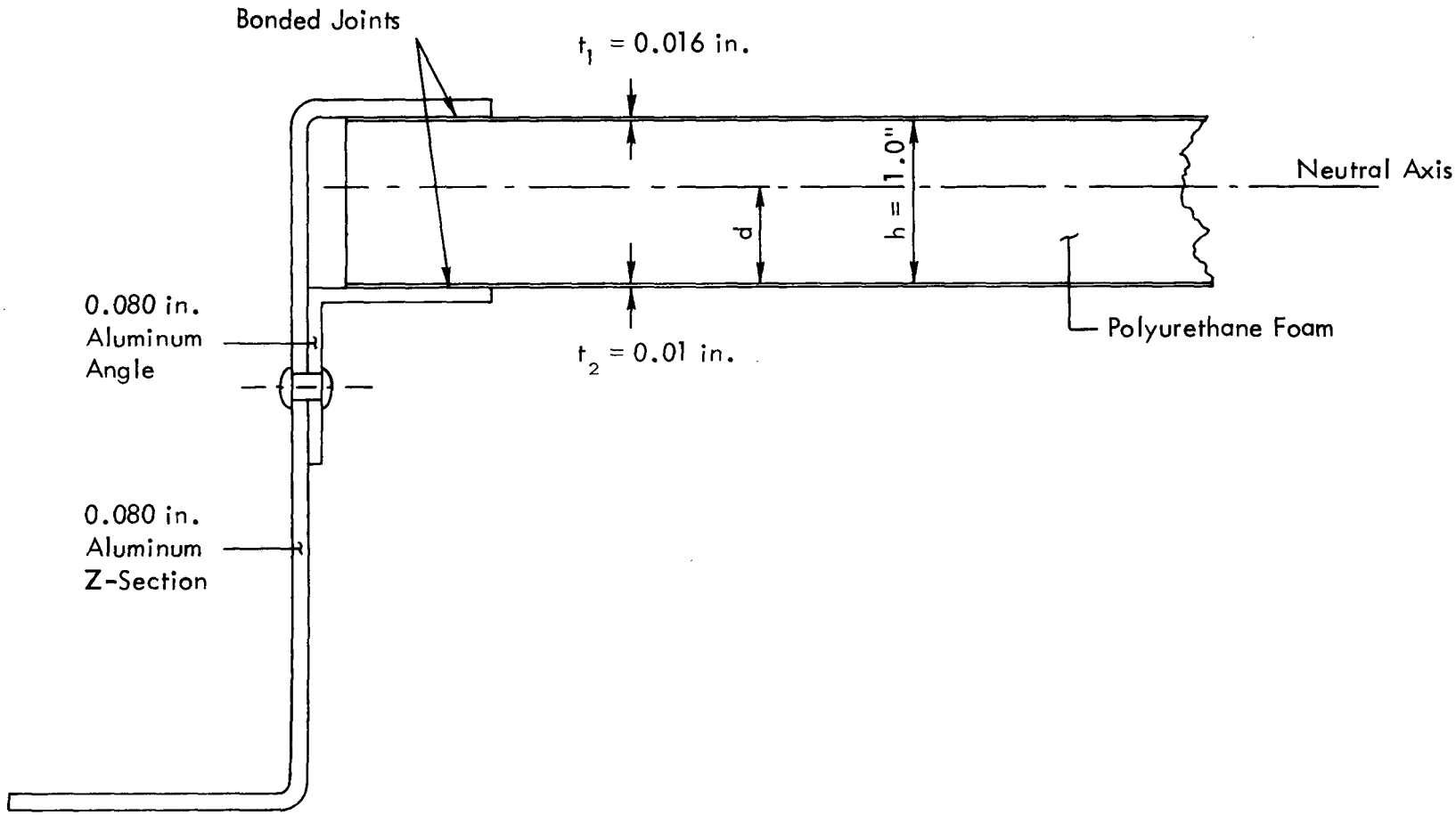

Figure 2. Cross-Section of Test Panel

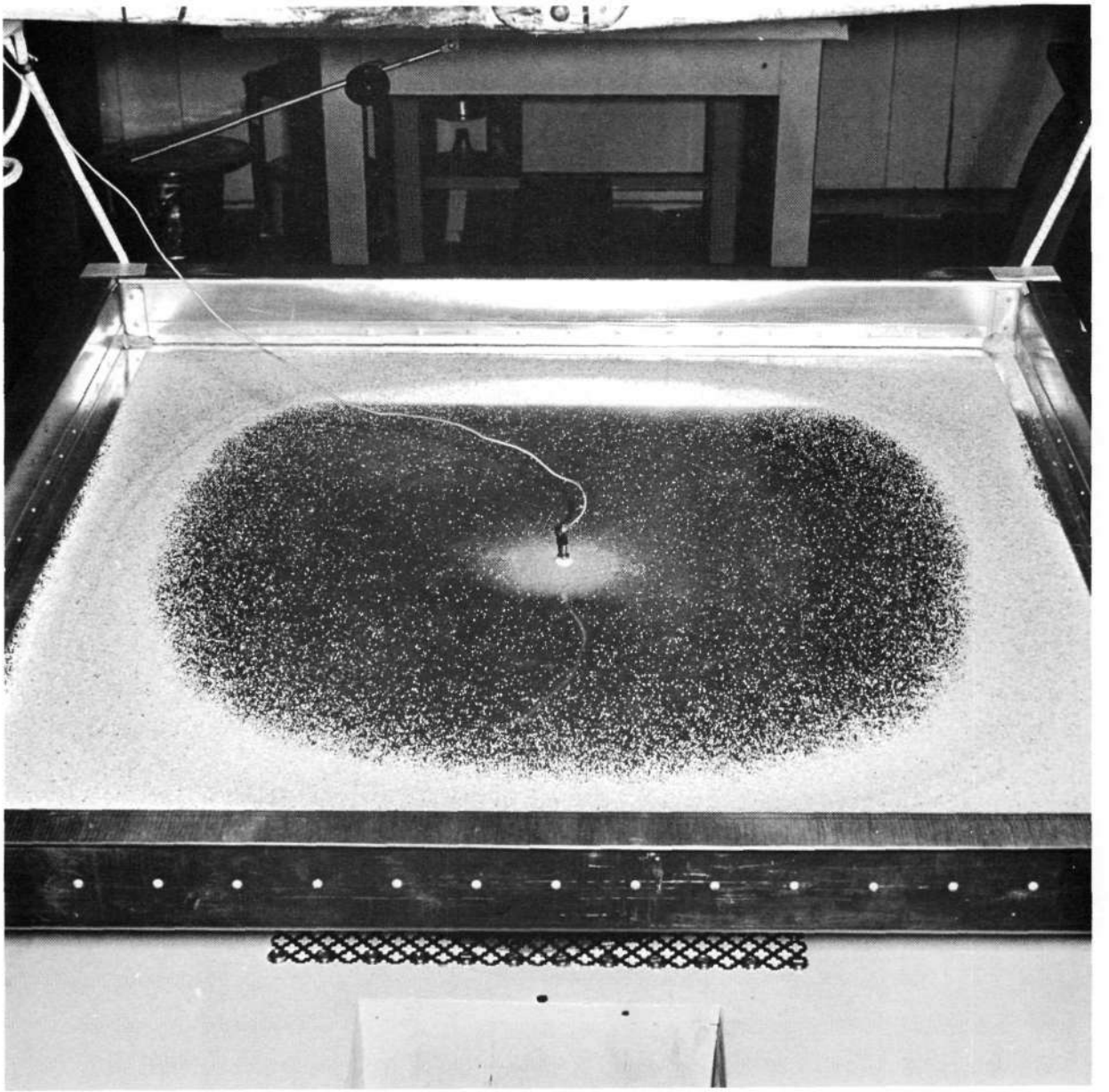

Figure 3. Modal Sand Pattern Obtained from Resonance Dwell at 112 Hz

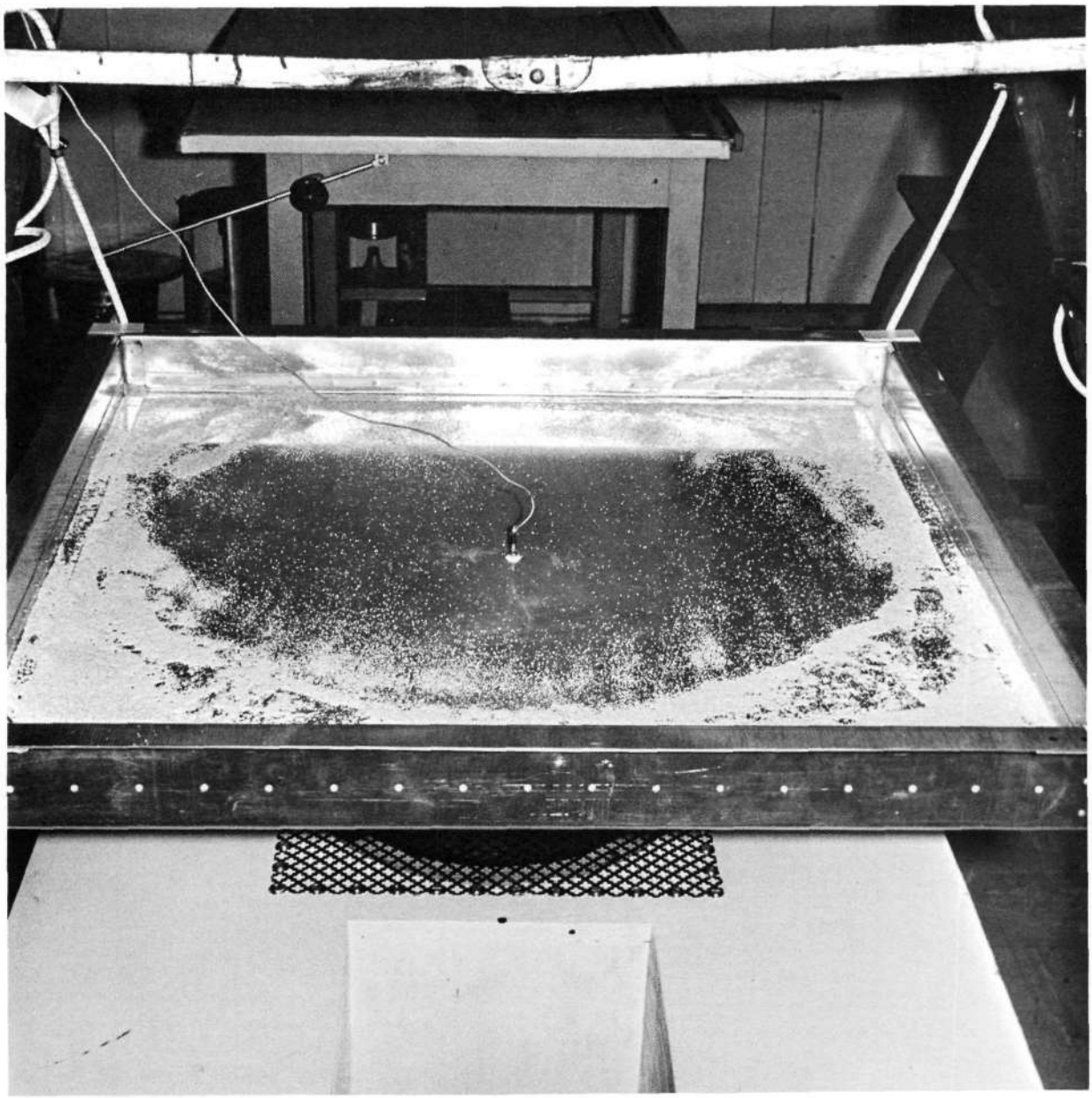

Figure 4. Modal Sand Pattern Obtained from Resonance Dwell at 198 Hz

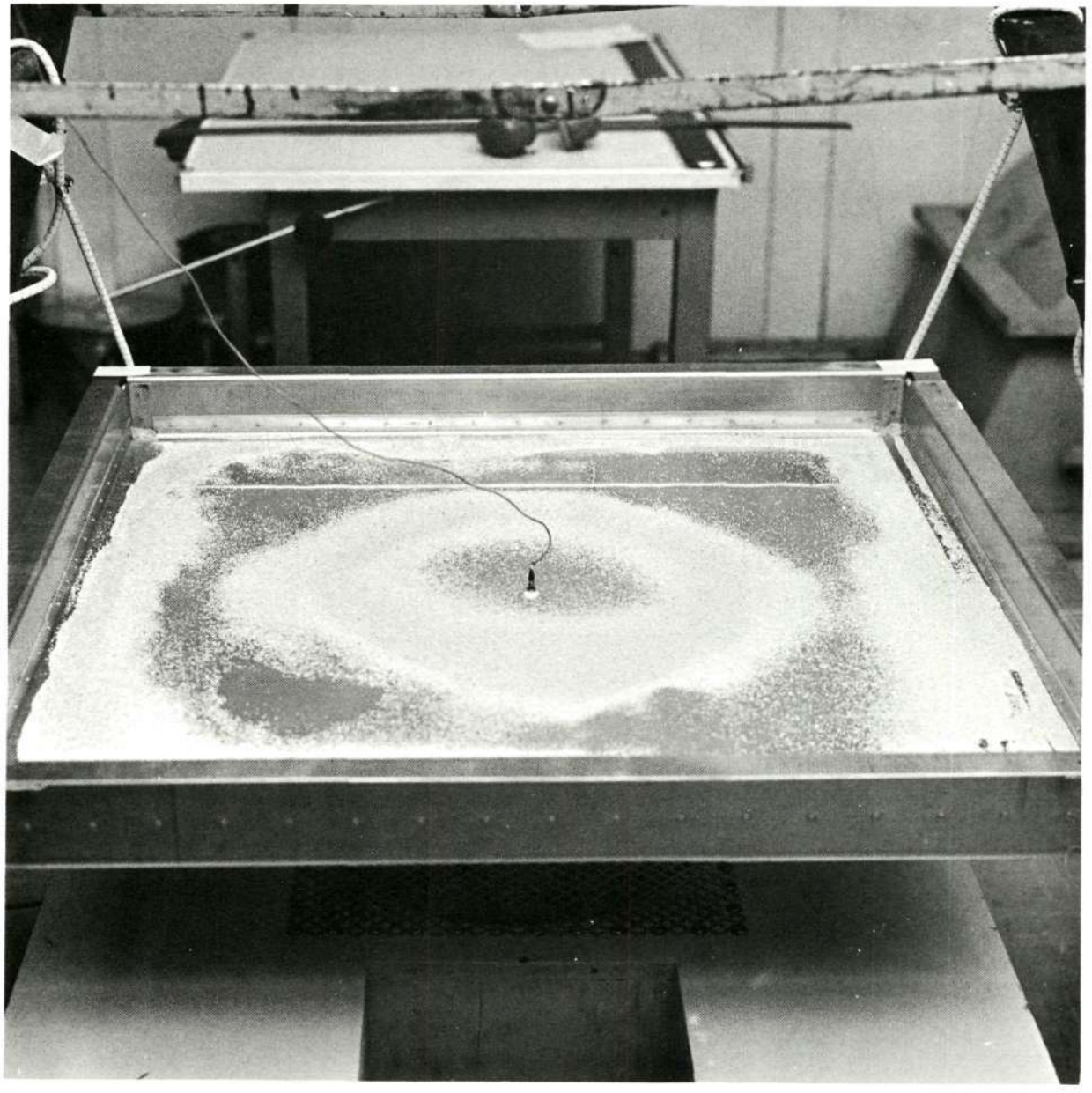

Figure 5. Modal Sand Pattern Obtained from Resonance Dwell at 268 Hz

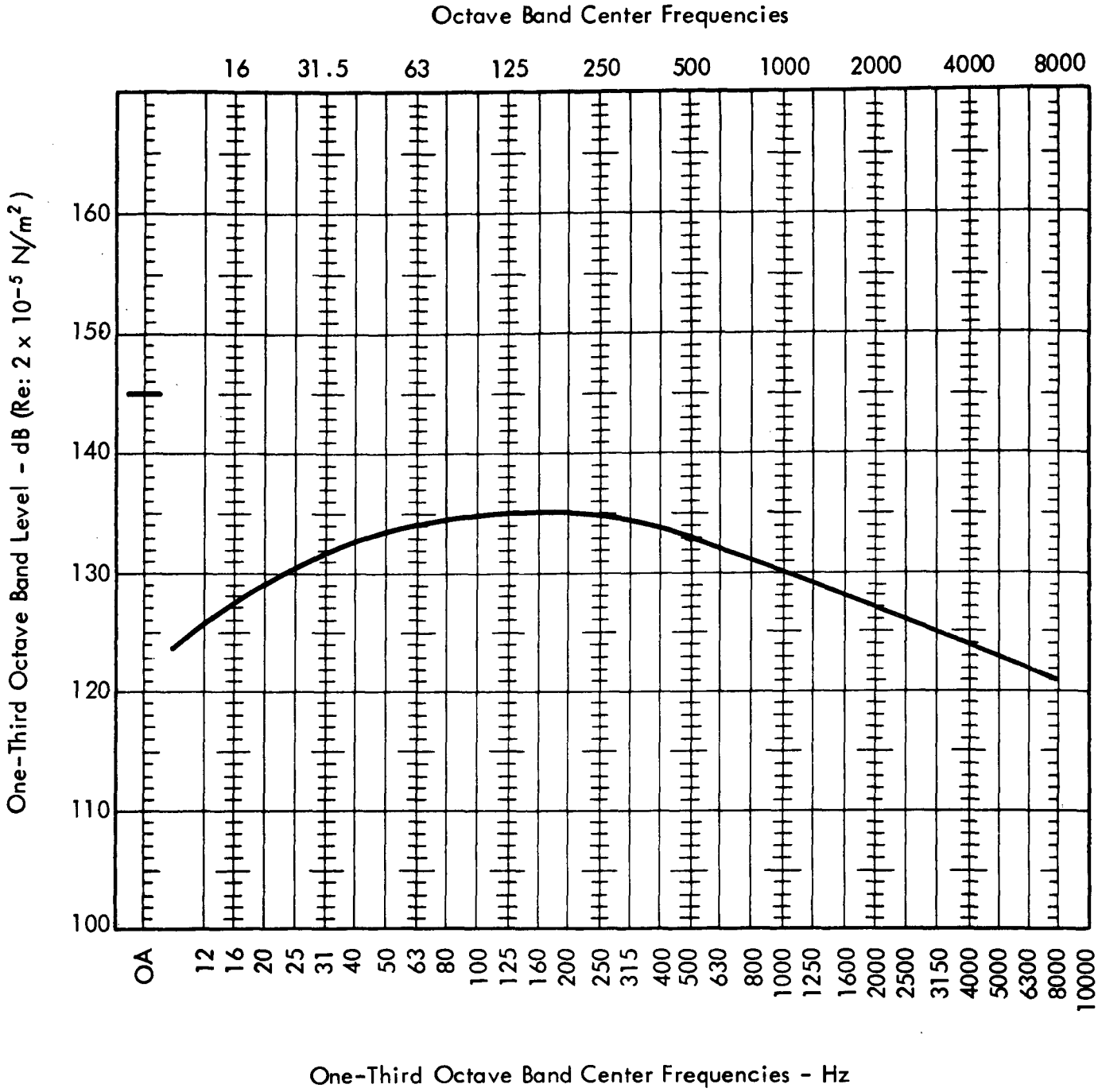

Figure 6. One-Third Octave Band Sound Pressure Levels Specified by MSFC for Interior of Shuttle Orbiter Cargo Bay at Lift-Off

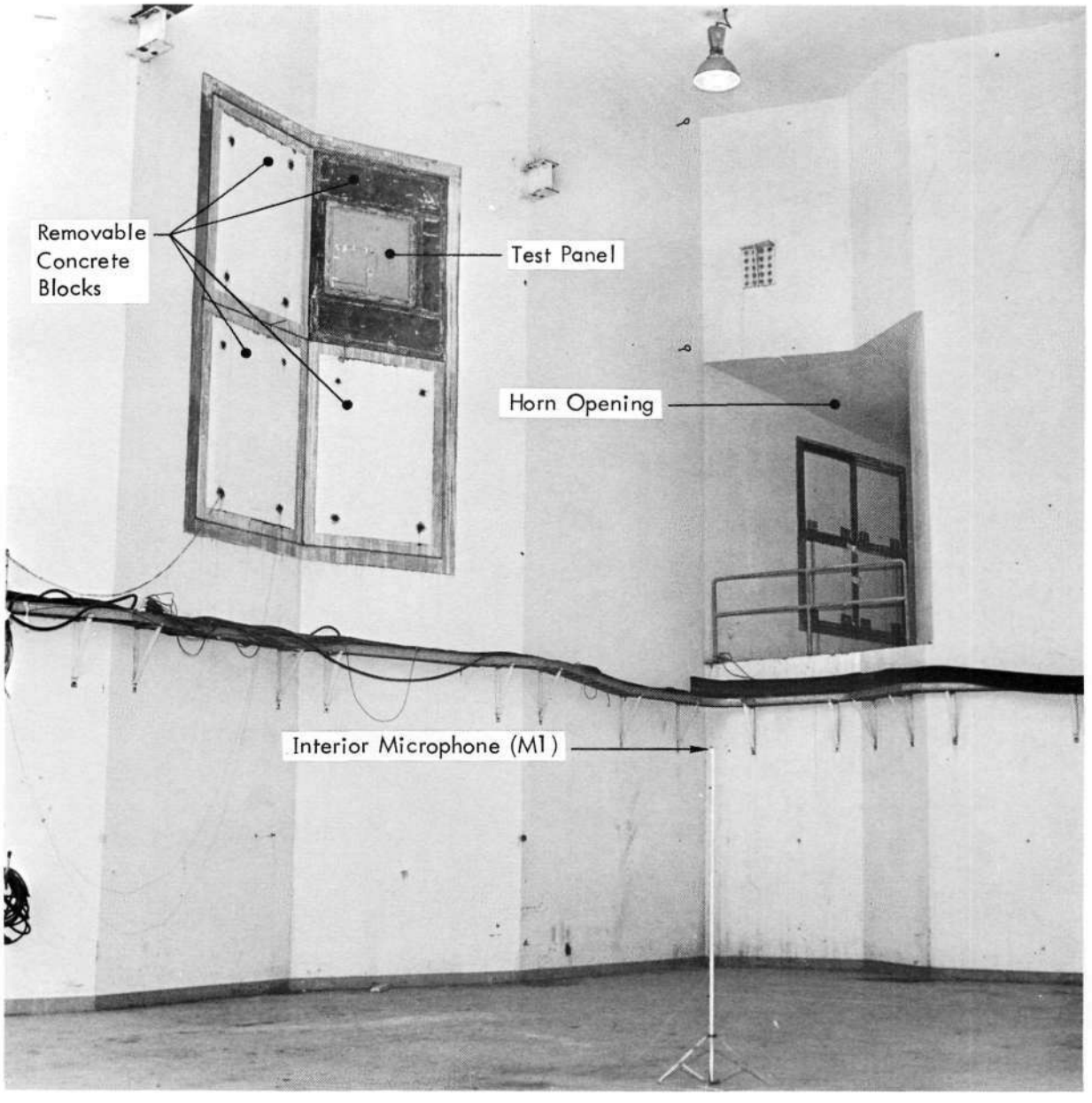

Figure 7. View of the Test Panel Set-Up from the Interior of the Wyle 100,000 ft^3 Reverberation Room

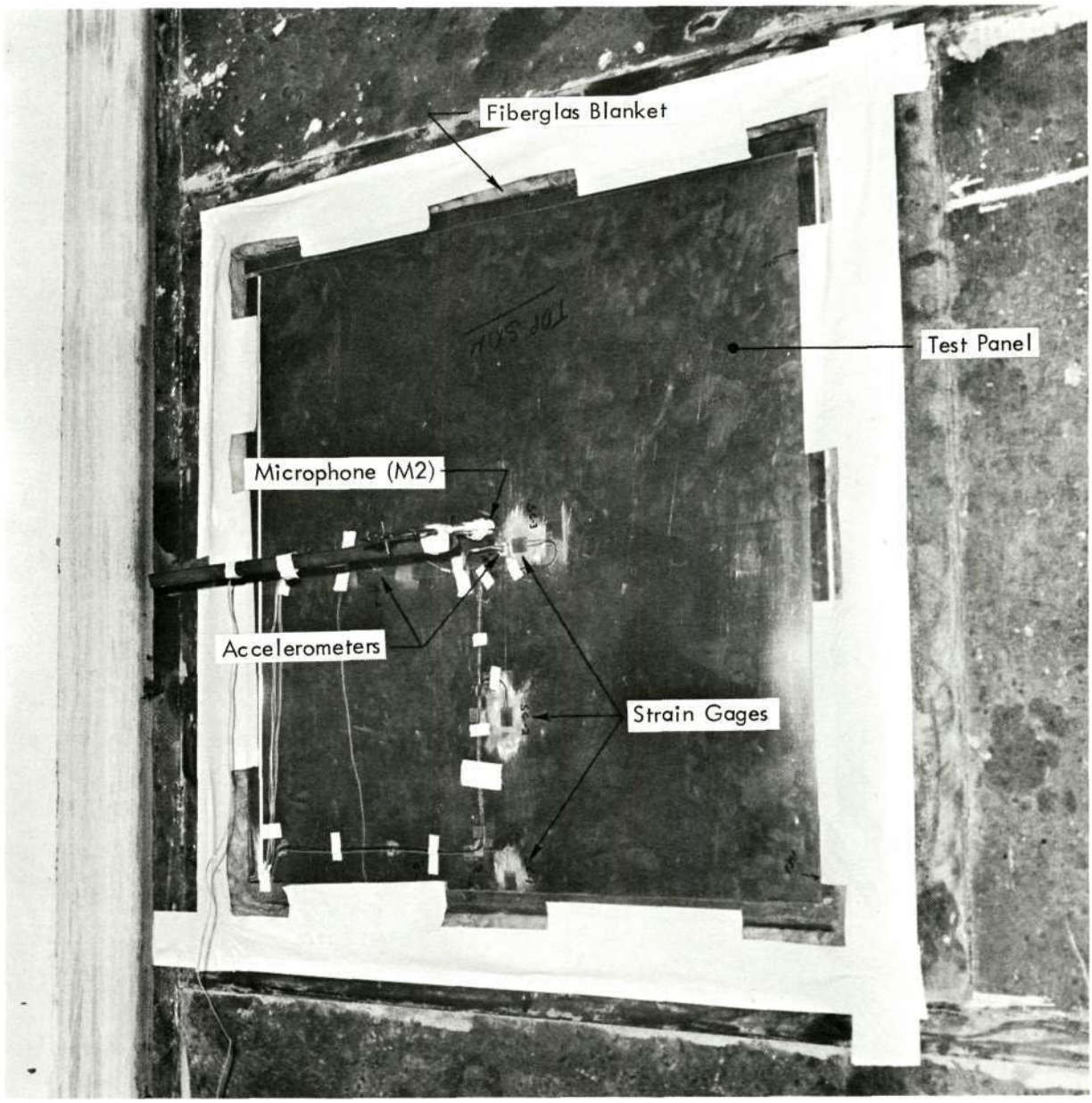

Figure 8. View of the Test Panel from the Interior of the Reverberation Room Showing the Method of Measuring the Panel Surface Sound Pressure Levels

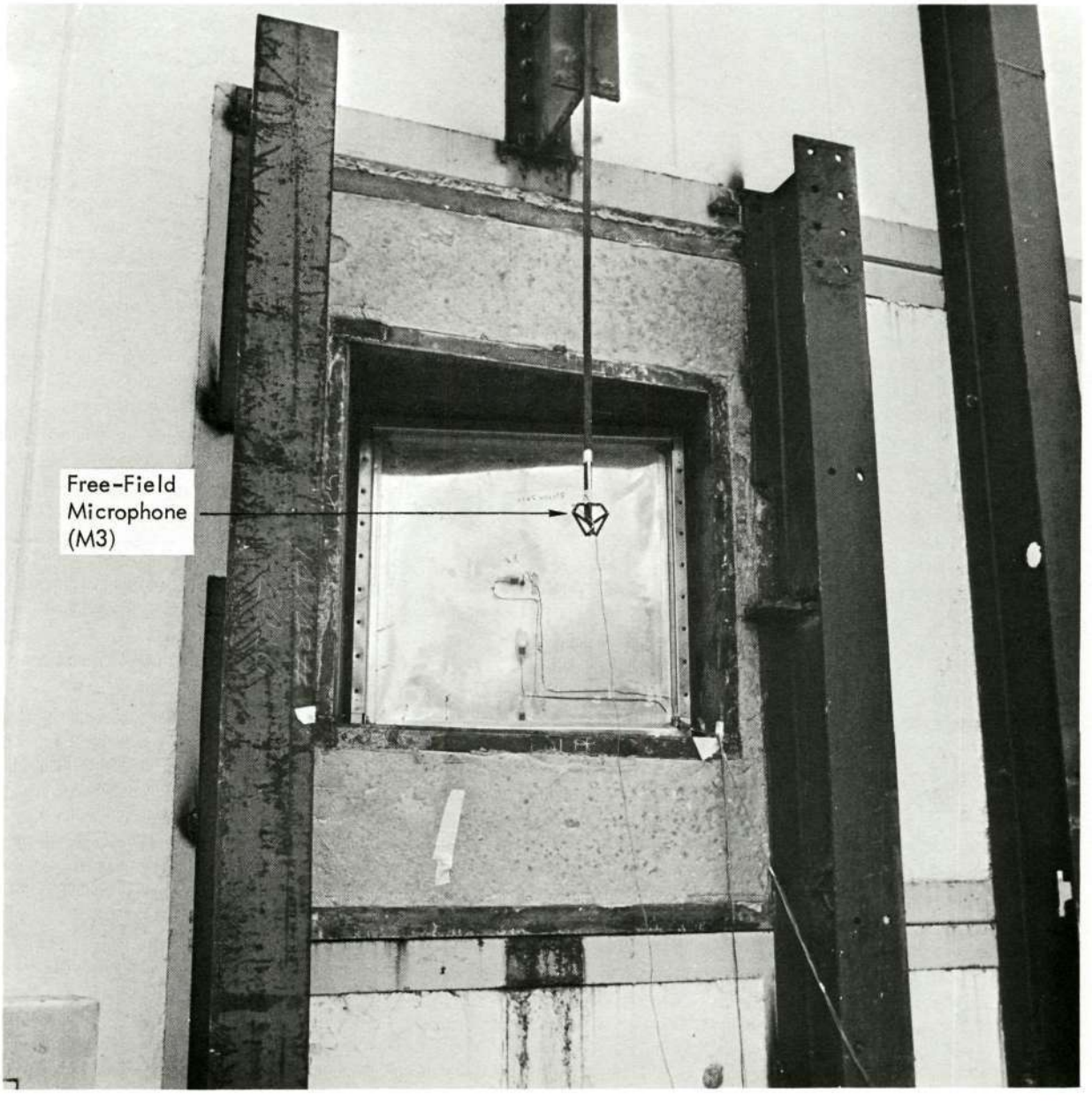

Figure 9. Exterior View of Test Panel in the Wall of the Wyle 100,000 ft^3 Reverberation Room

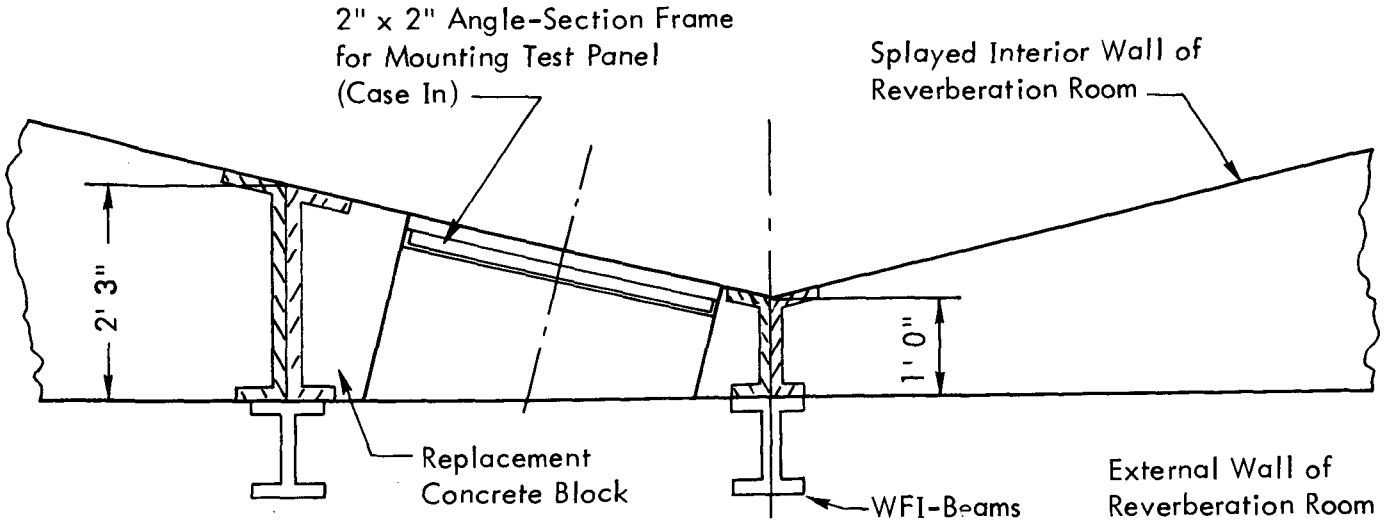

(a) Section Through Wall of Reverberation Room
Showing Geometry of Concrete Block Fixture

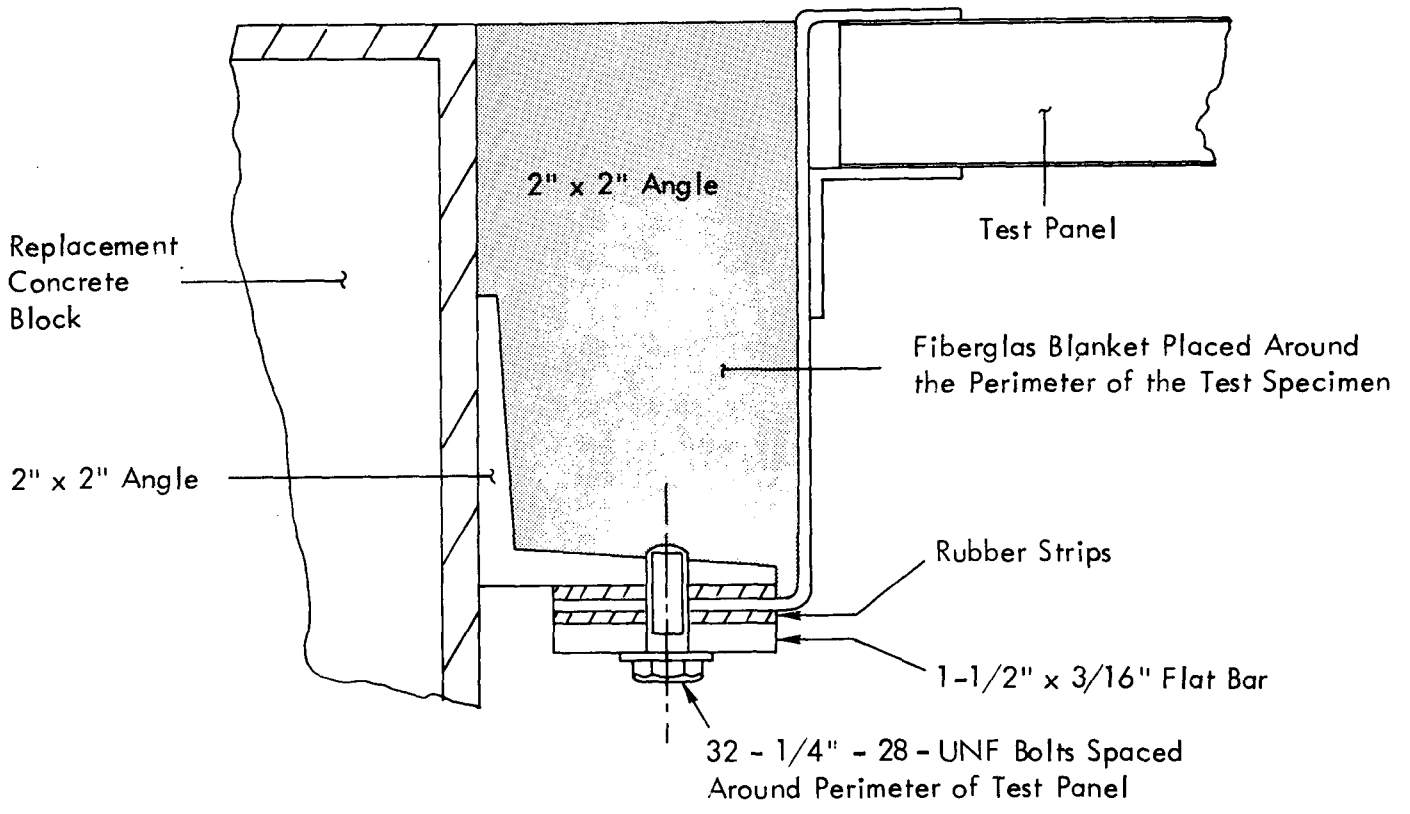

(b) View of Panel Mounting Arrangement

Figure 10. Panel and Fixture Details

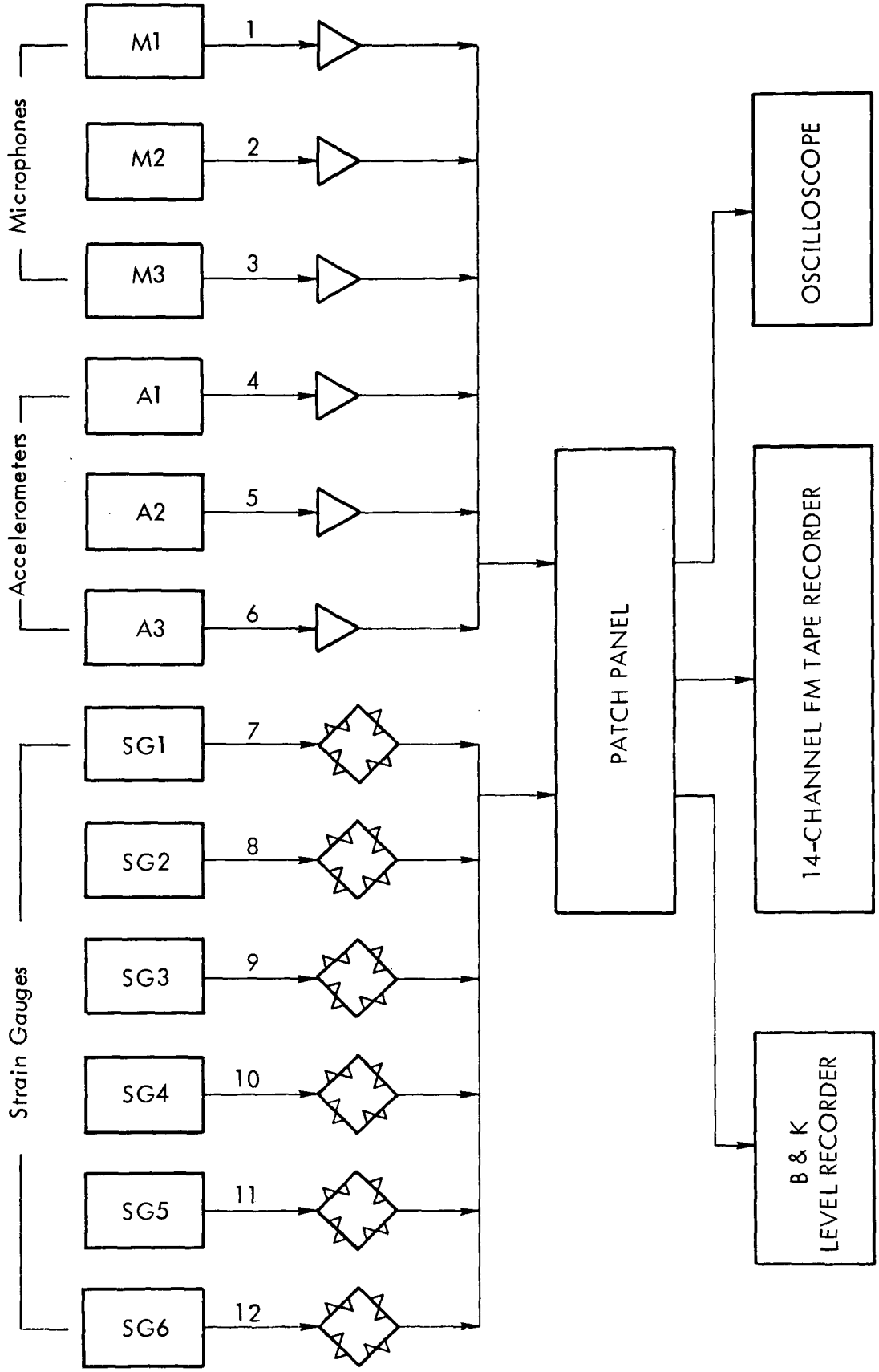

Figure 11. Block Diagram of Instrumentation for Fatigue Testing of RAM Structural Panel

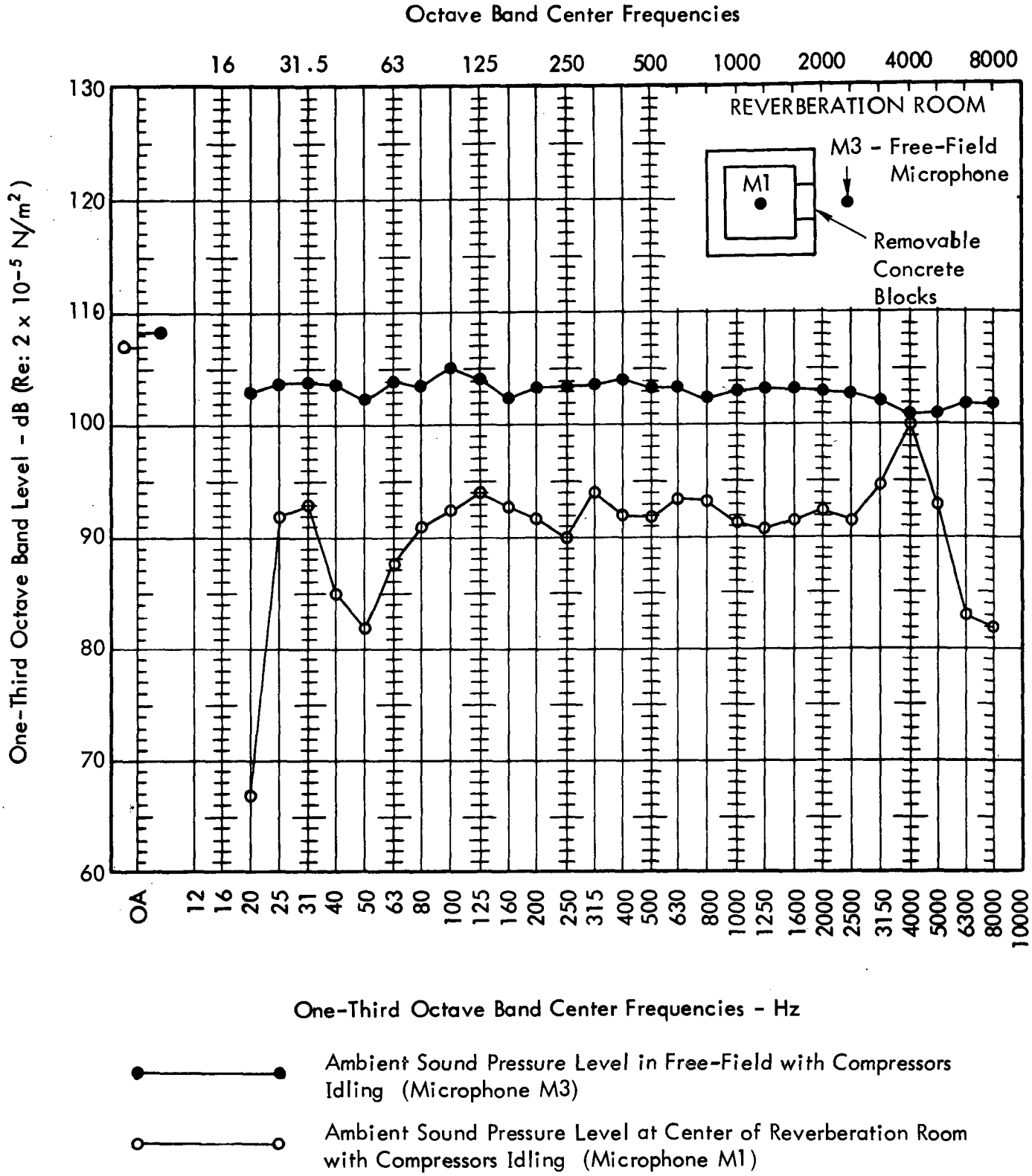

Figure 12. Ambient Sound Pressure Levels Measured Prior to Operation of Reverberant Facility

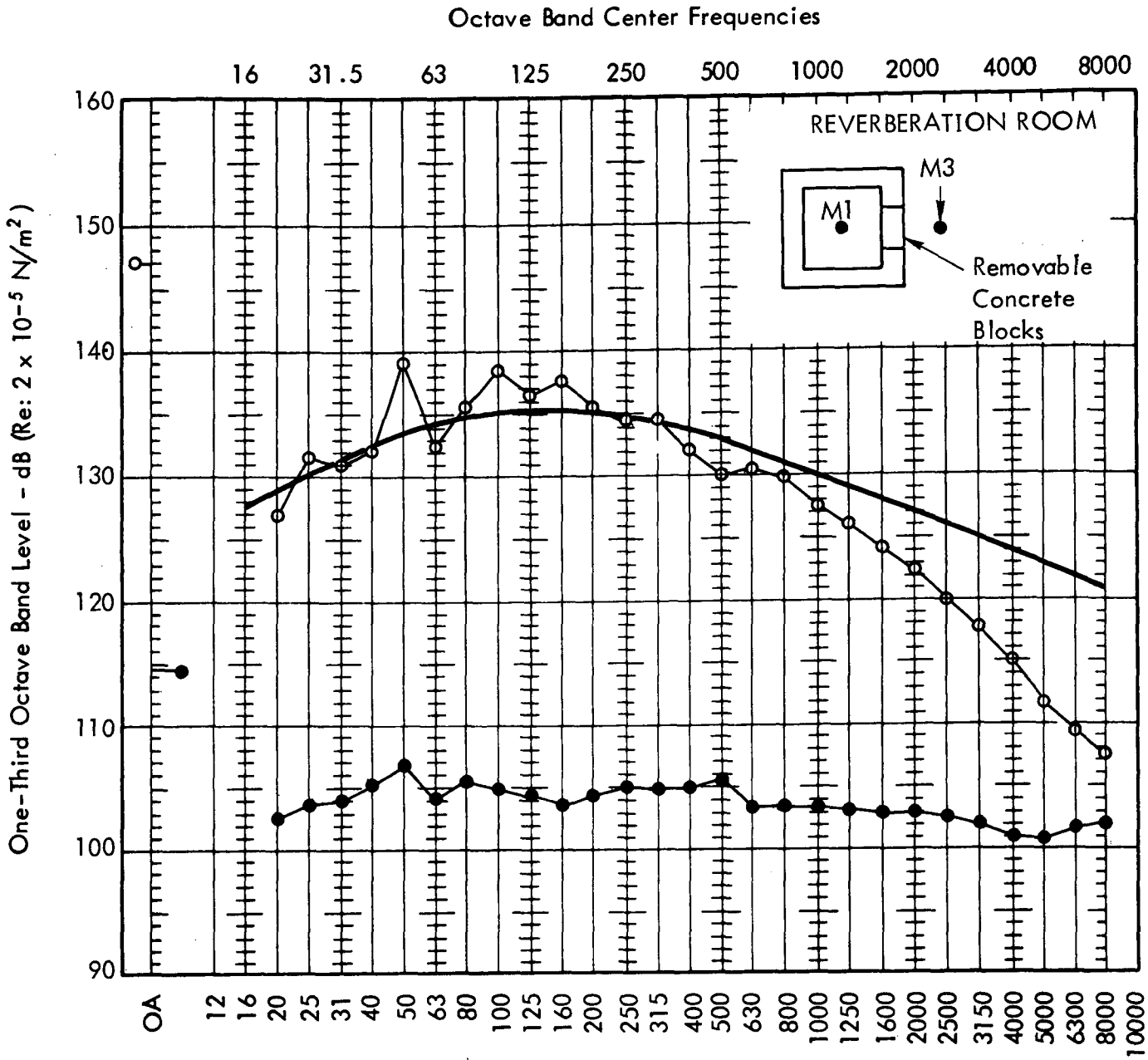

Figure 13. Measured Sound Pressure Levels During Calibration Run

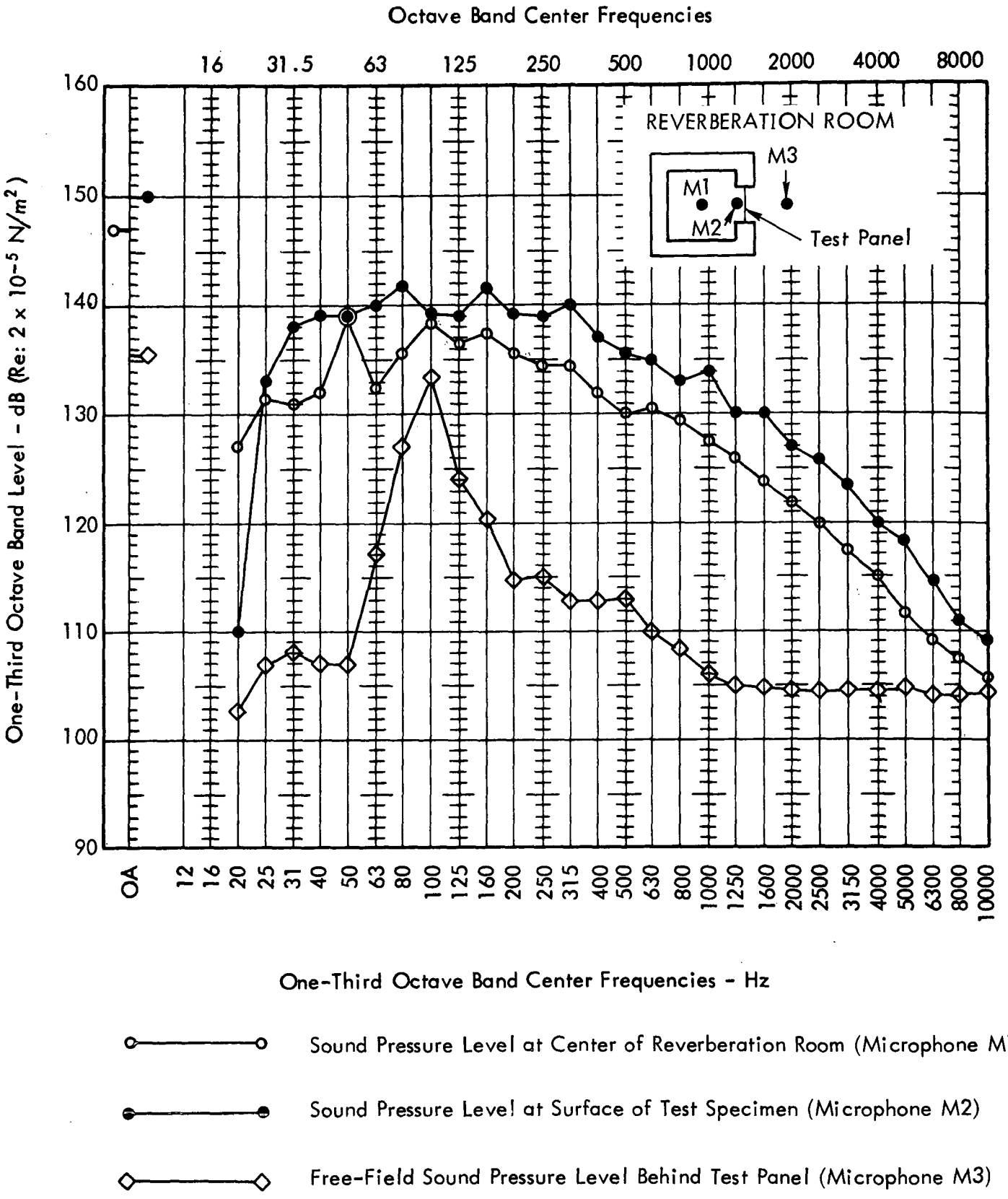

Figure 14. Internal and External Sound Pressure Levels Measured During Acoustic Fatigue Test: Test Run Number 1

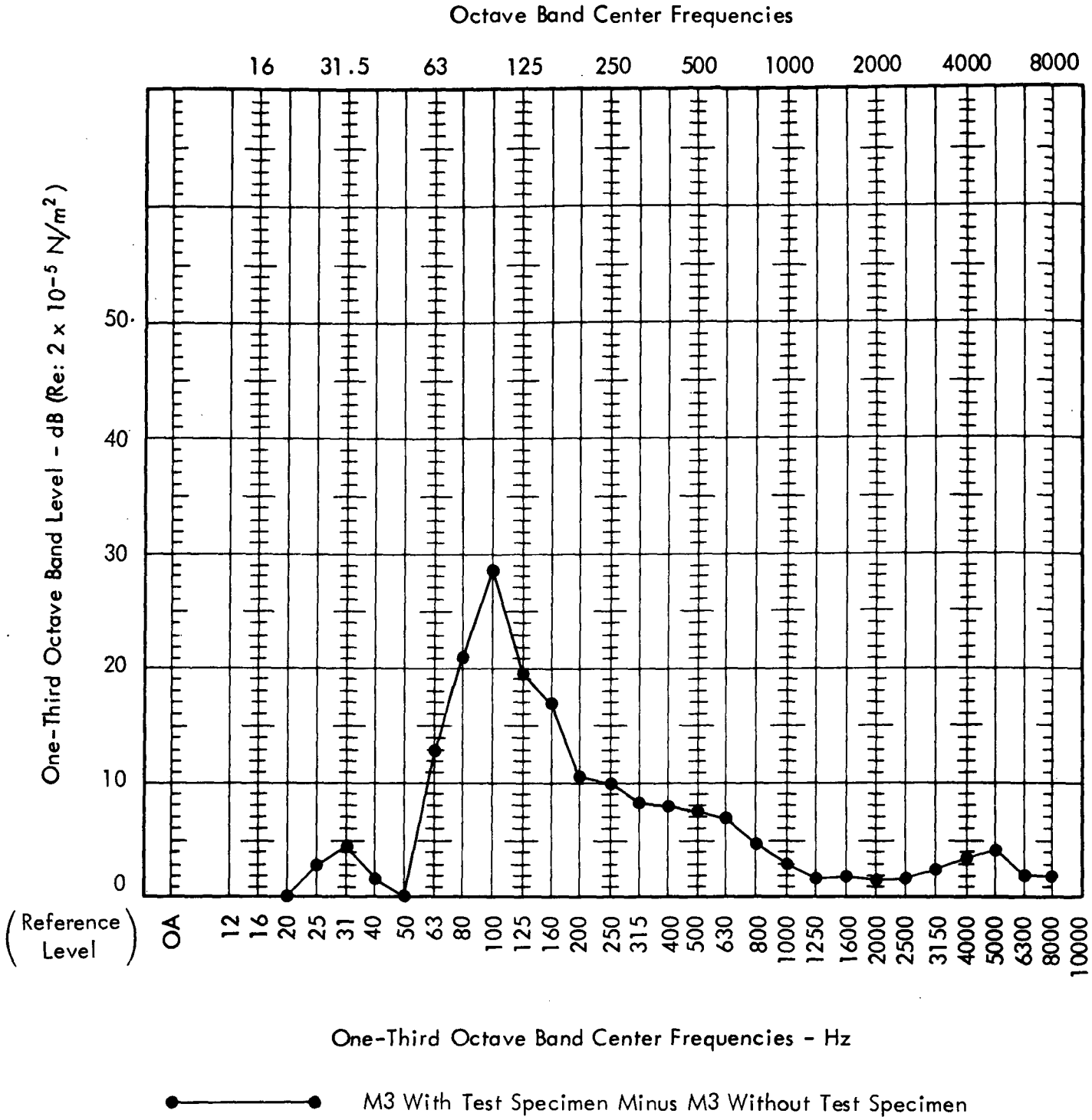

Figure 15. Effective Sound Transmission Through Test Panel

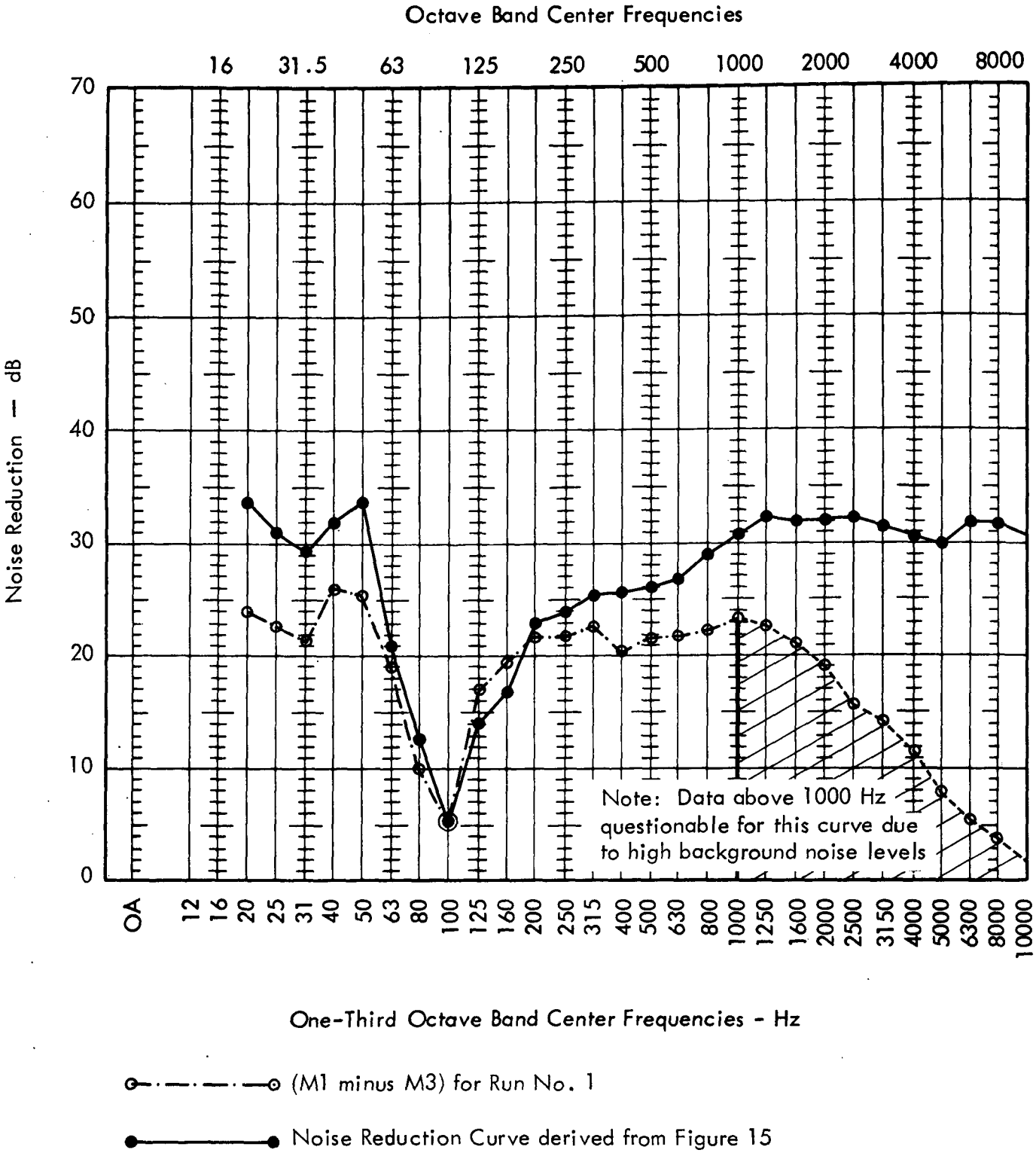

Figure 16. Panel Noise Reduction Data

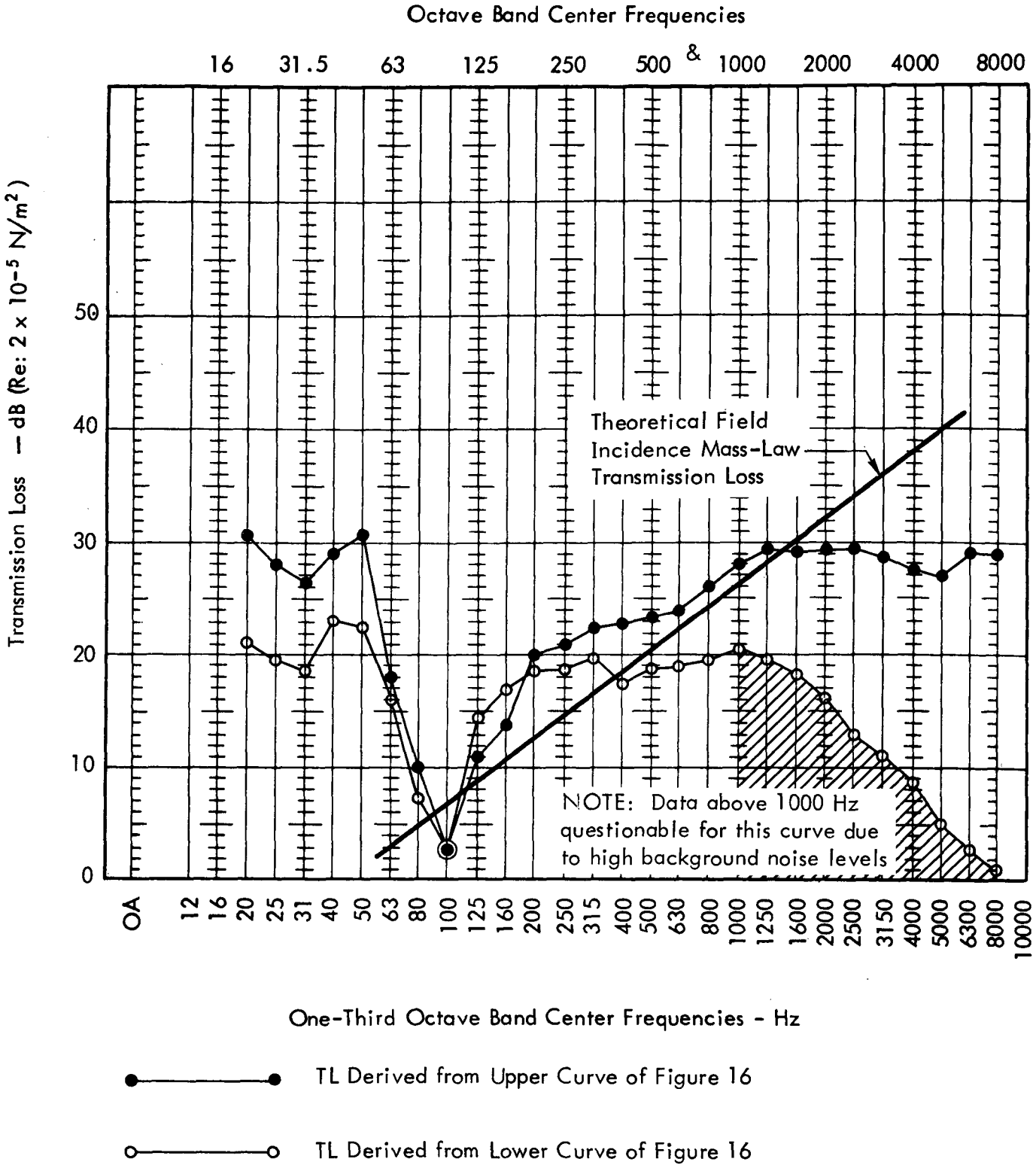

Figure 17. Estimated Transmission Loss of Test Panel

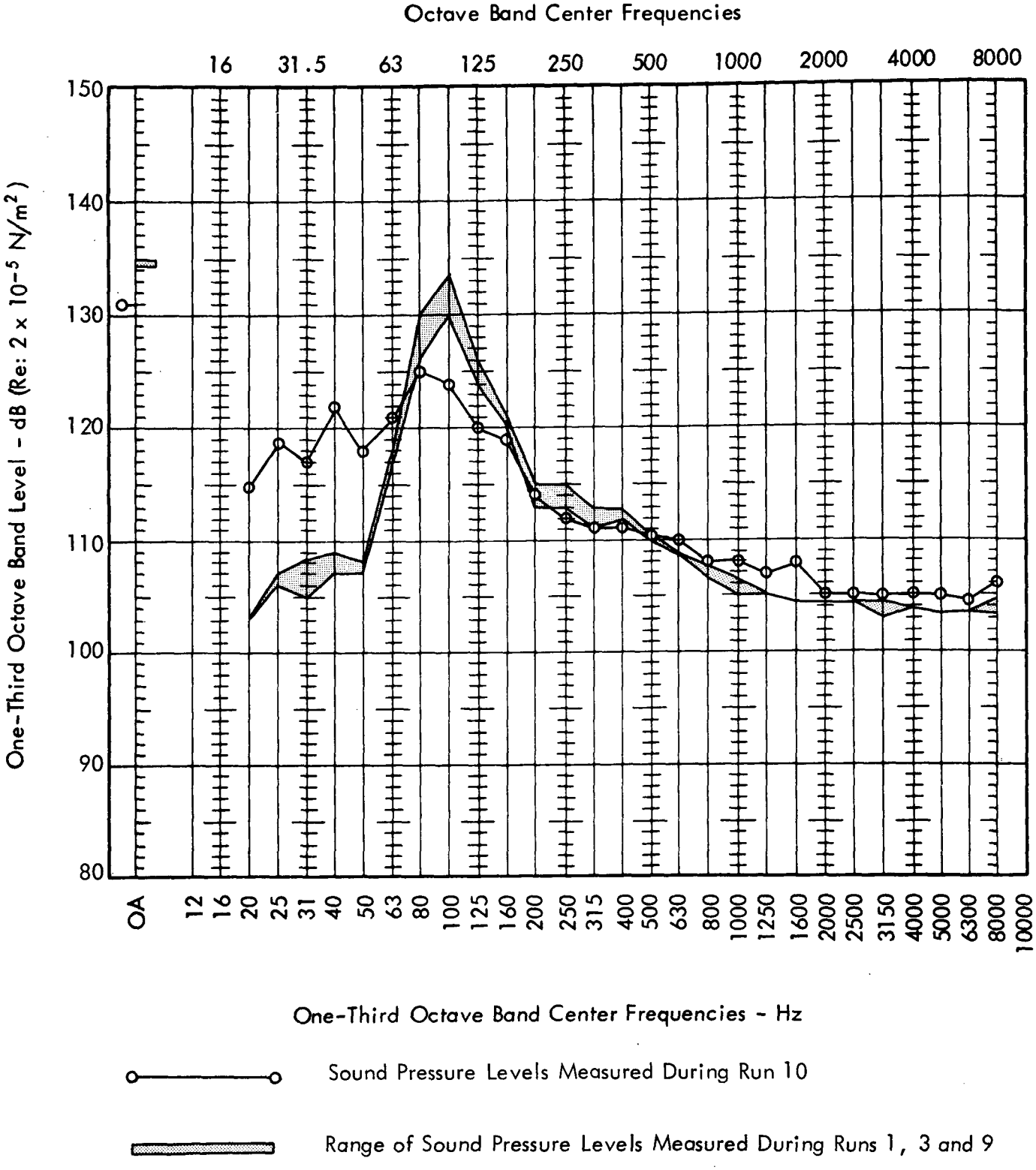

Figure 18. Change in the Measured Free-Field Sound Pressure Levels (M3) Following Micro-Meteoroid Impact

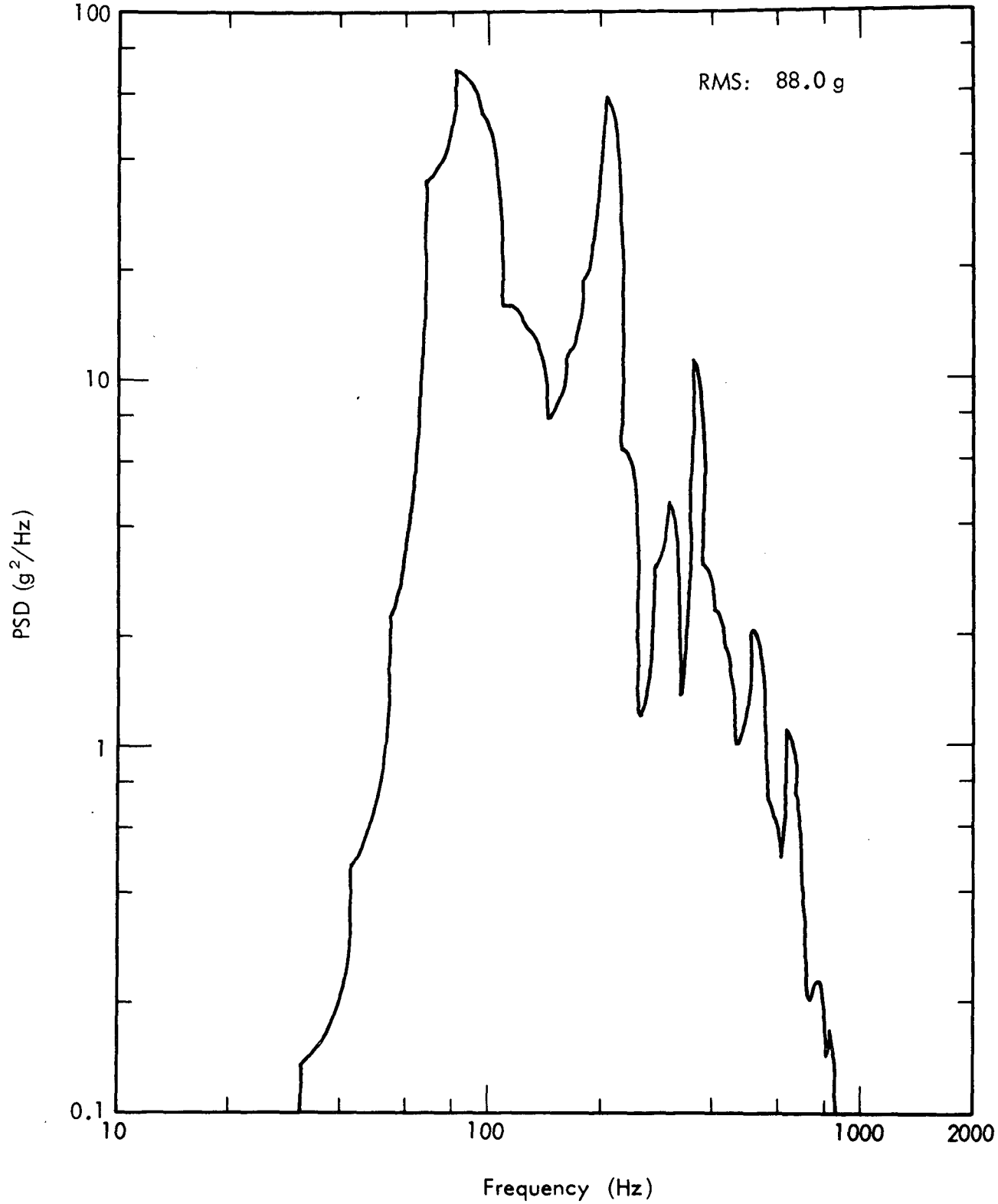

Figure 19. PSD of Accelerometer A1 — Run 3

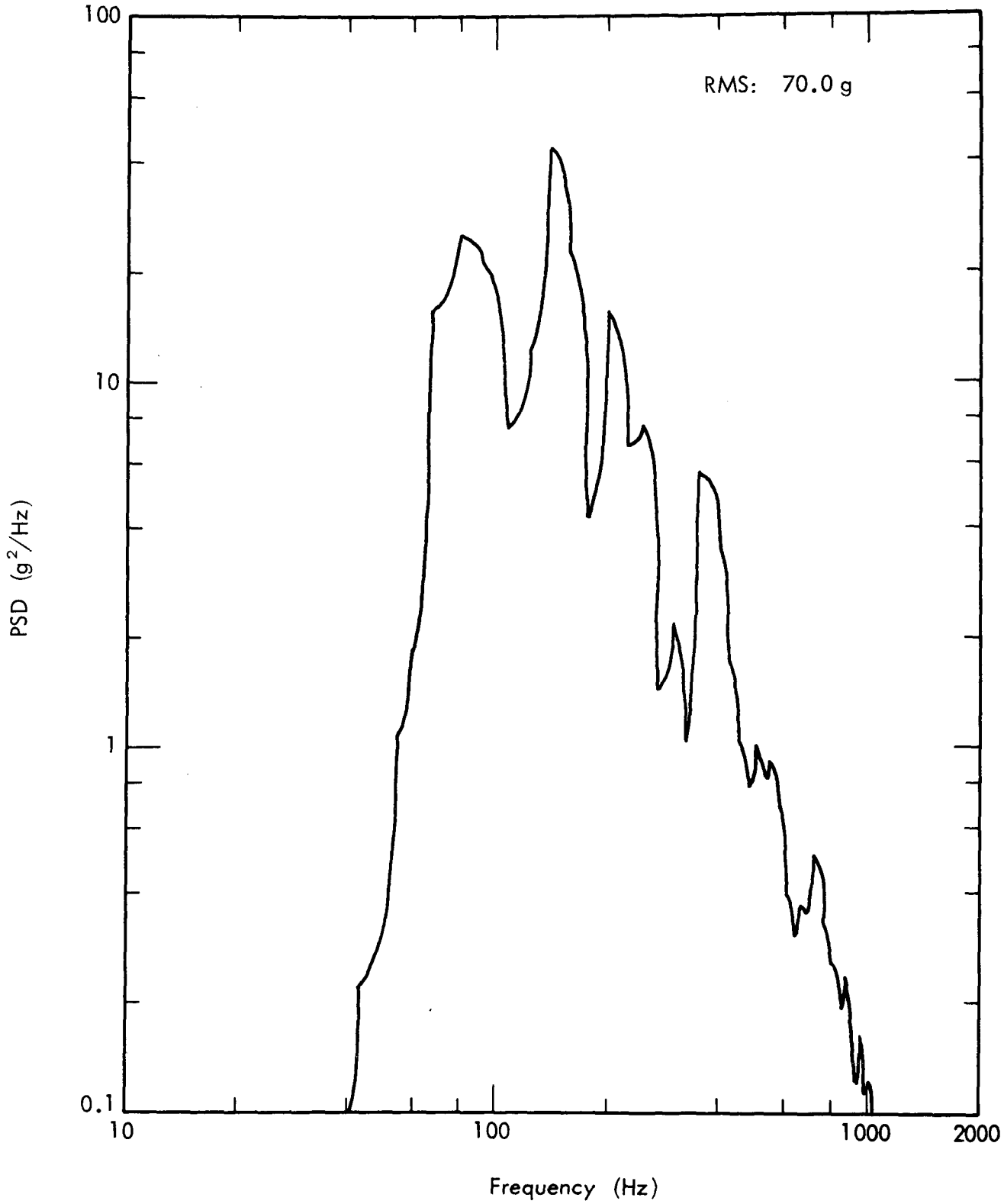

Figure 20. PSD of Accelerometer A2 — Run 3

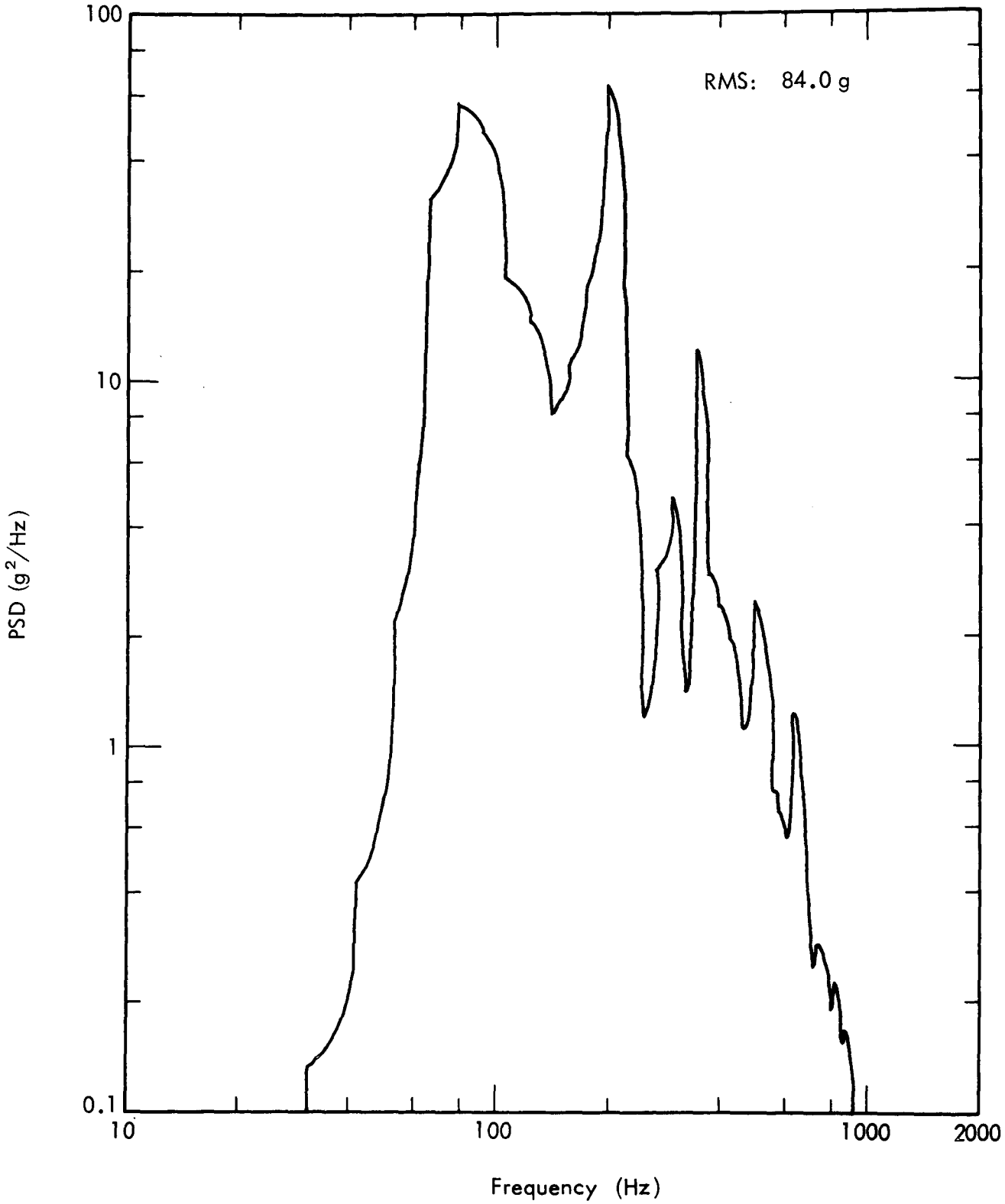

Figure 21. PSD of Accelerometer A3 — Run 3

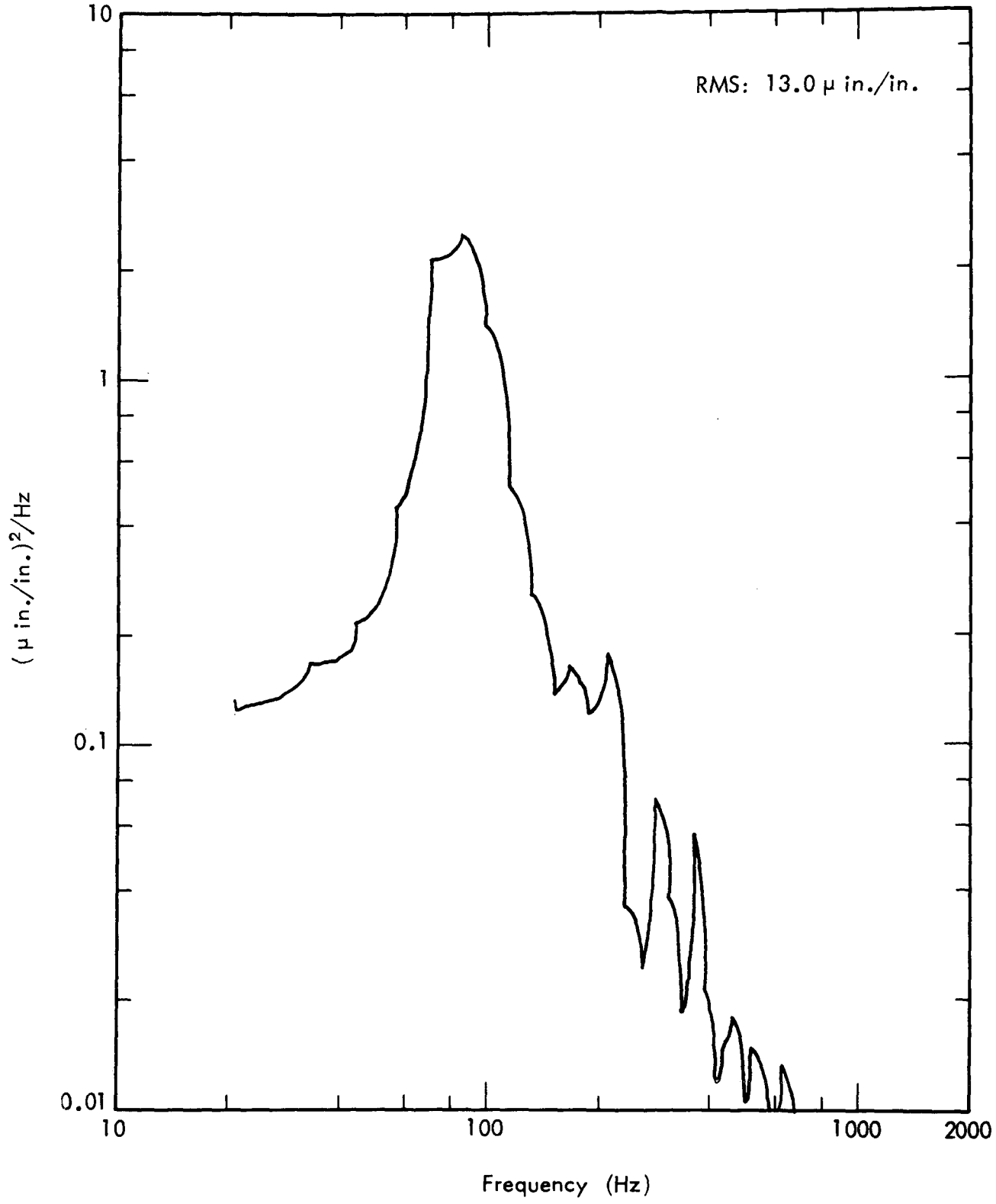

Figure 22. PSD of Strain Gage SG1 — Run 3

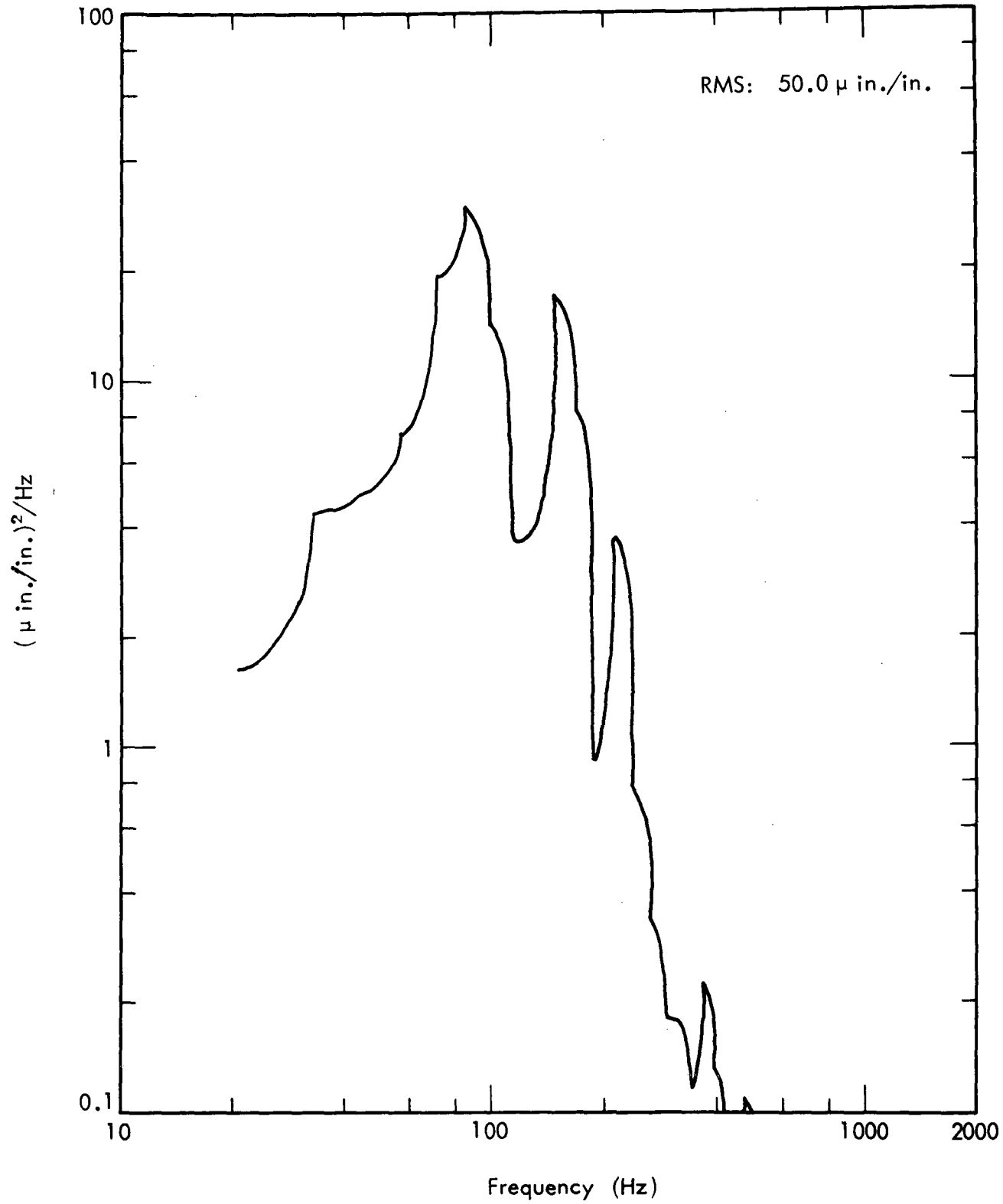

Figure 23. PSD of Strain Gage SG2 — Run 3

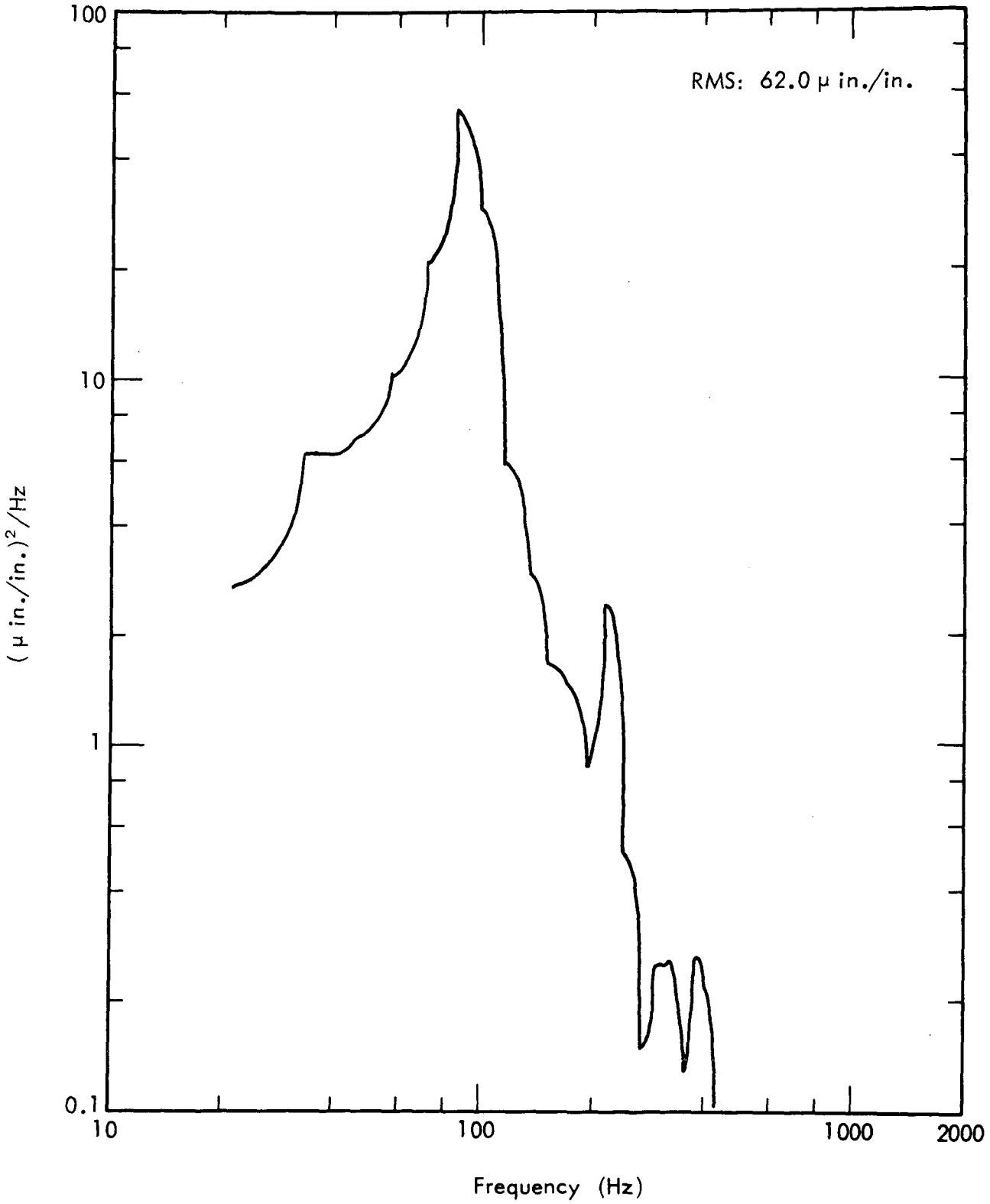

Figure 24. PSD of Strain Gage SG3 — Run 3

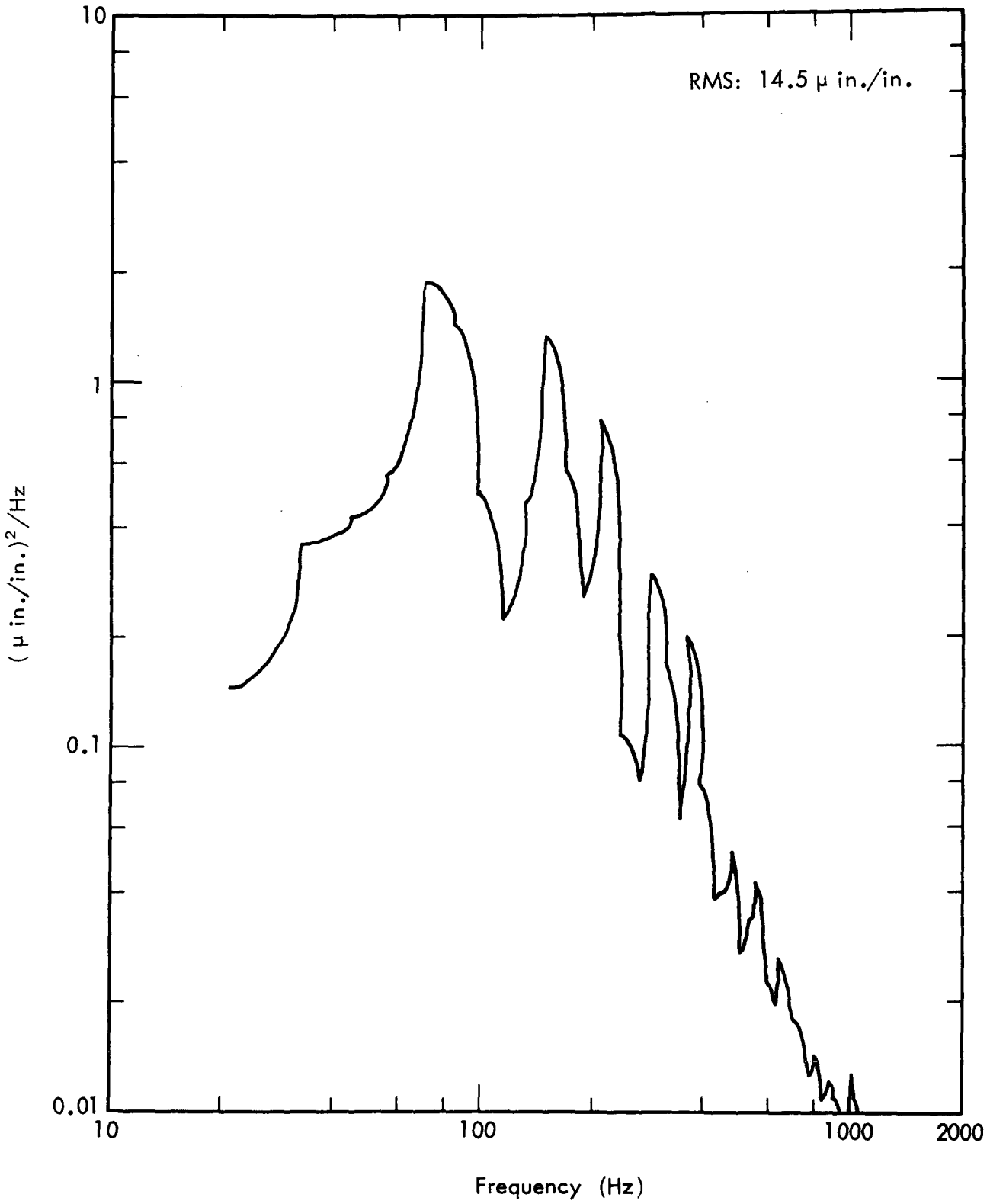

Figure 25. PSD of Strain Gage SG4 — Run 3

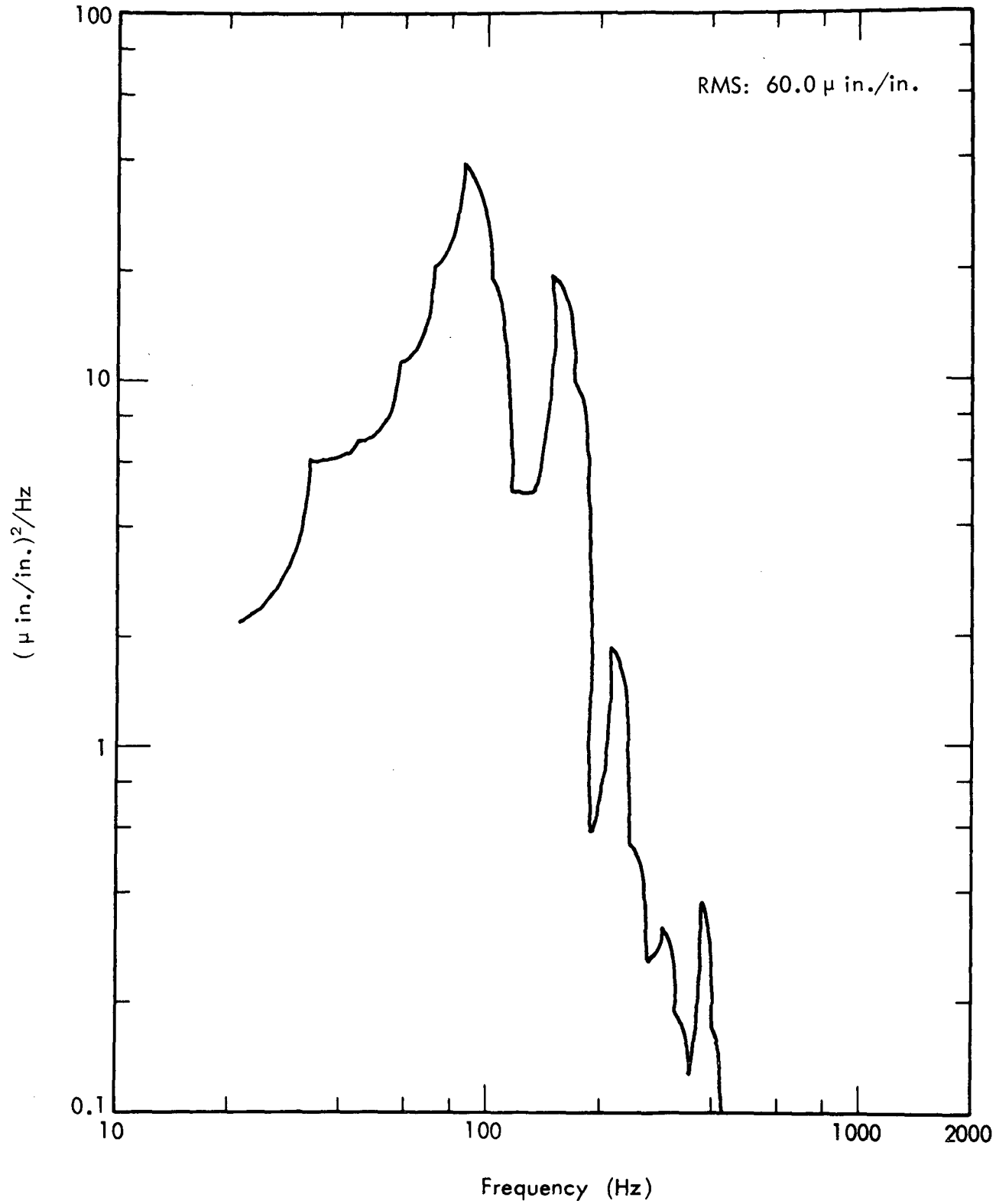

Figure 26. PSD of Strain Gage SG5 — Run 3

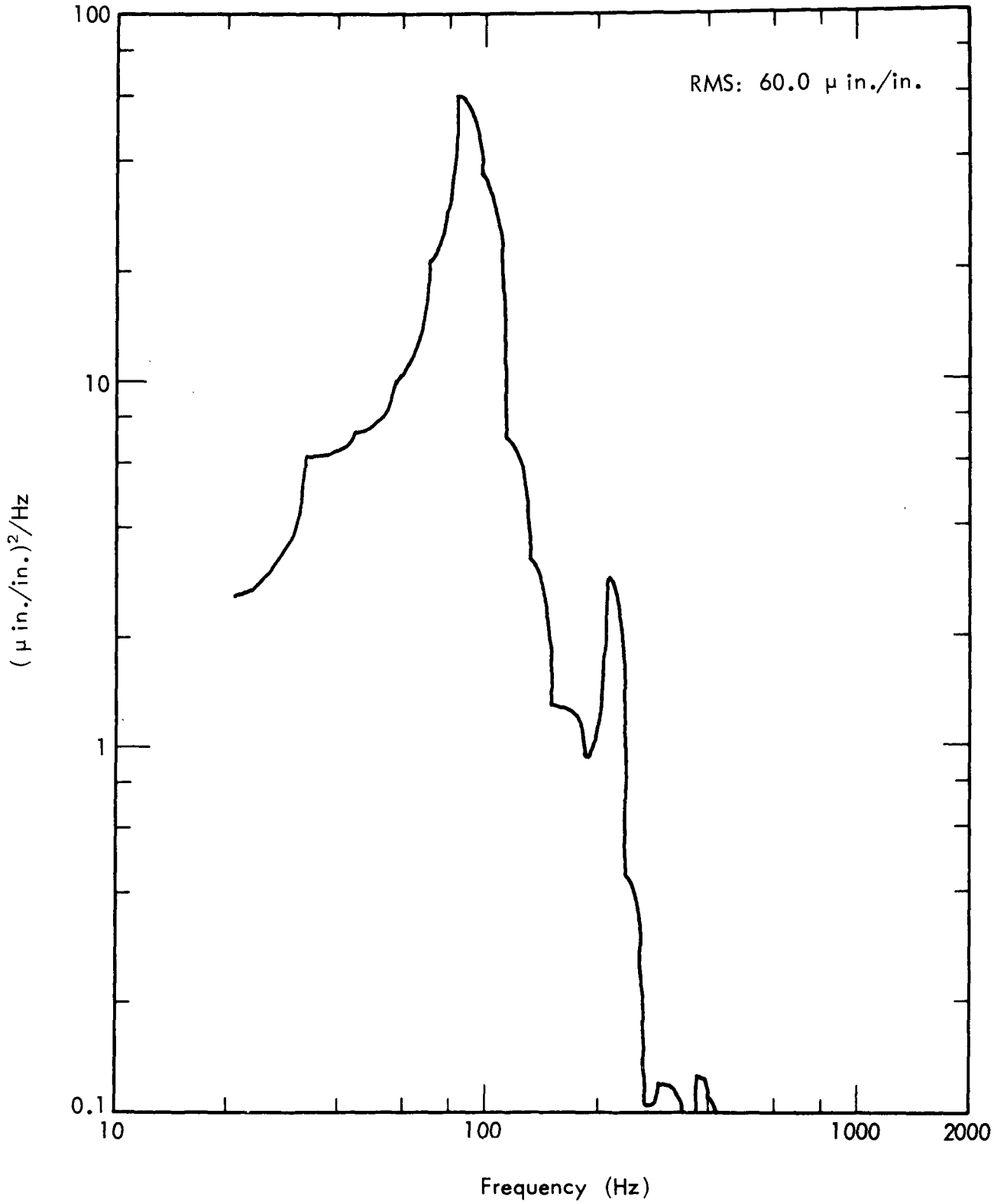

Figure 27. PSD of Strain Gage SG6 — Run 3

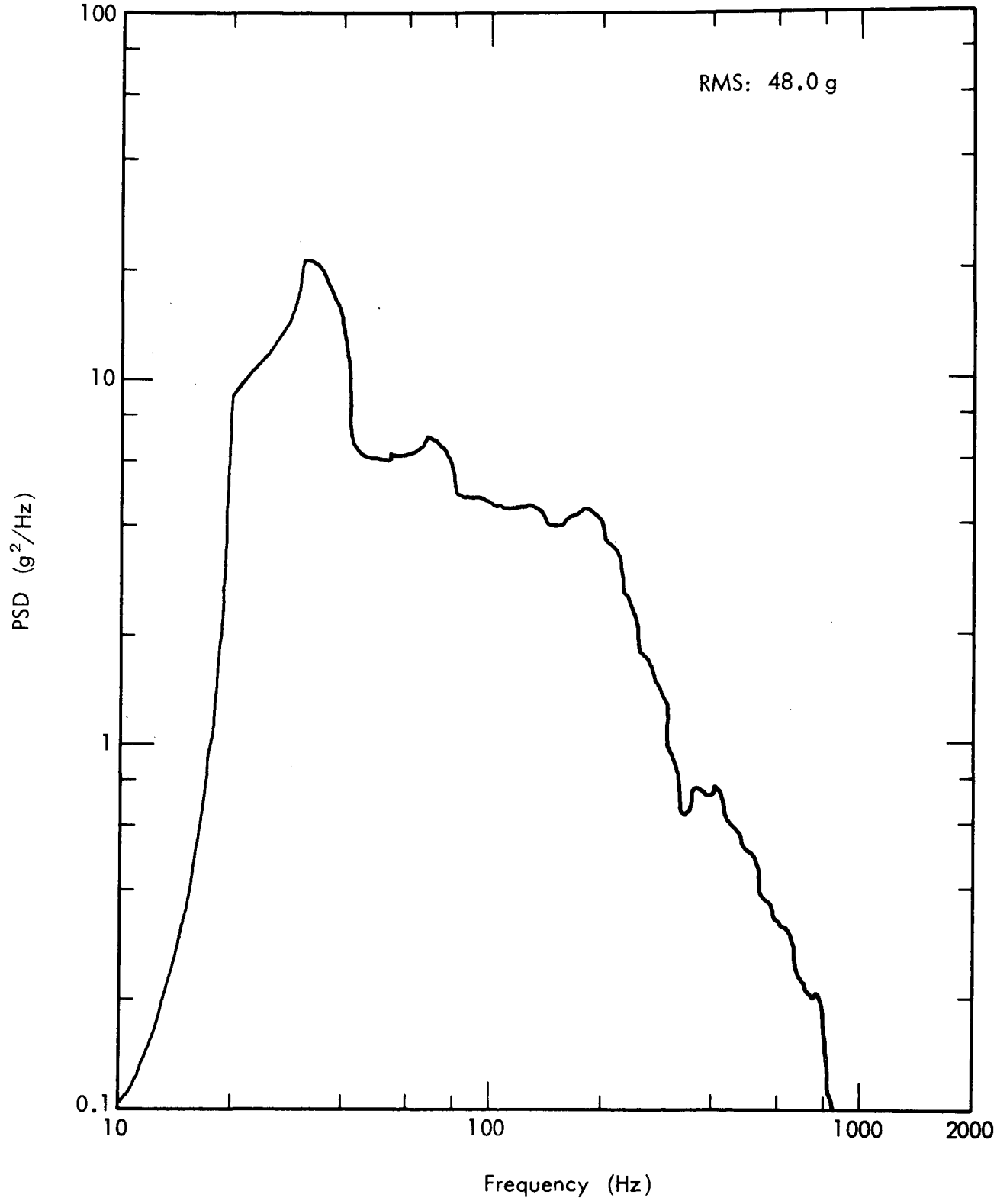

Figure 28. PSD of Accelerometer A2 — Run 10

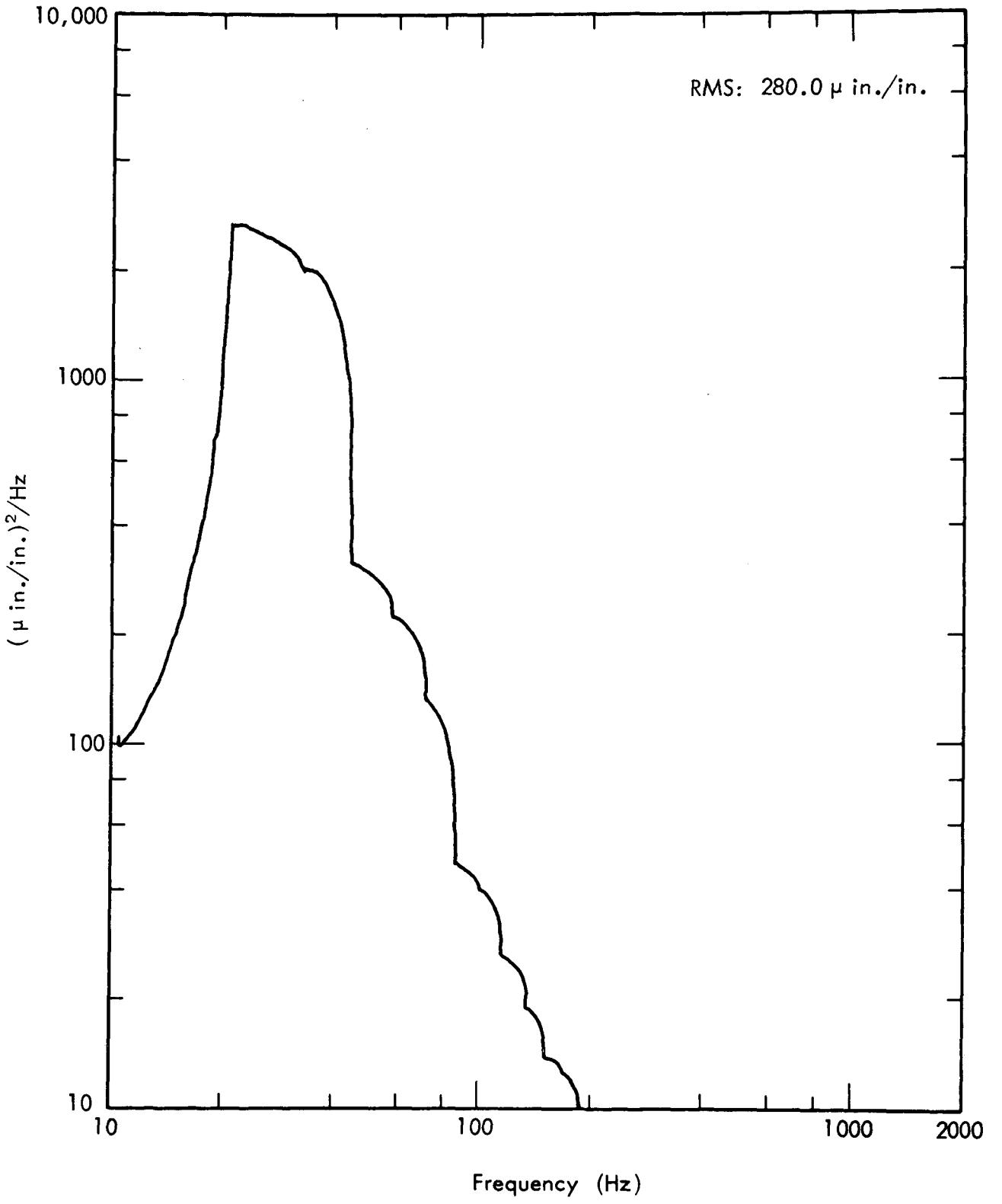

Figure 29. PSD of Strain Gage SG1 — Run 10

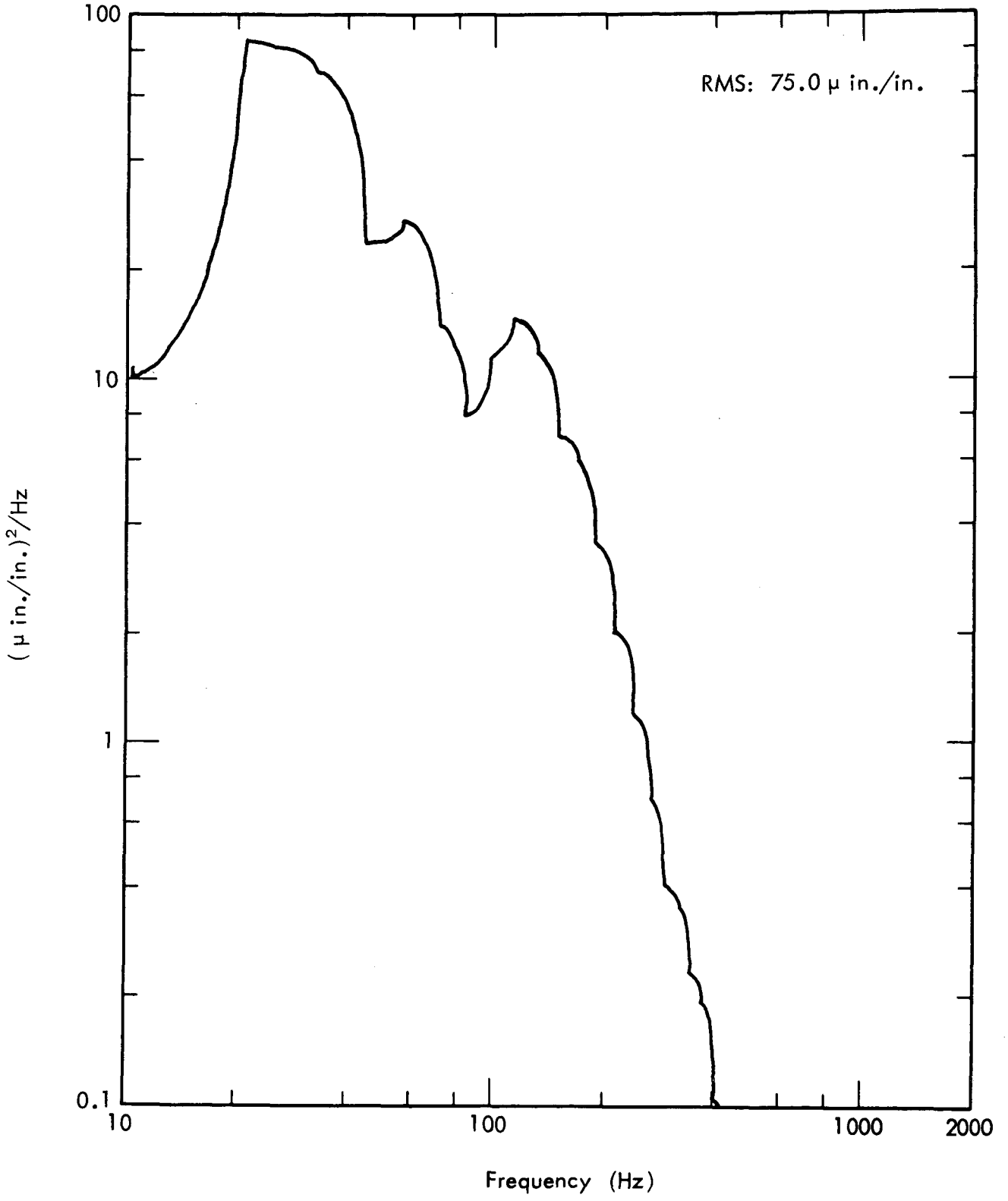

Figure 30. PSD of Strain Gage SG2 — Run 10

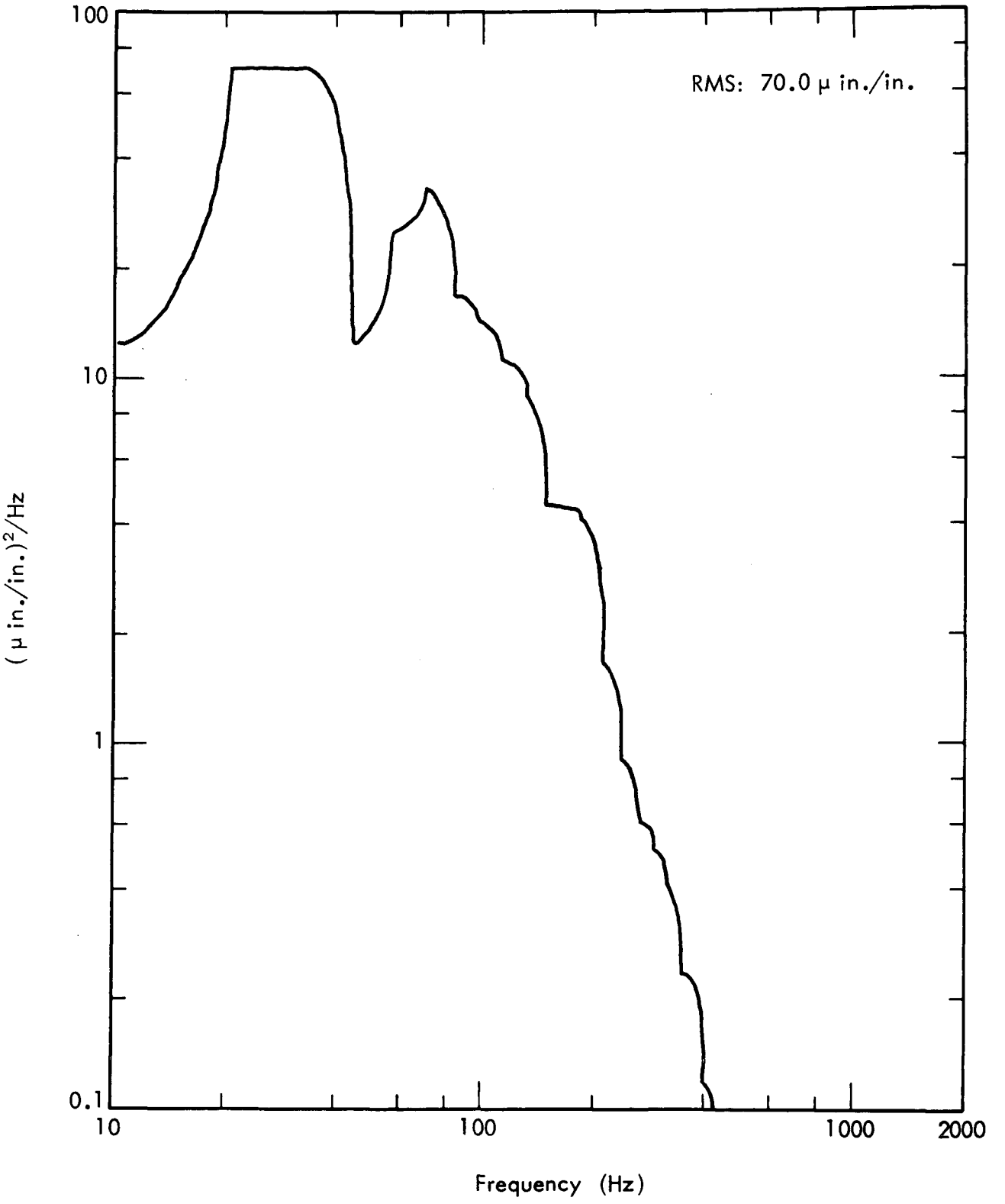

Figure 31. PSD of Strain Gage SG3 — Run 10

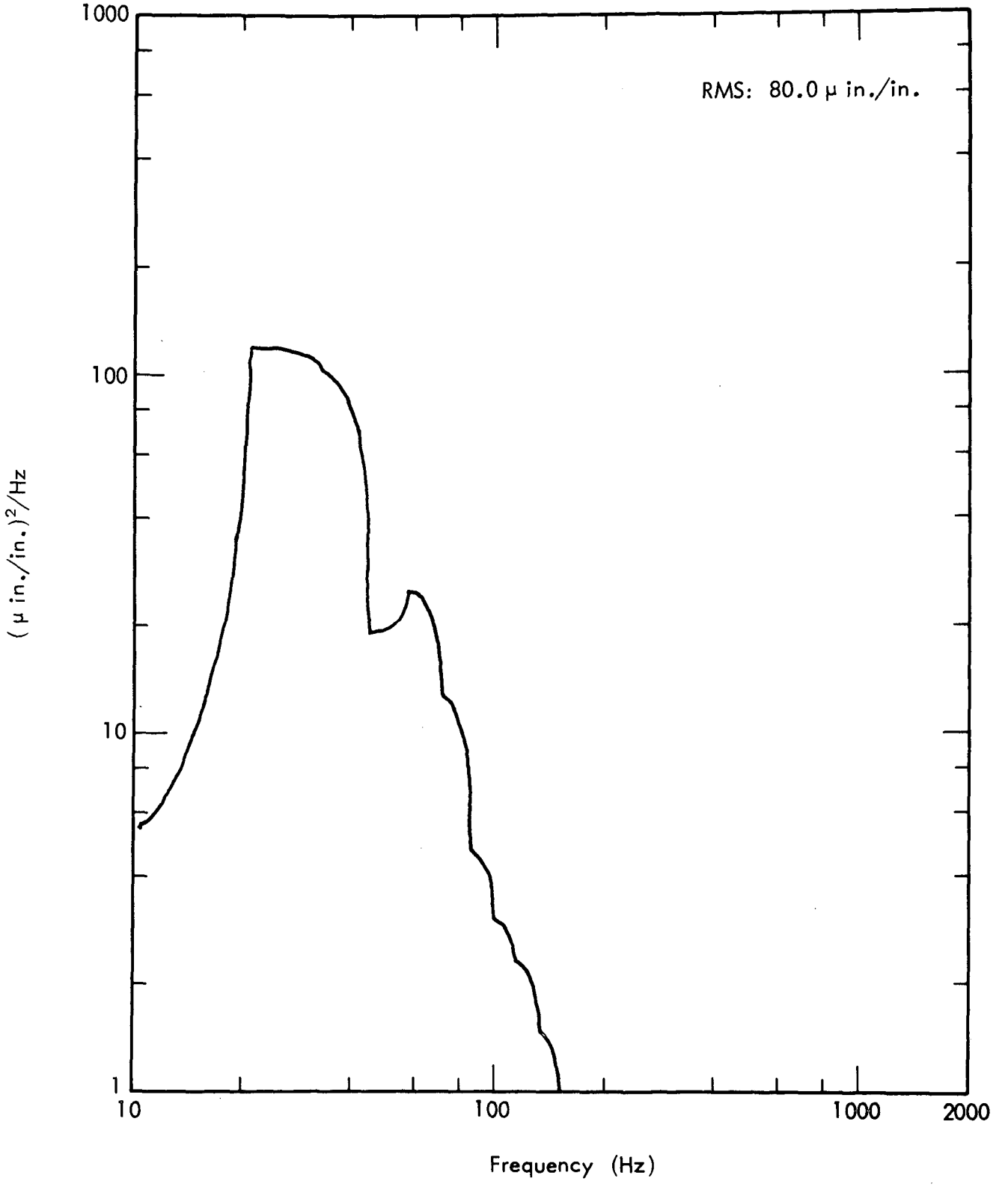

Figure 32. PSD of Strain Gage SG4 — Run 10

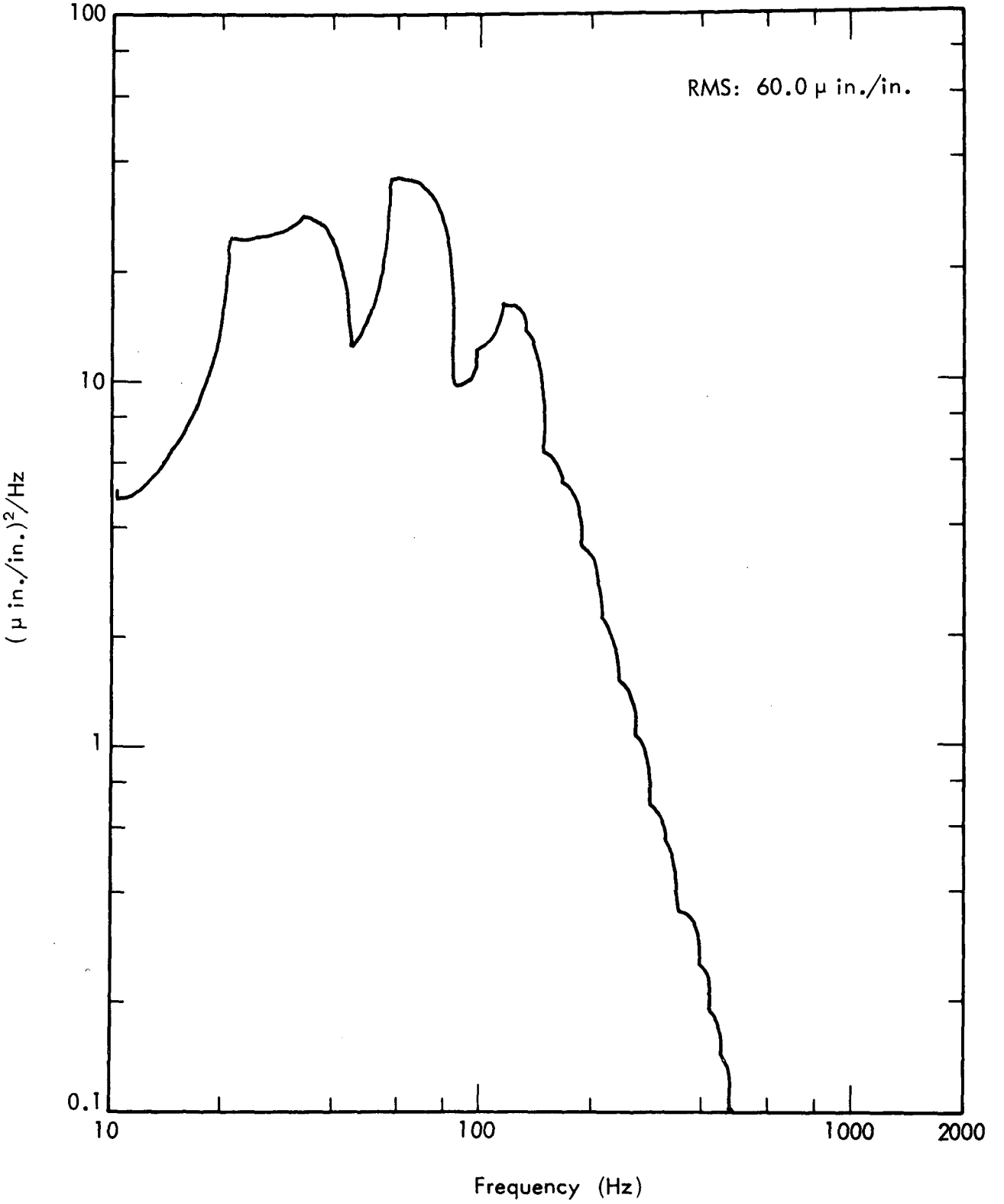

Figure 33. PSD of Strain Gage SG5 — Run 10

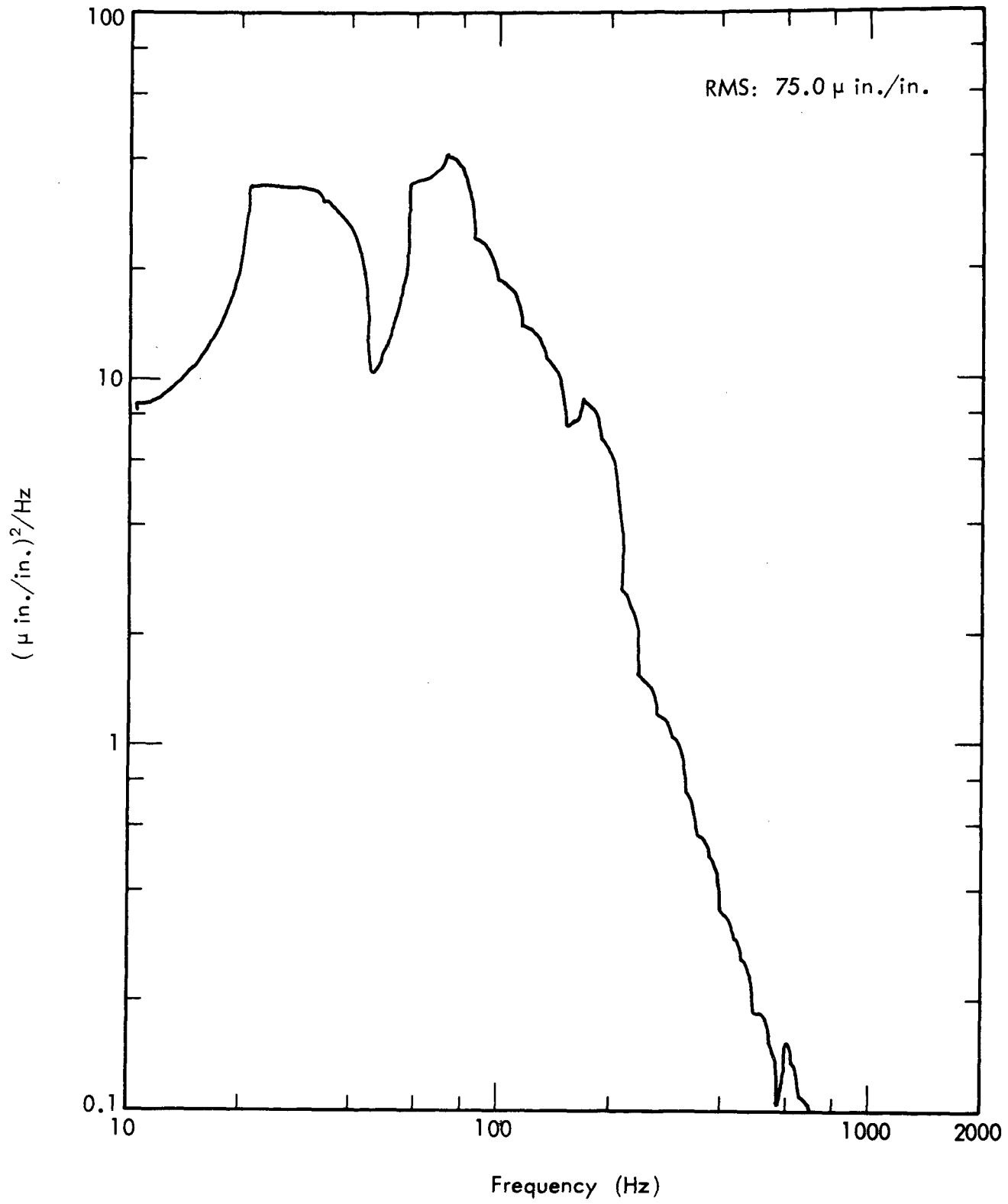

Figure 34. PSD of Strain Gage SG6 — Run 10

Figure 35. Photograph from Interior of Reverberation Room Showing Partial De-bonding Panel Edge

APPENDIX A

MICROPHONE AND ADDITIONAL RESPONSE DATA

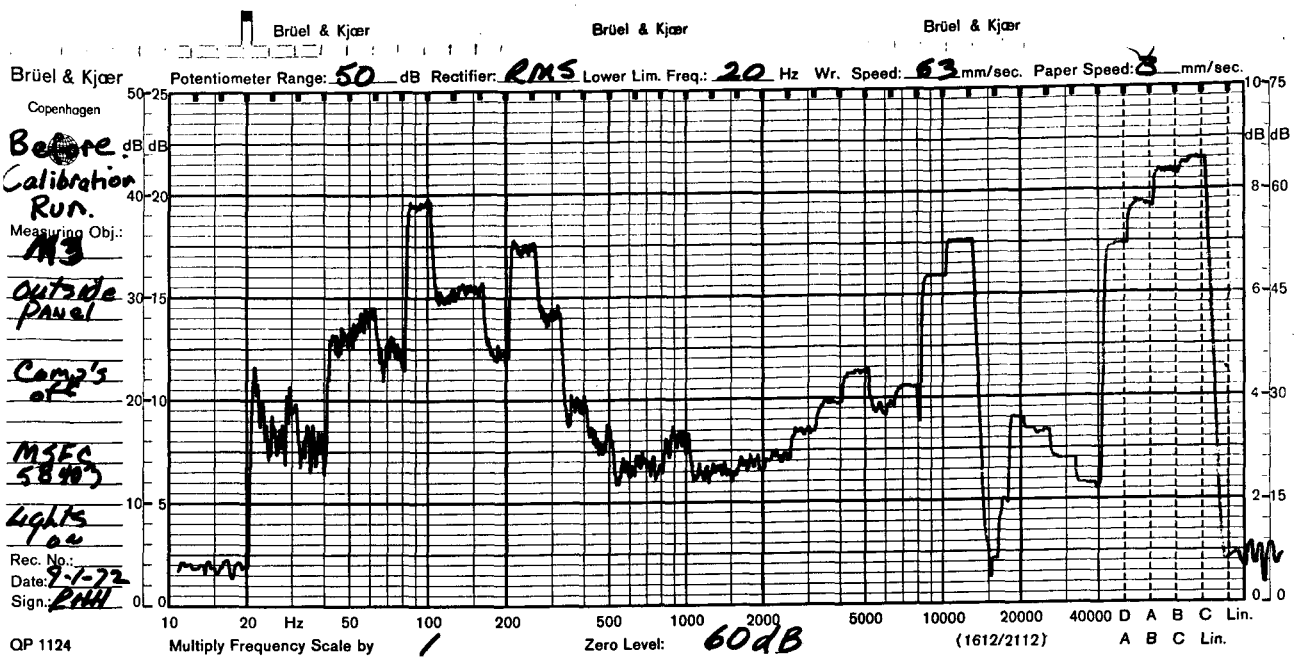

(a) Microphone M3 Prior to Calibration

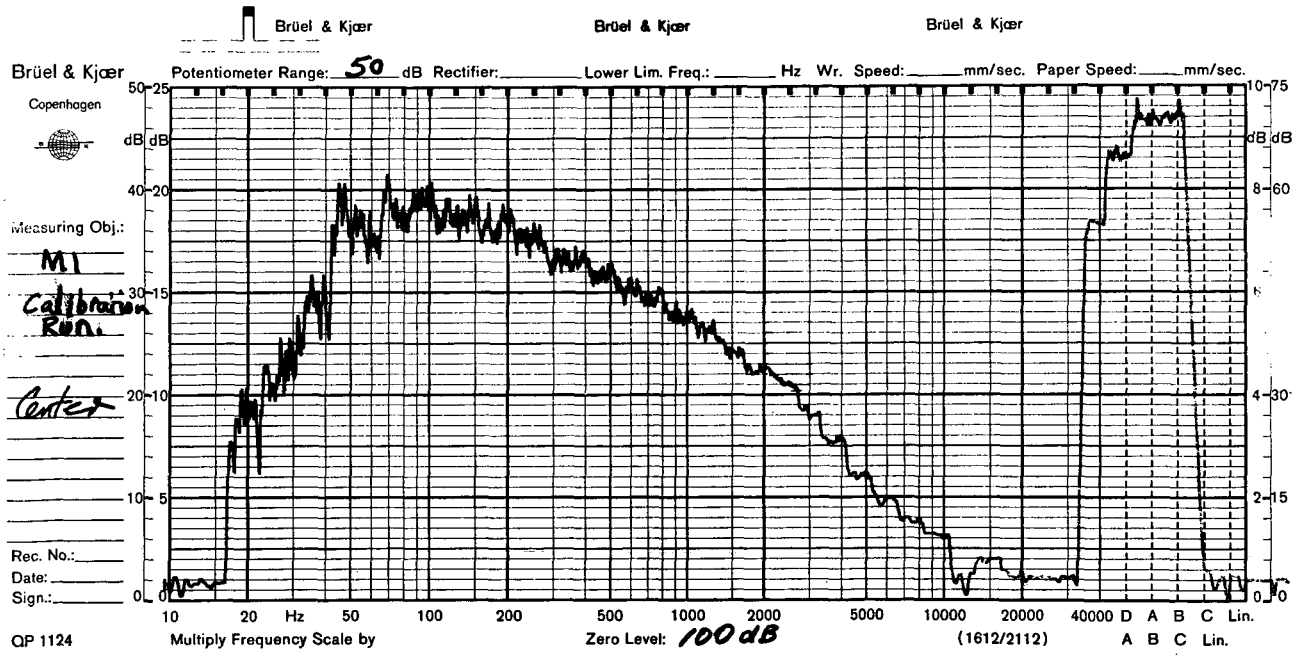

(b) Microphone M1 During Calibration

Figure A-1. Sound Pressure Levels During Facility Calibration

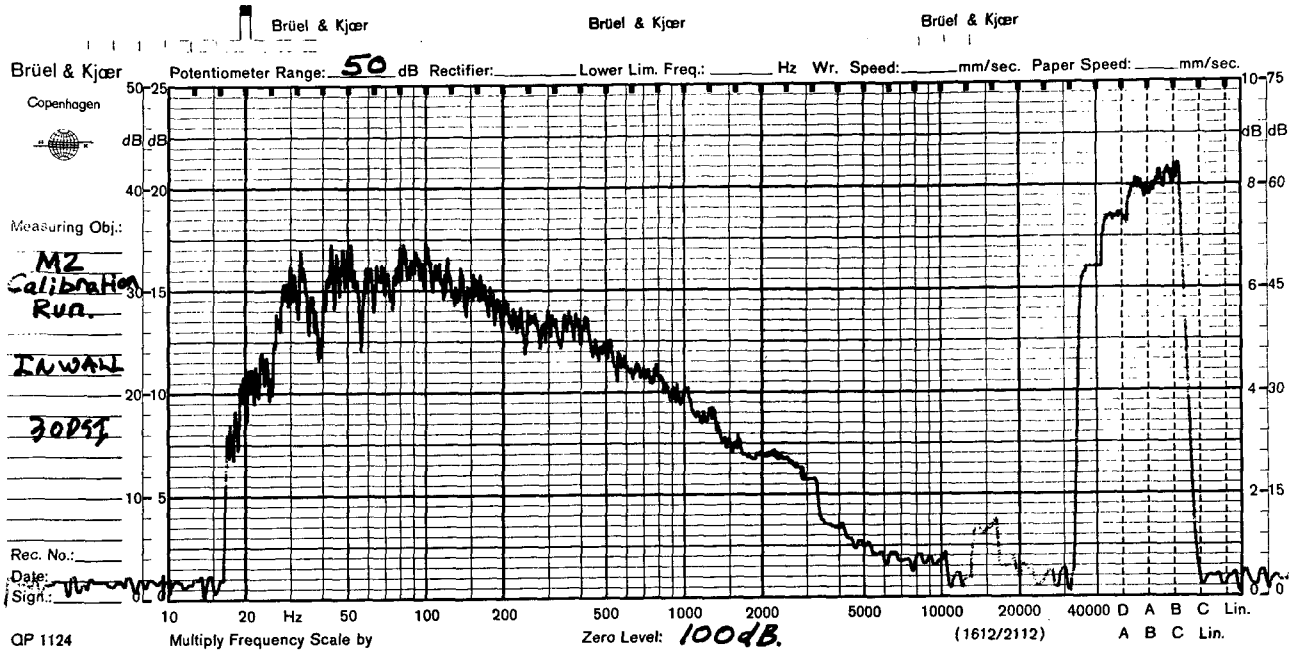

(c) Microphone M2 During Calibration

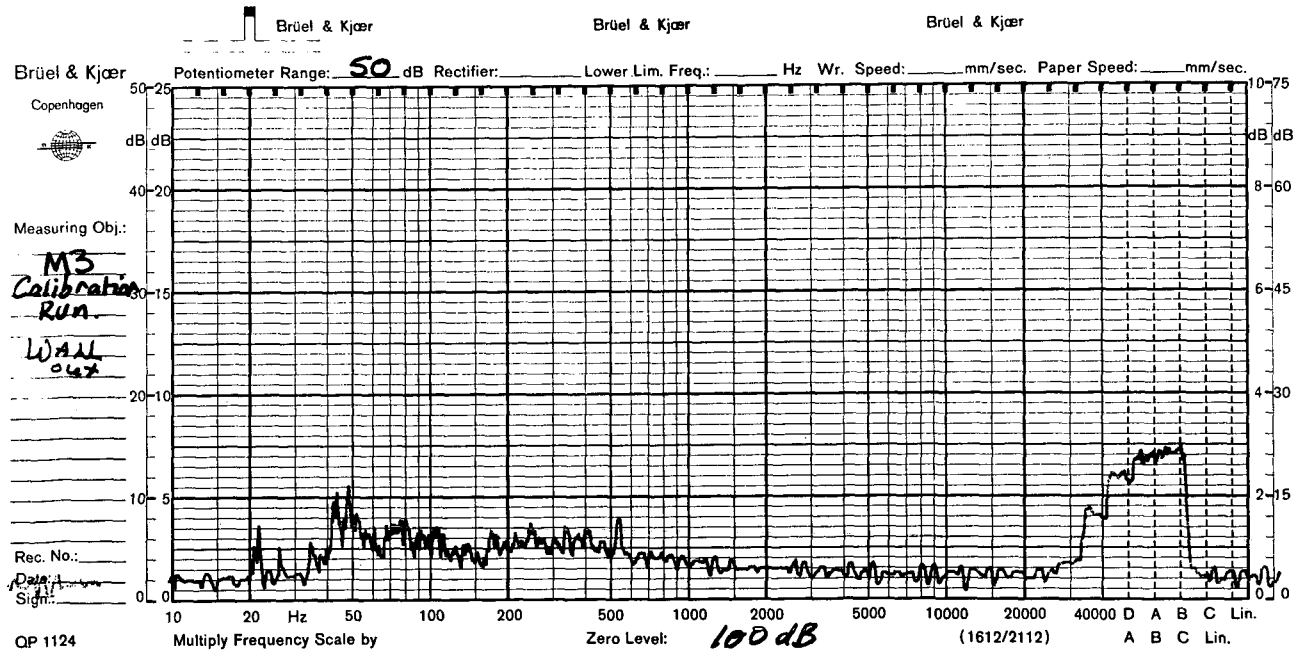

(d) Microphone M3 During Calibration

Figure A-1. (Concluded)

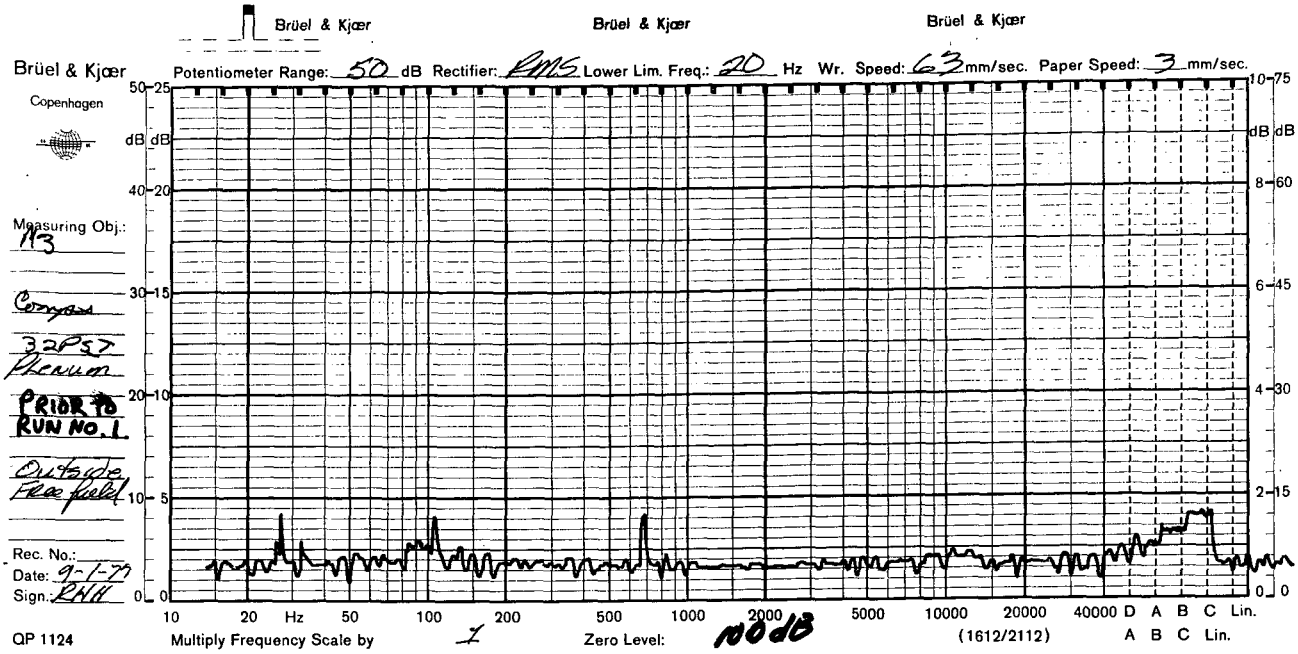

(a) Microphone M3 Prior to Test Run

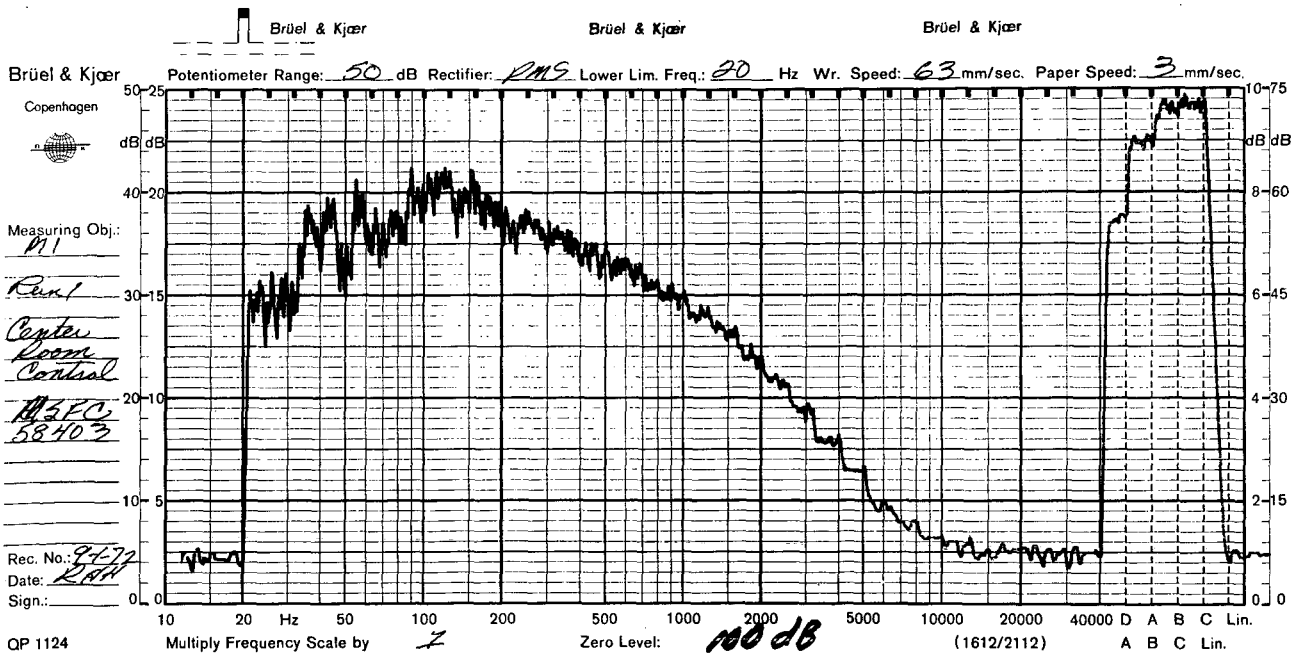

(b) Microphone M1 During Test Run

Figure A-2. Sound Pressure Levels During Acoustic Test Run Number 1

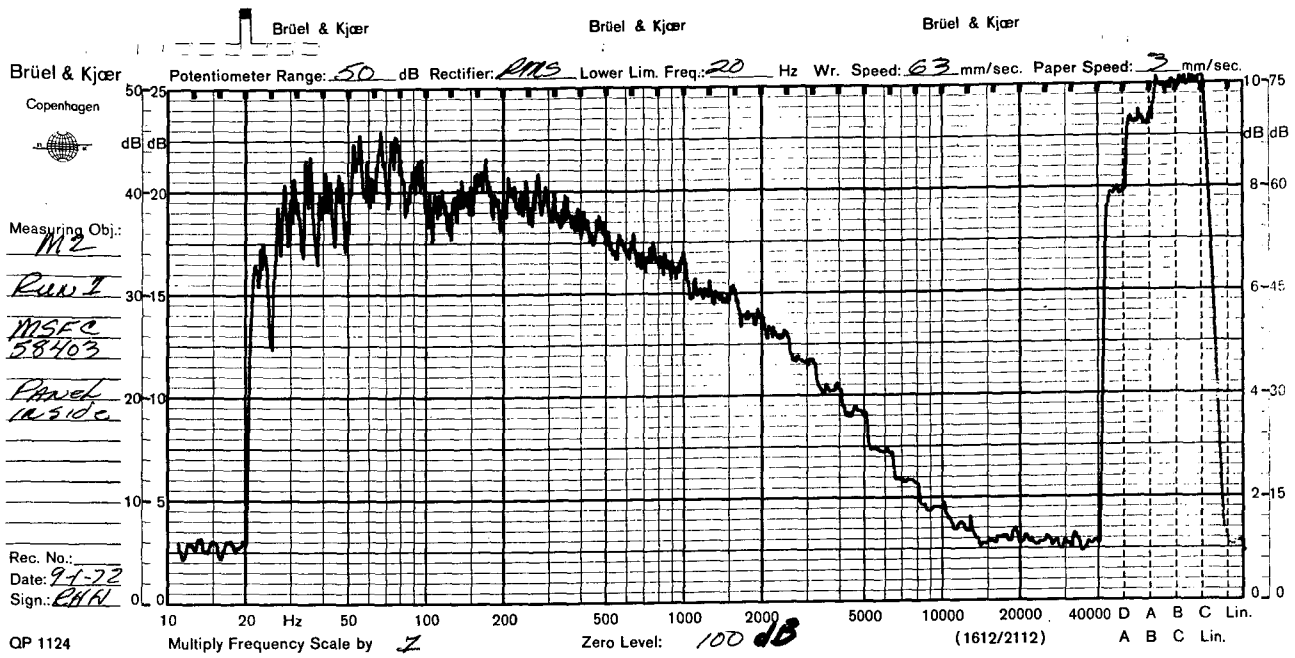

(c) Microphone M2 During Test Run

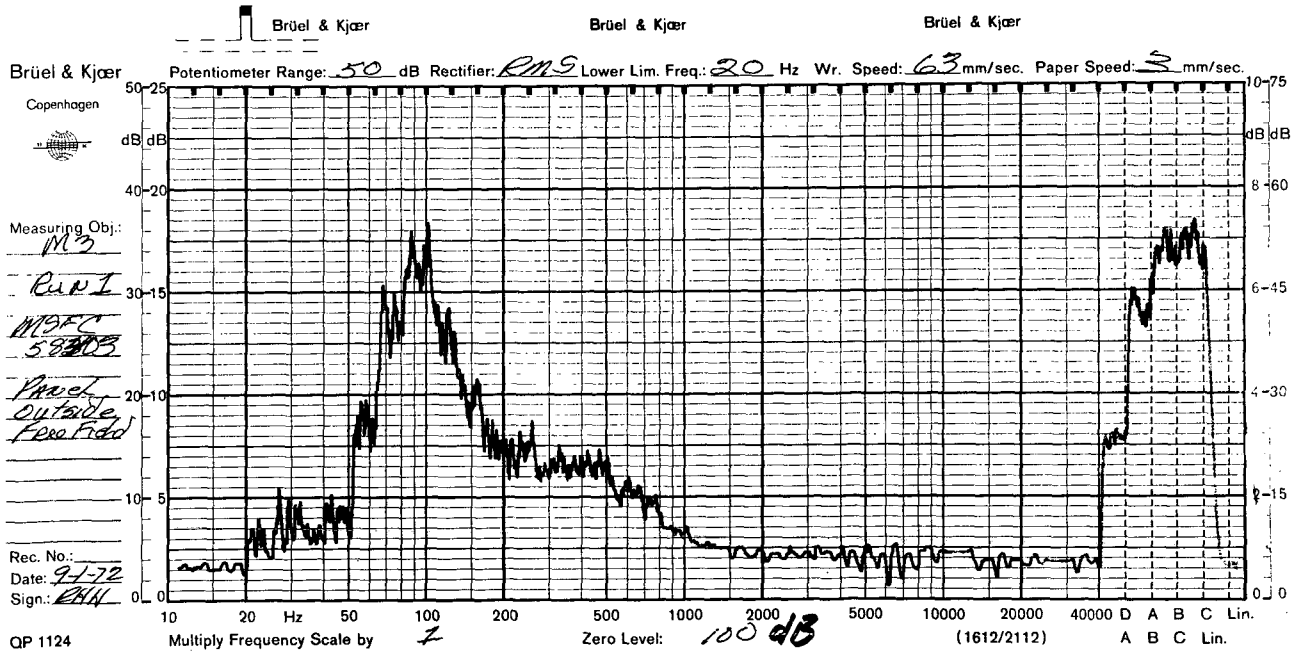

(d) Microphone M3 During Test Run

Figure A-2. (Concluded)

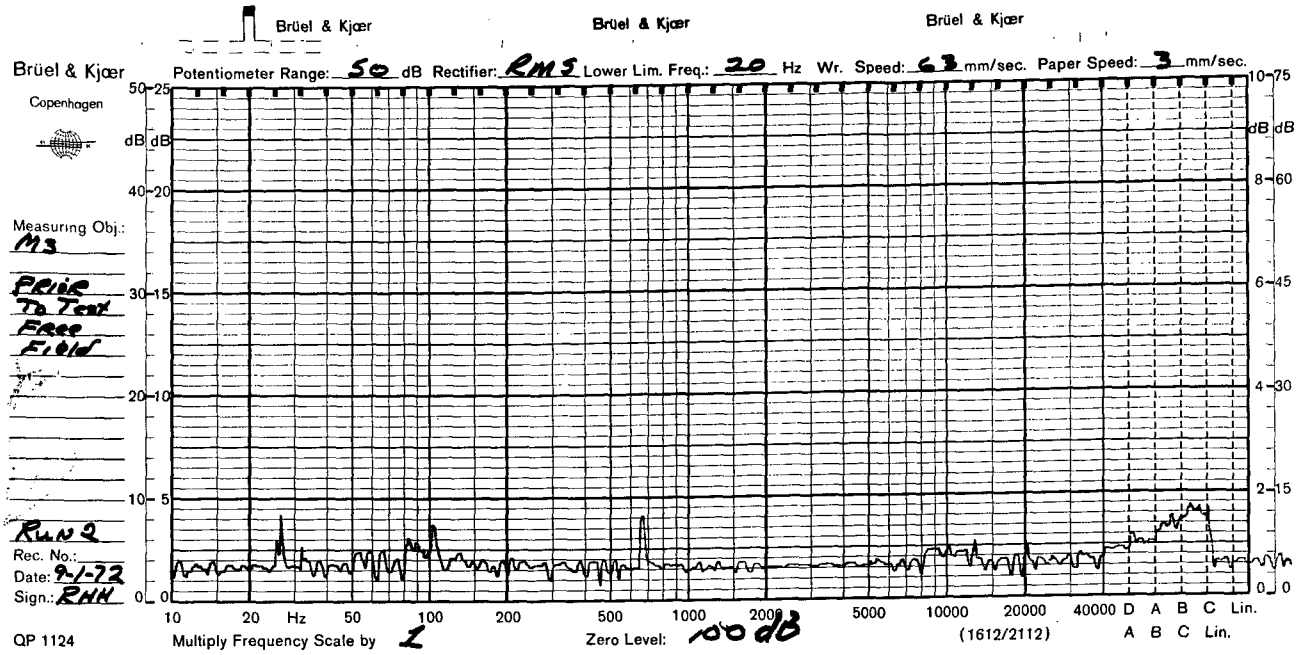

(a) Microphone M3 Prior to Test Run

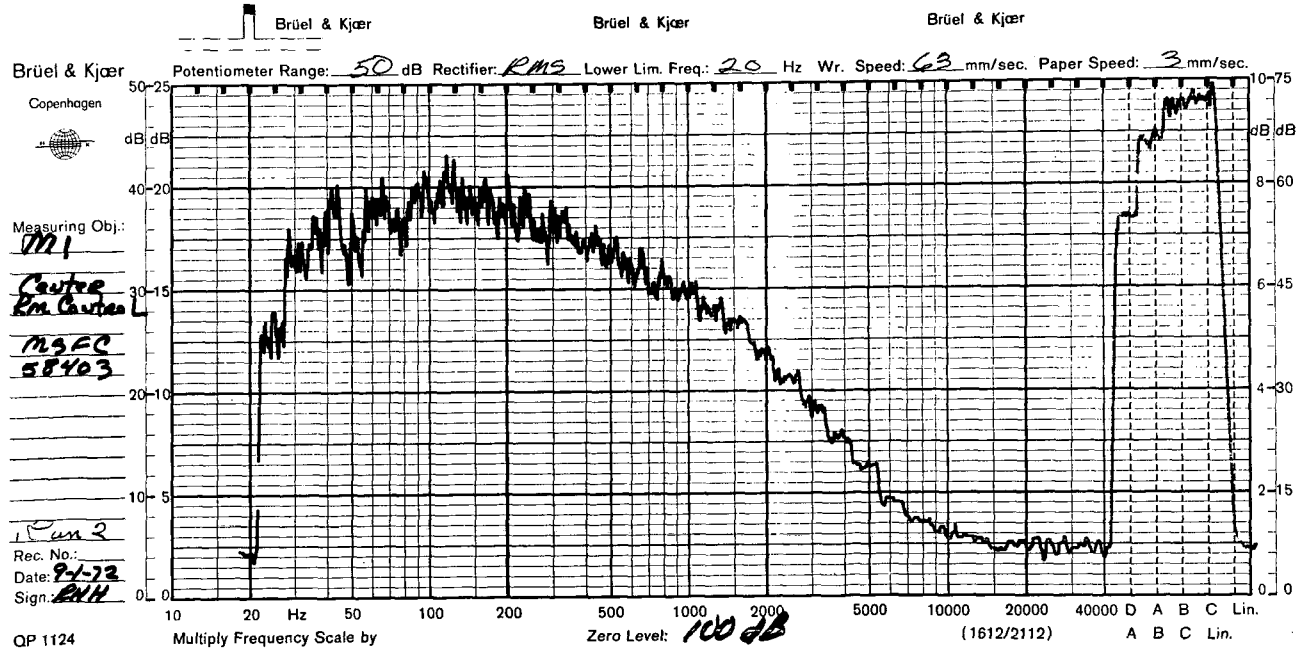

(b) Microphone M1 During Test Run

Figure A-3. Sound Pressure Levels During Acoustic Test Run Number 2

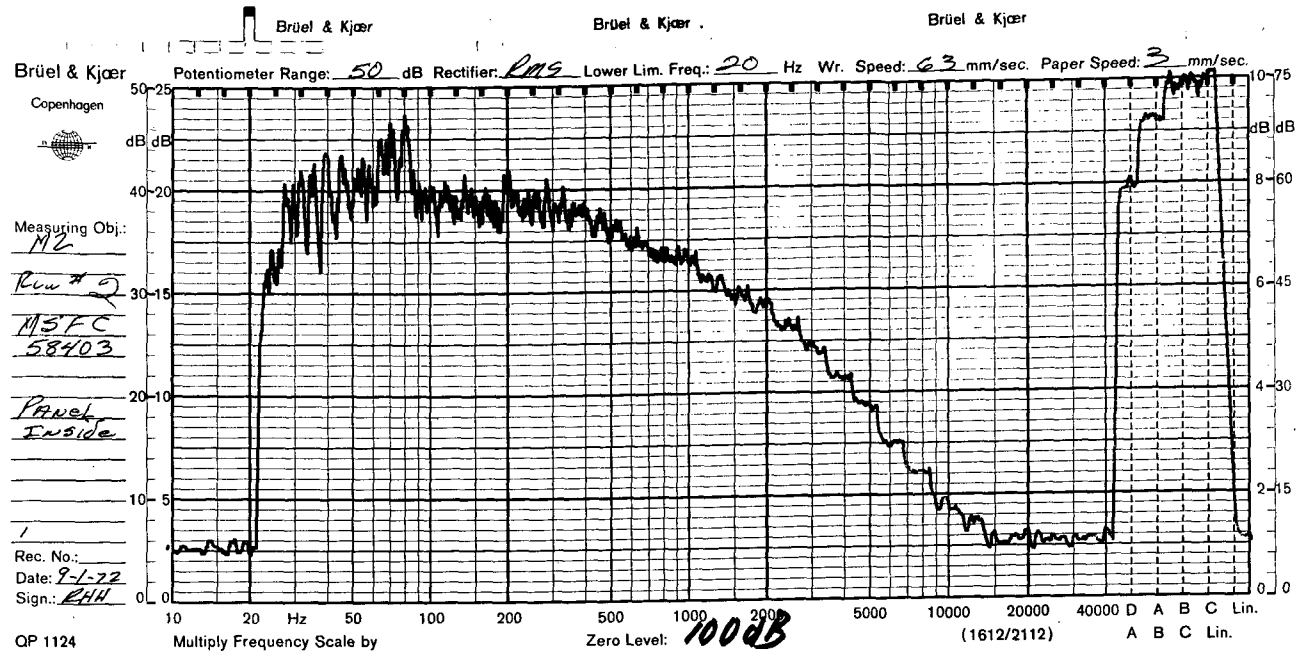

(c) Microphone M2 During Test Run

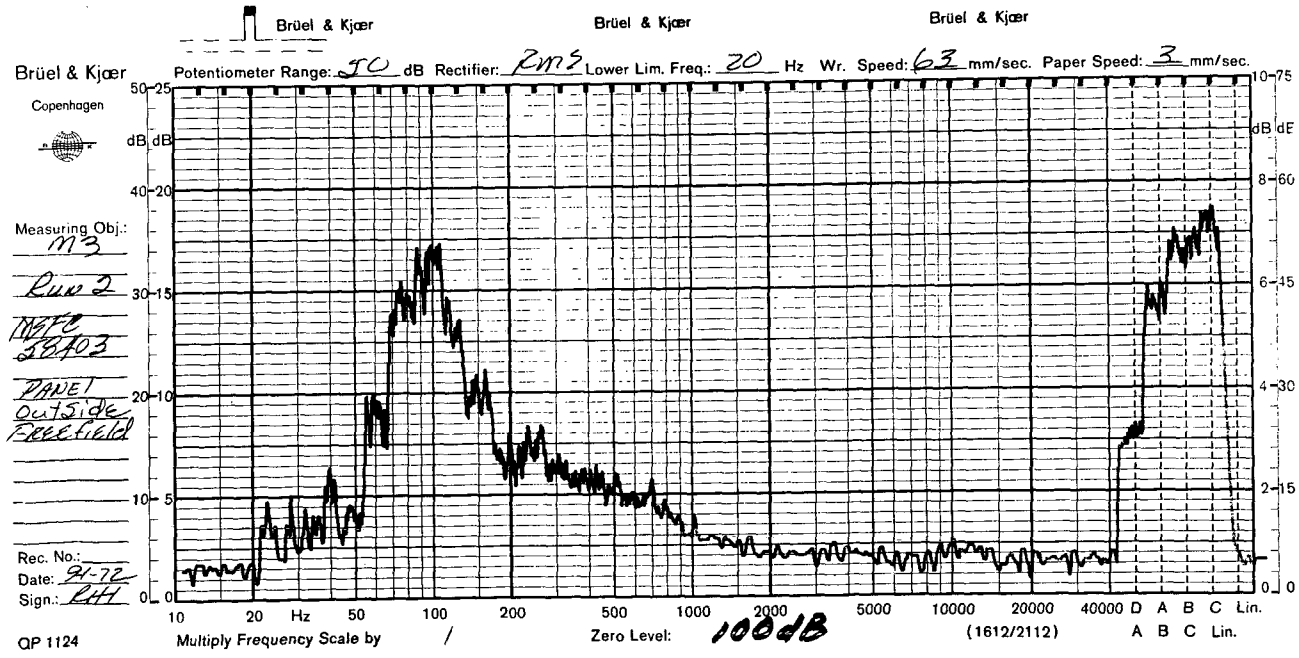

(d) Microphone M3 During Test Run

Figure A-3. (Concluded)

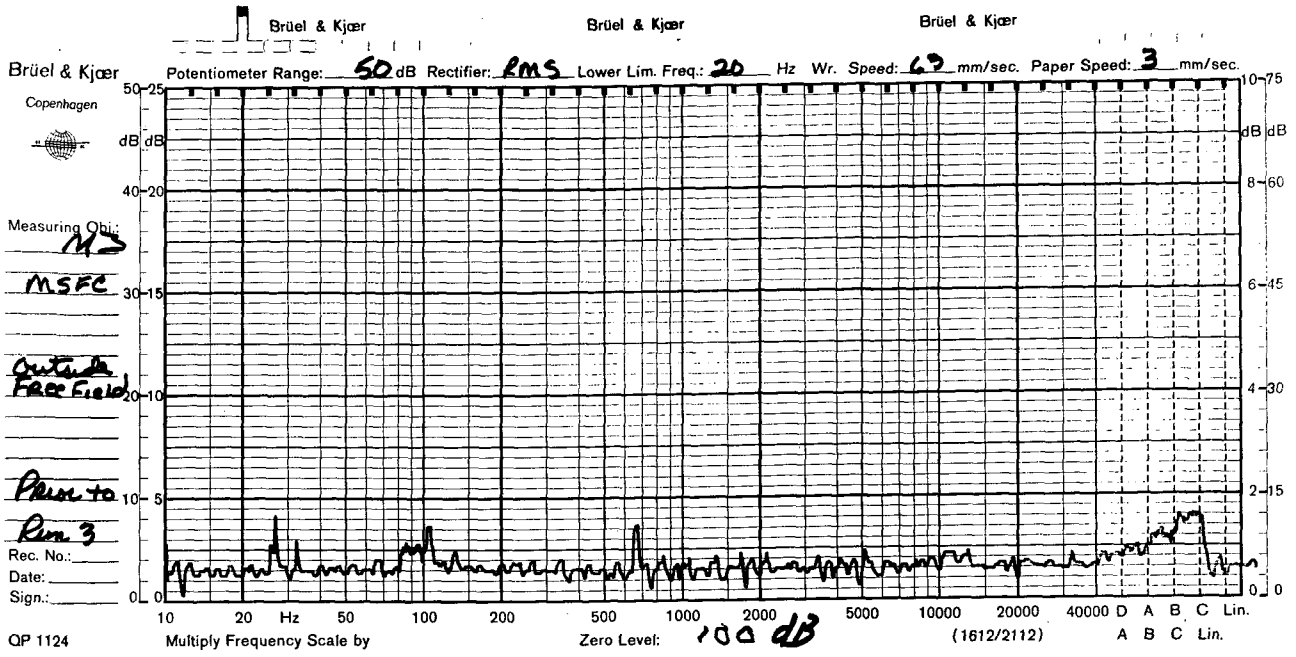

(a) Microphone M3 Prior to Test Run

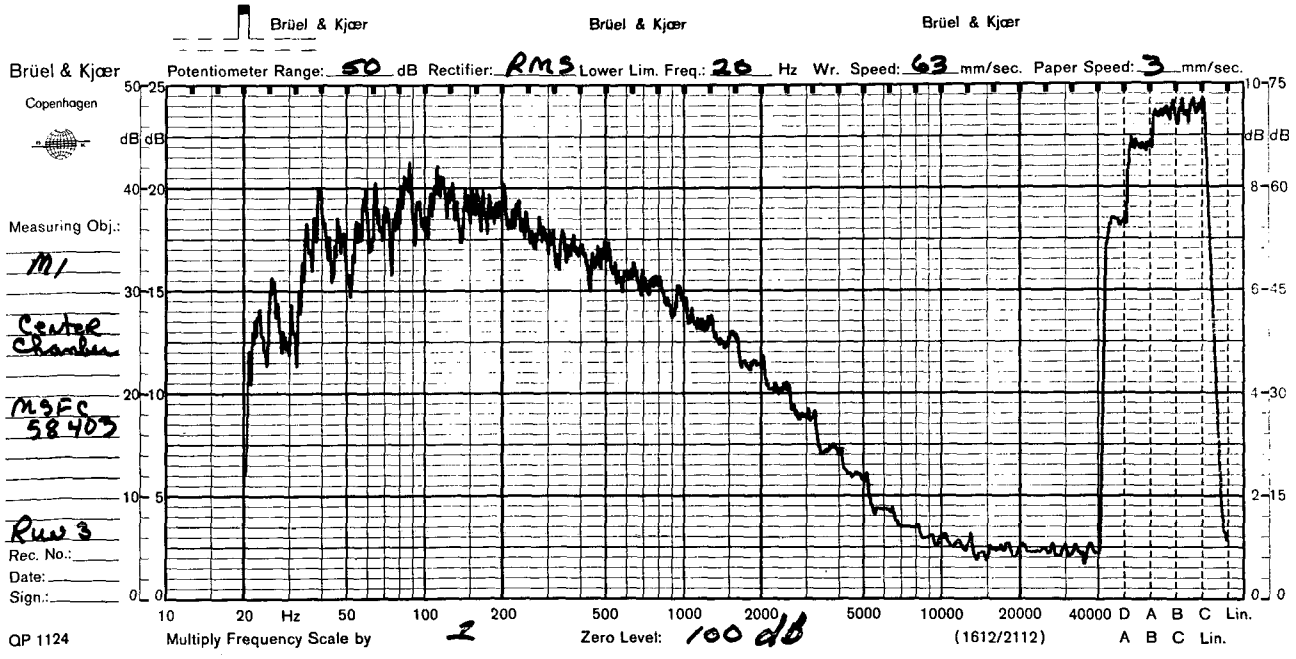

(b) Microphone M1 During Test Run

Figure A-4. Sound Pressure Levels During Acoustic Test Run Number 3

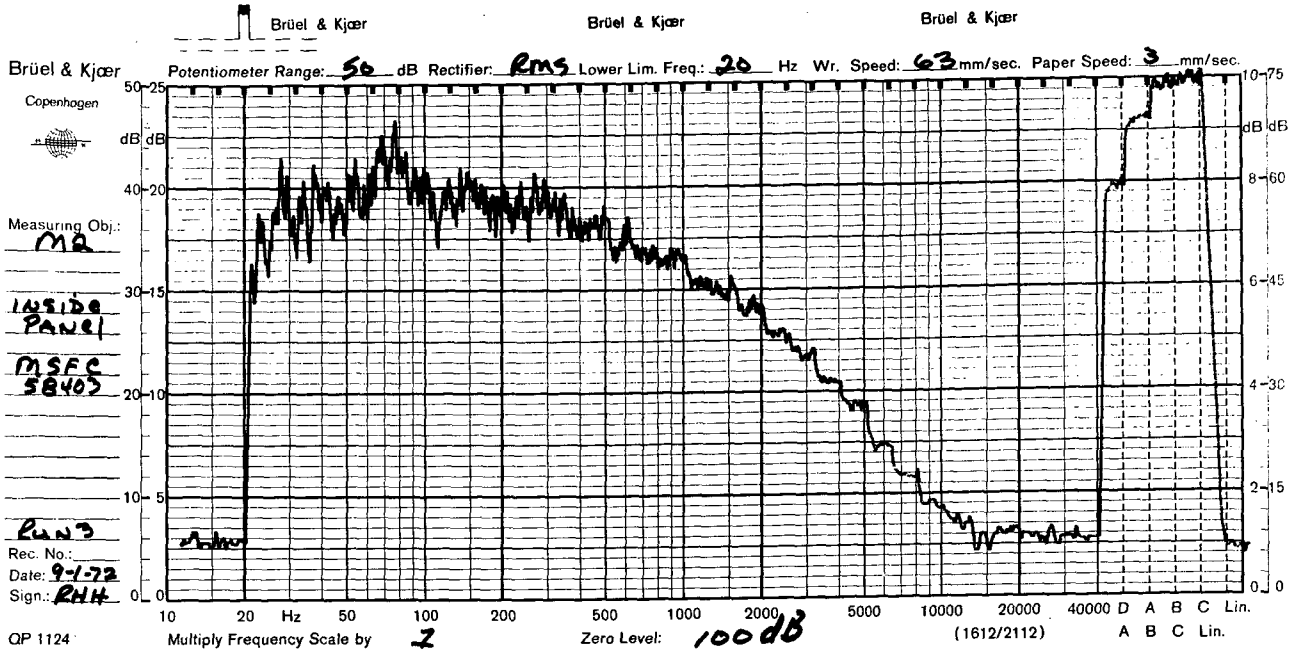

(c) Microphone M2 During Test Run

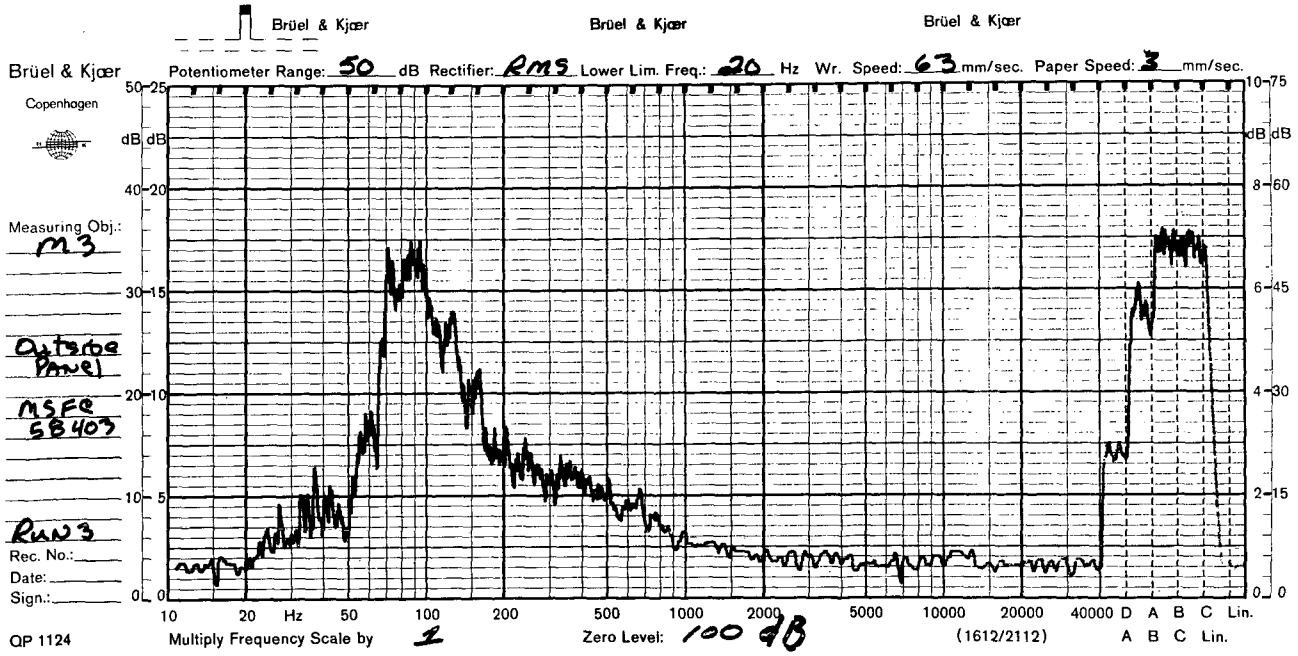

(d) Microphone M3 During Test Run

Figure A-4. (Concluded)

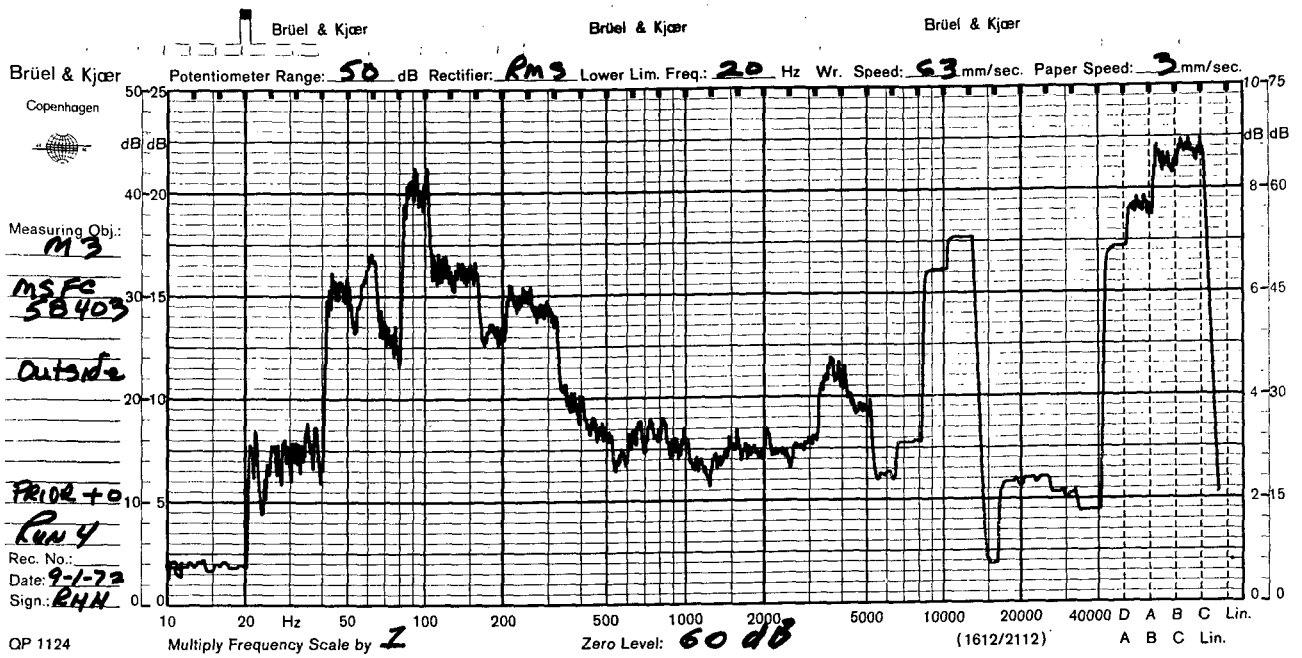

(a) Microphone M3 Prior to Test Run

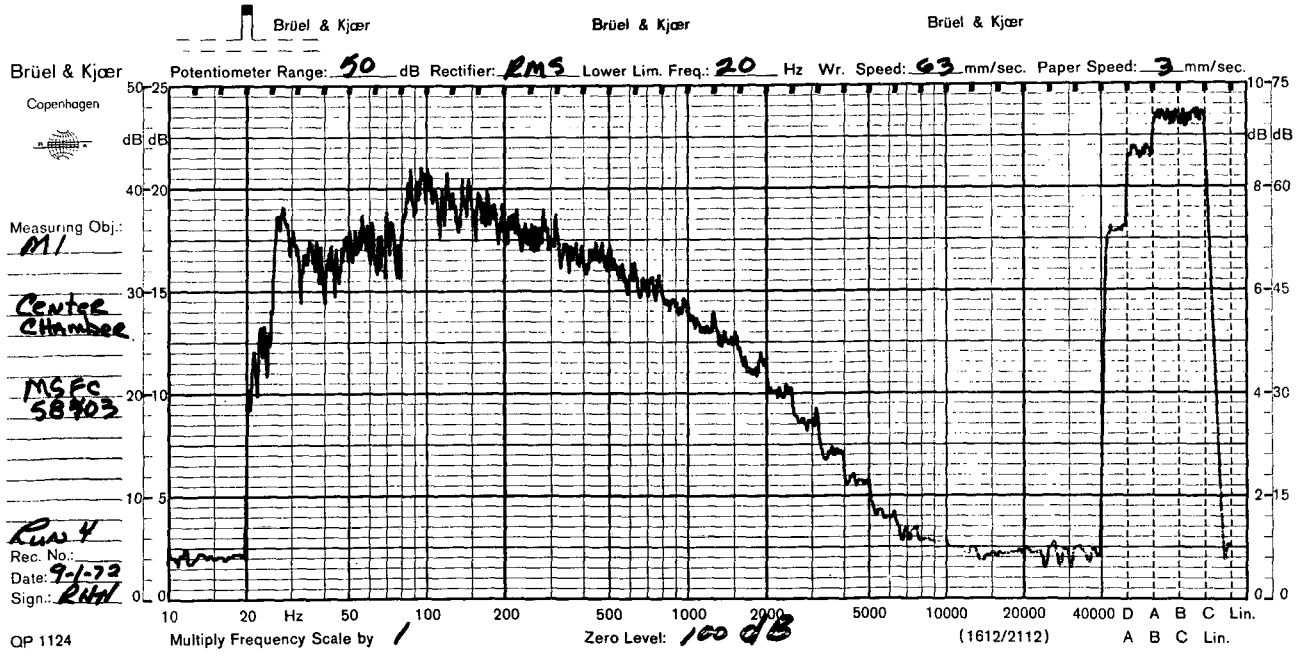

(b) Microphone M1 During Test Run

Figure A-5. Sound Pressure Levels During Acoustic Test Run Number 4

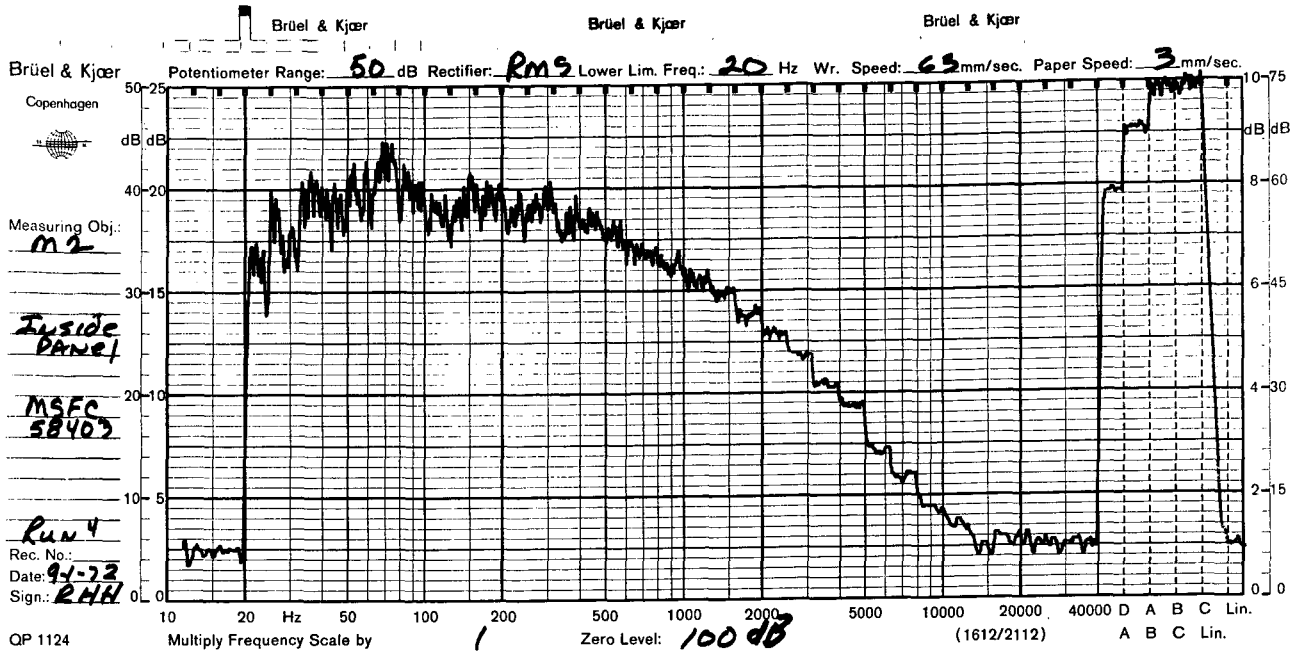

(c) Microphone M2 During Test Run

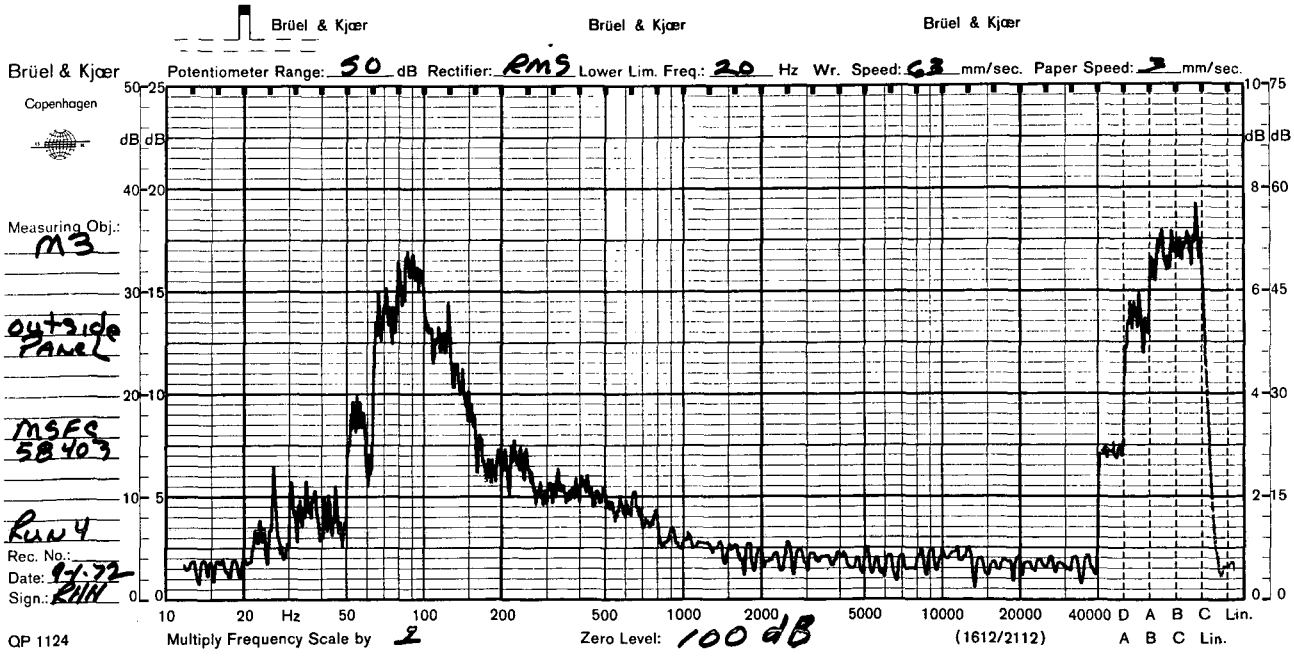

(d) Microphone M3 During Test Run

Figure A-5. (Concluded)

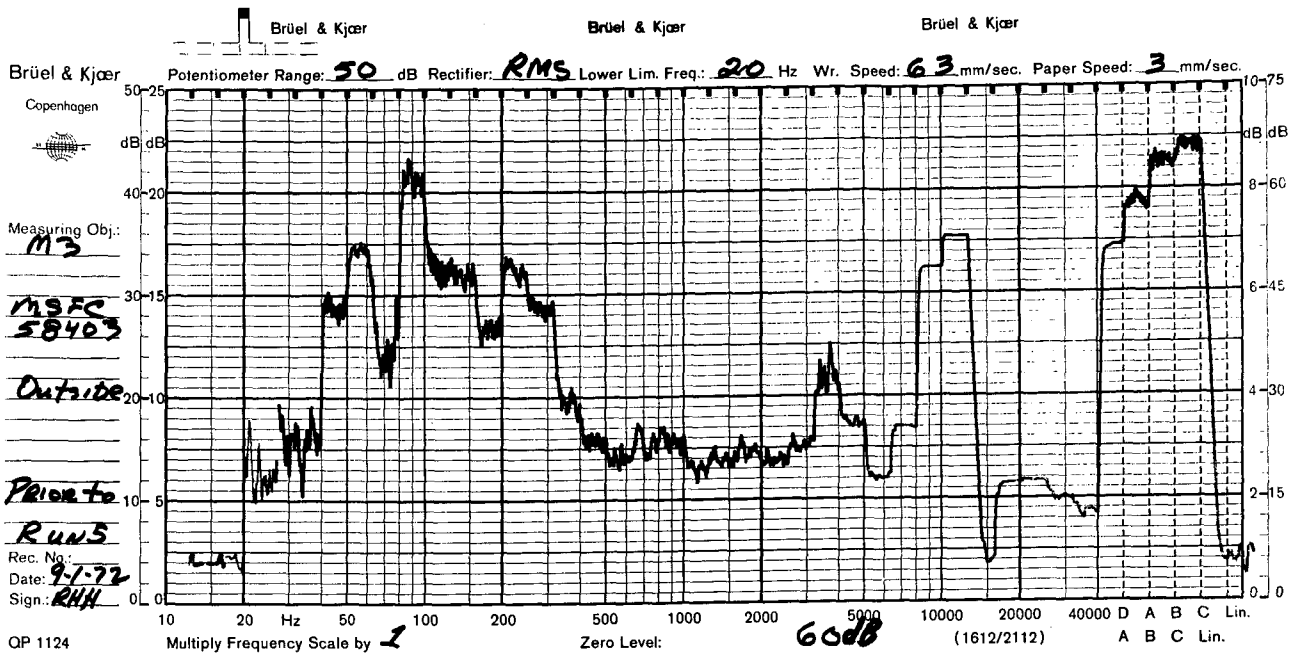

(a) Microphone M3 Prior to Test Run

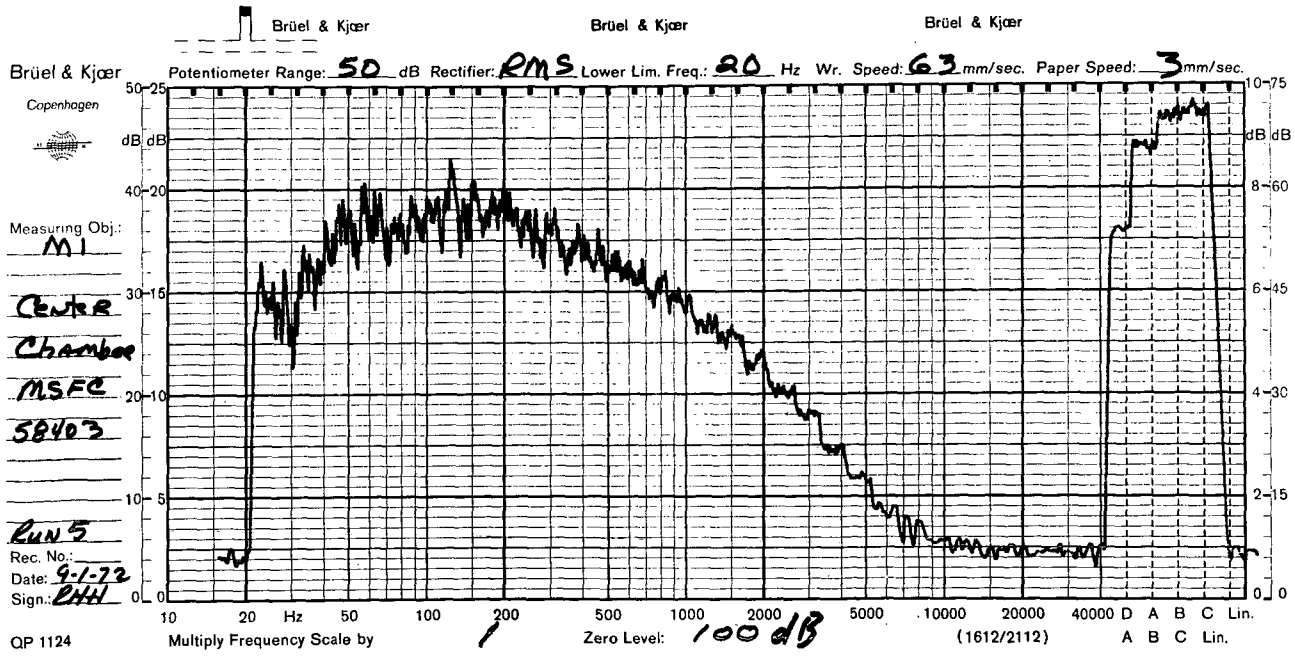

(b) Microphone M1 During Test Run

Figure A-6. Sound Pressure Levels During Acoustic Test Run Number 5

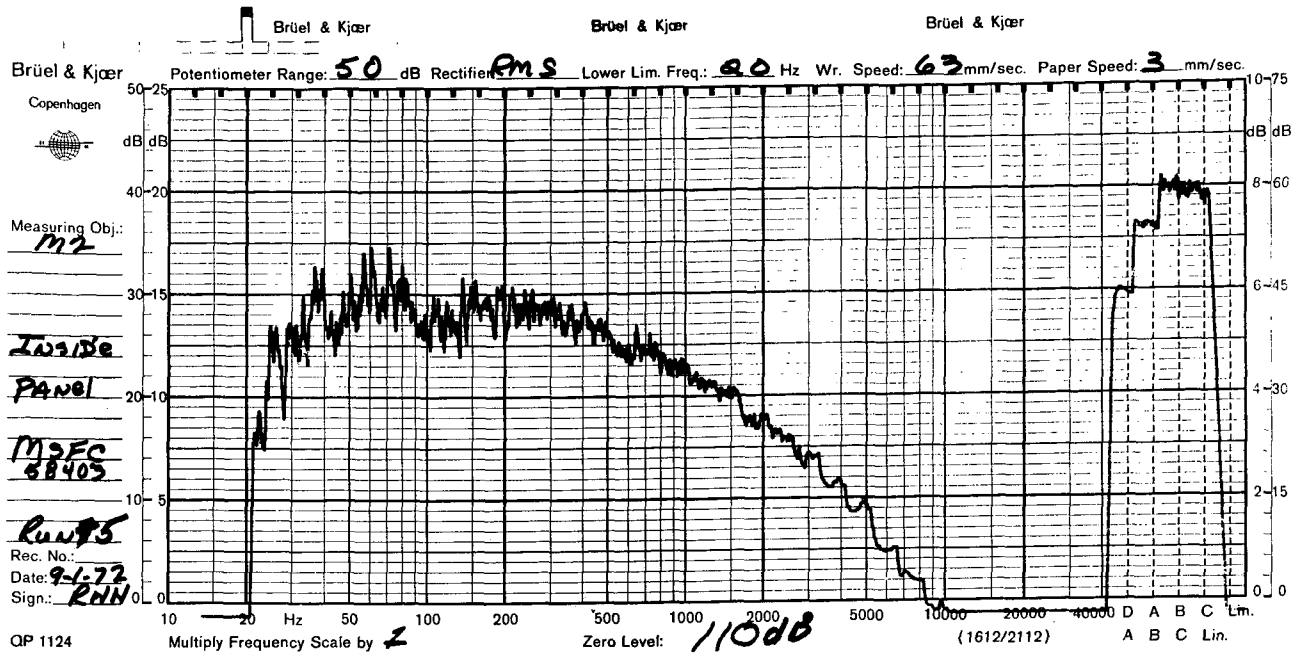

(c) Microphone M2 During Test Run

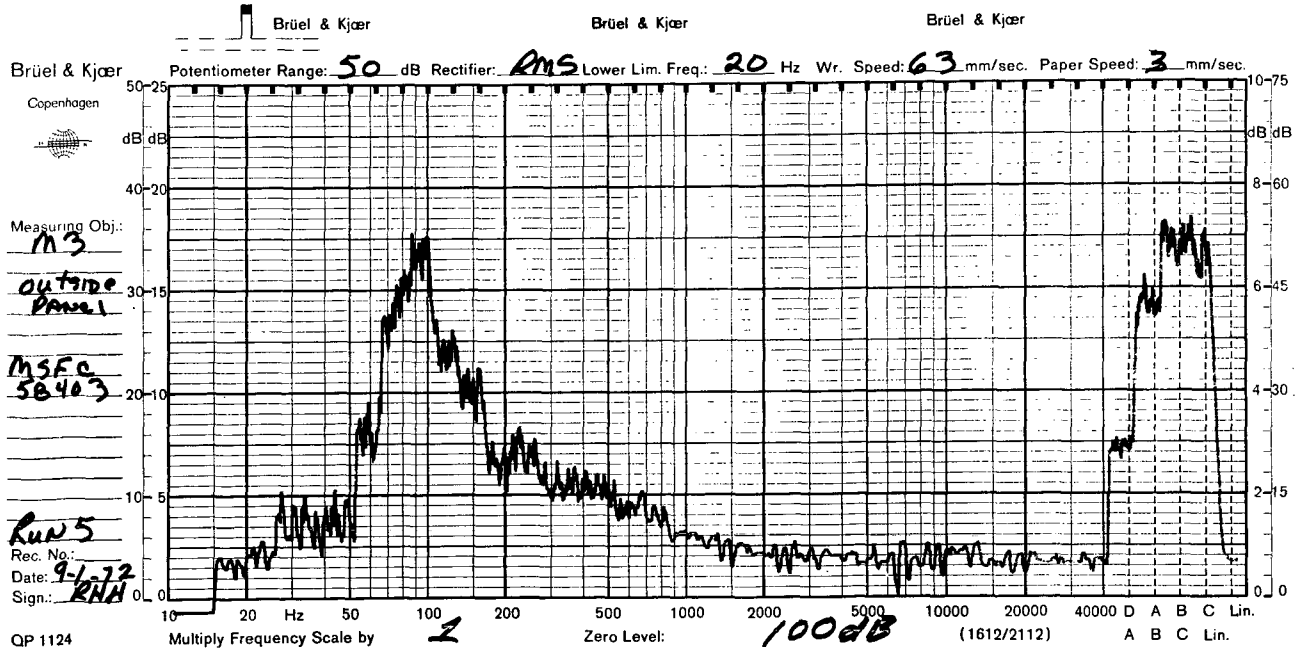

(d) Microphone M3 During Test Run

Figure A-6. (Concluded)

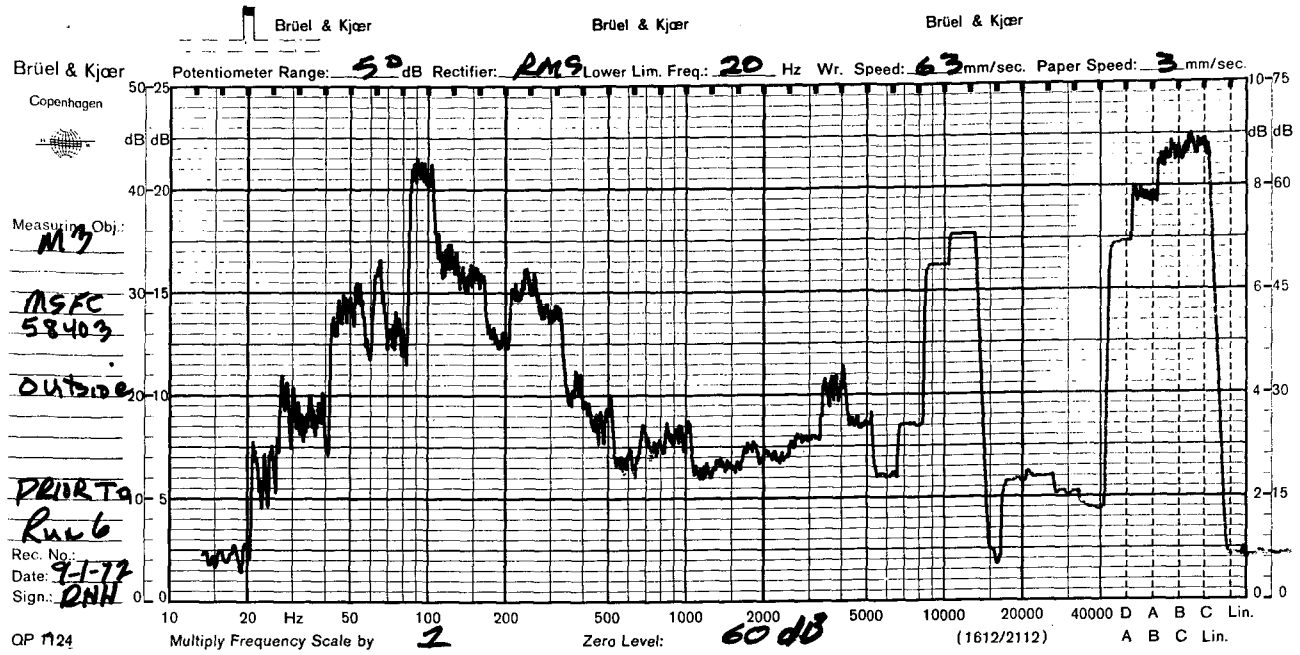

(a) Microphone M3 Prior to Test Run

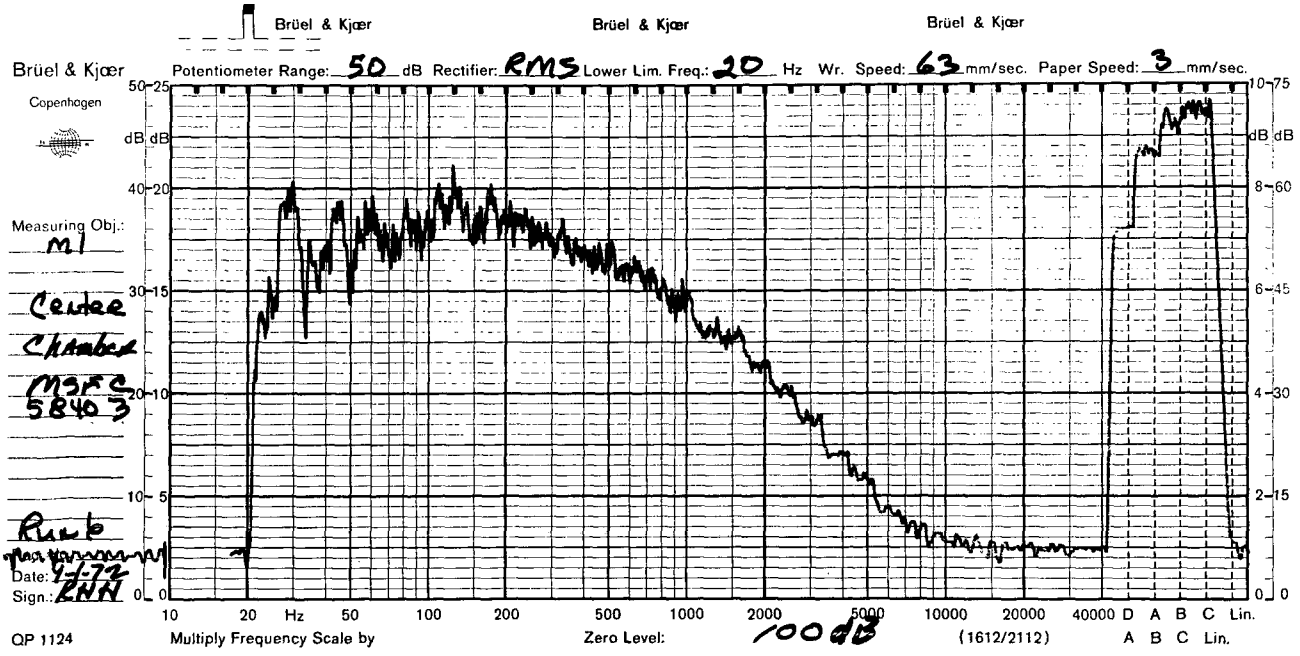

(b) Microphone M1 During Test Run

Figure A-7. Sound Pressure Levels During Acoustic Test Run Number 6

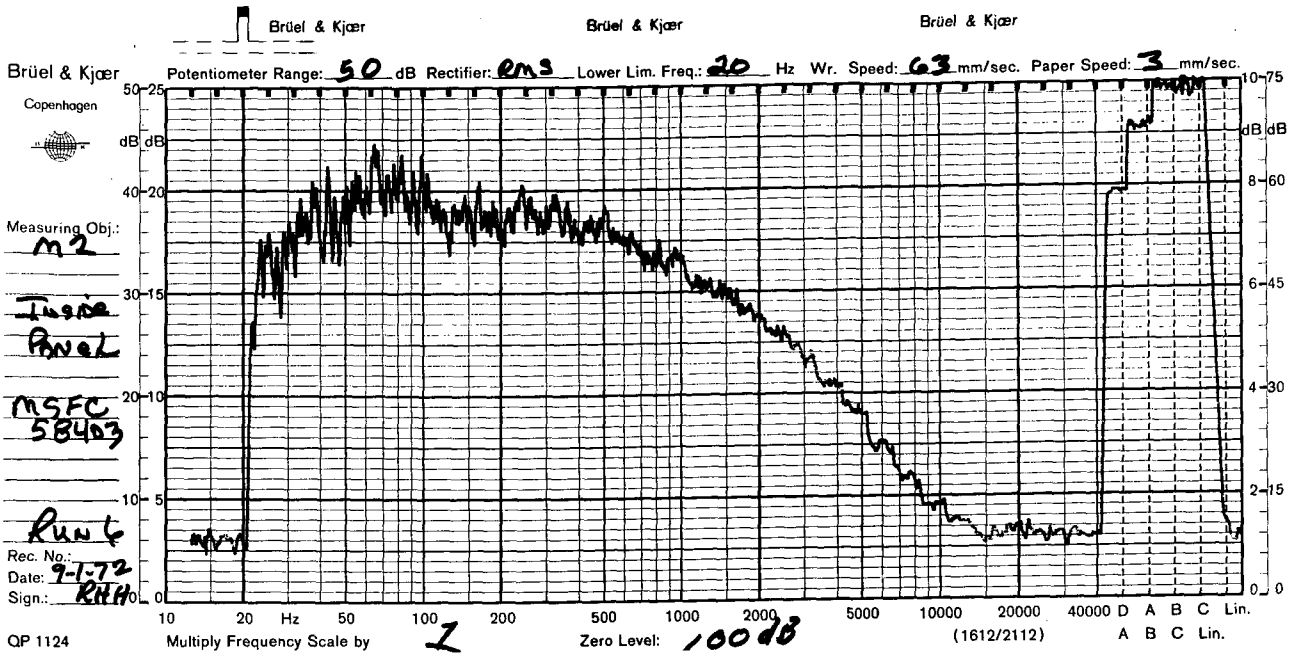

(c) Microphone M2 During Test Run

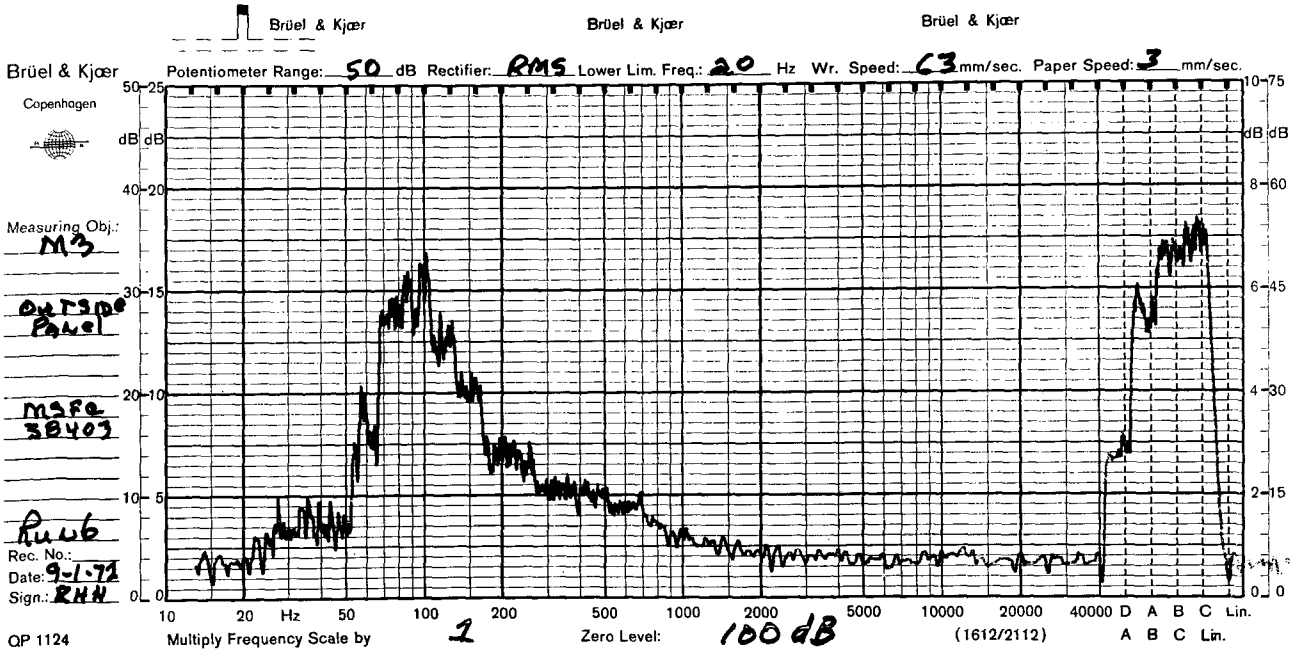

(d) Microphone M3 During Test Run

Figure A-7. (Concluded)

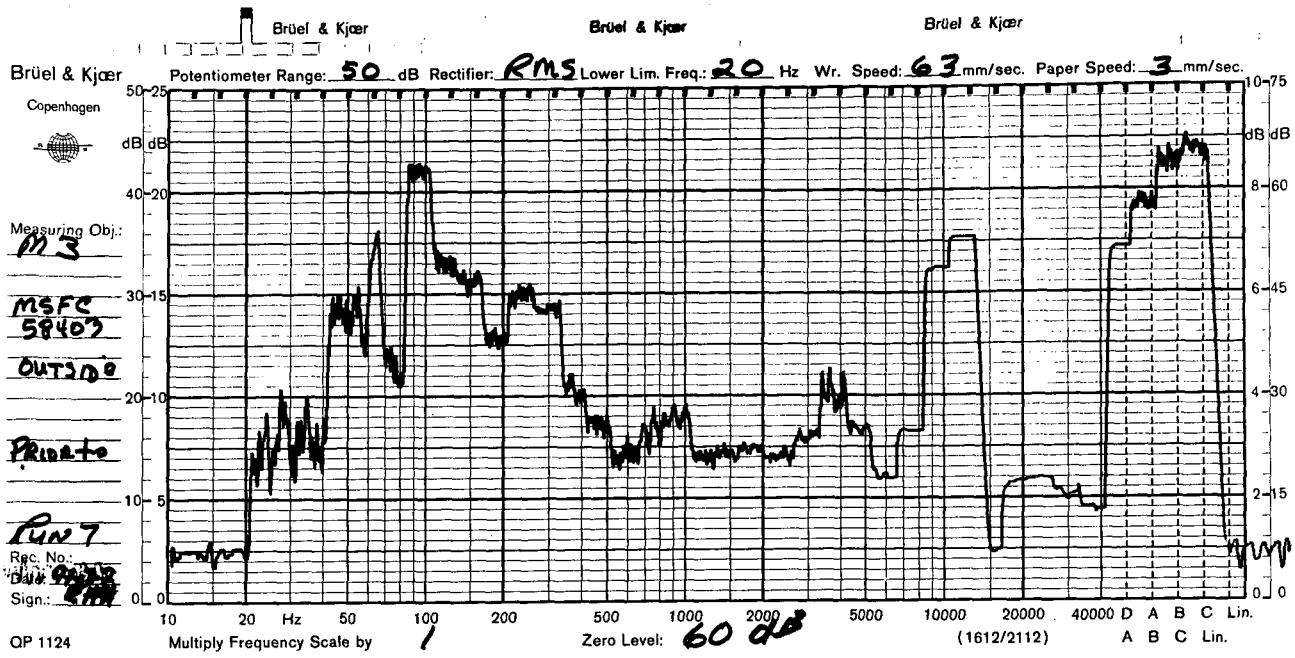

(a) Microphone M3 Prior to Test Run

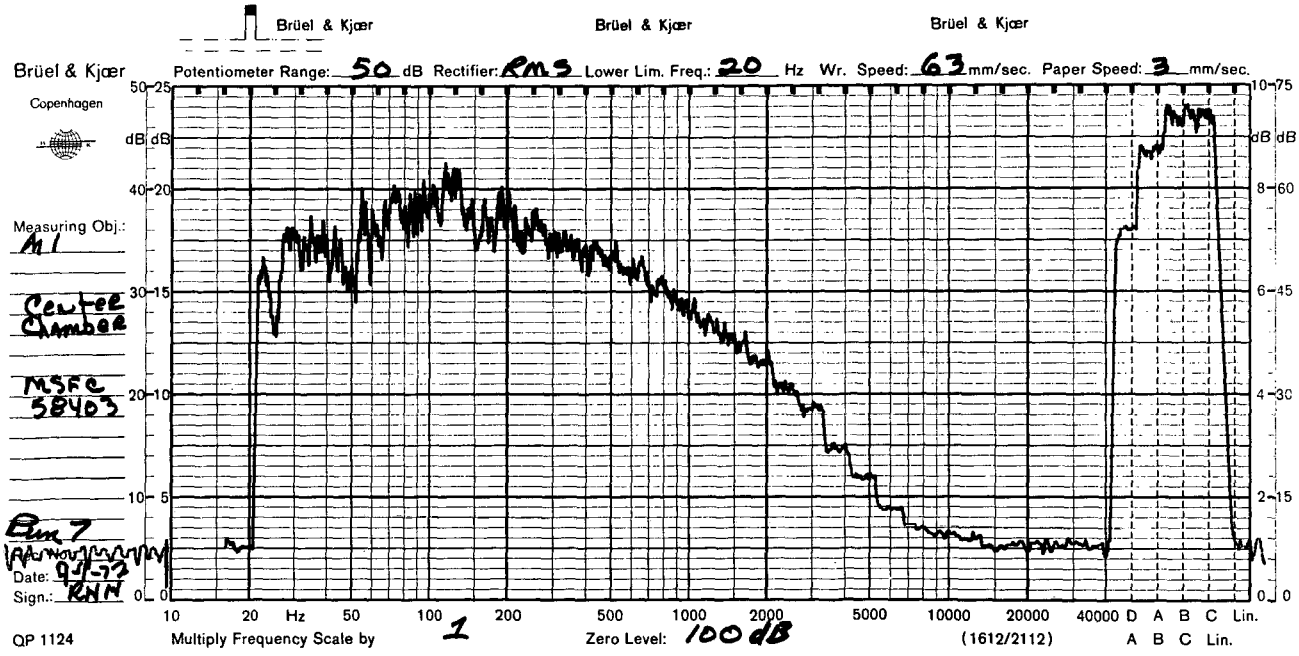

(b) Microphone M1 During Test Run

Figure A-8. Sound Pressure Levels During Acoustic Test Run Number 7

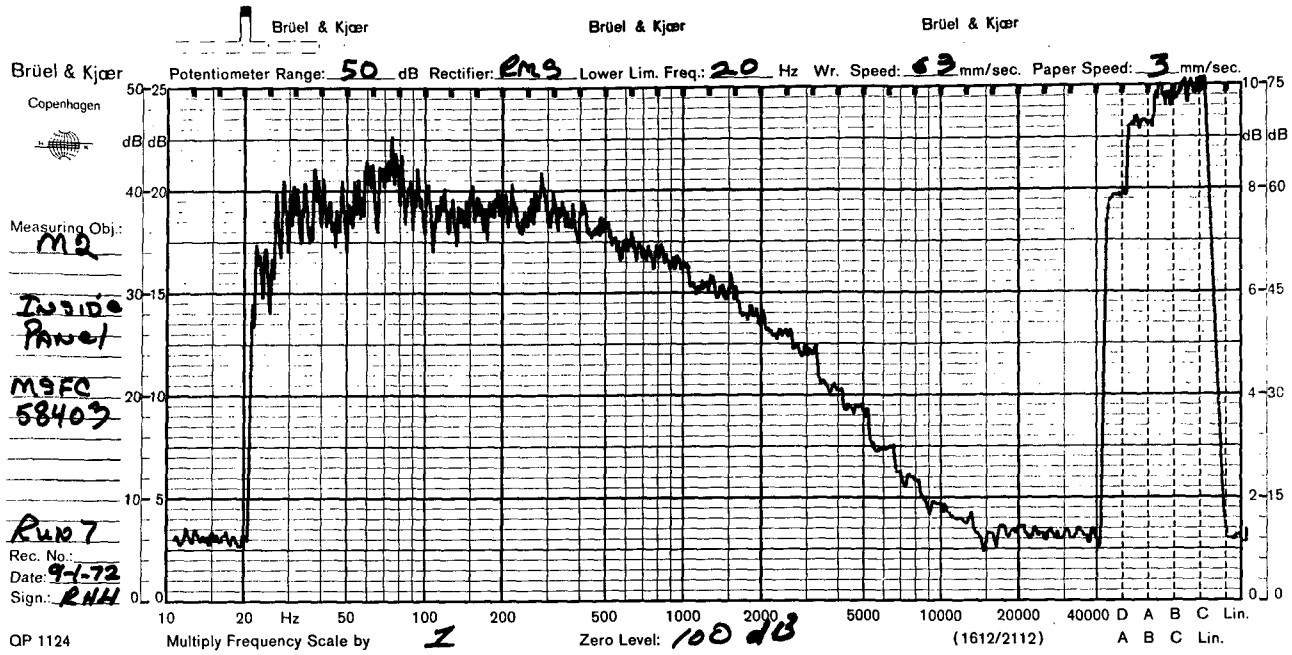

(c) Microphone M2 During Test Run

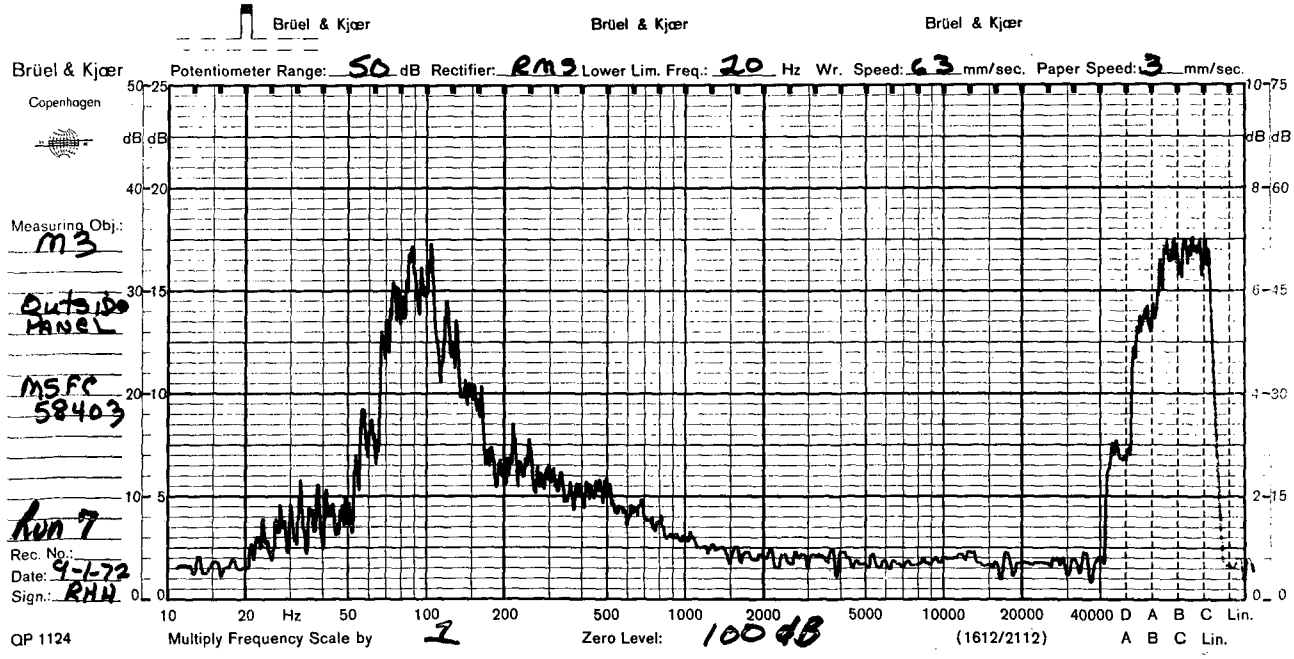

(d) Microphone M3 During Test Run

Figure A-8. (Concluded)

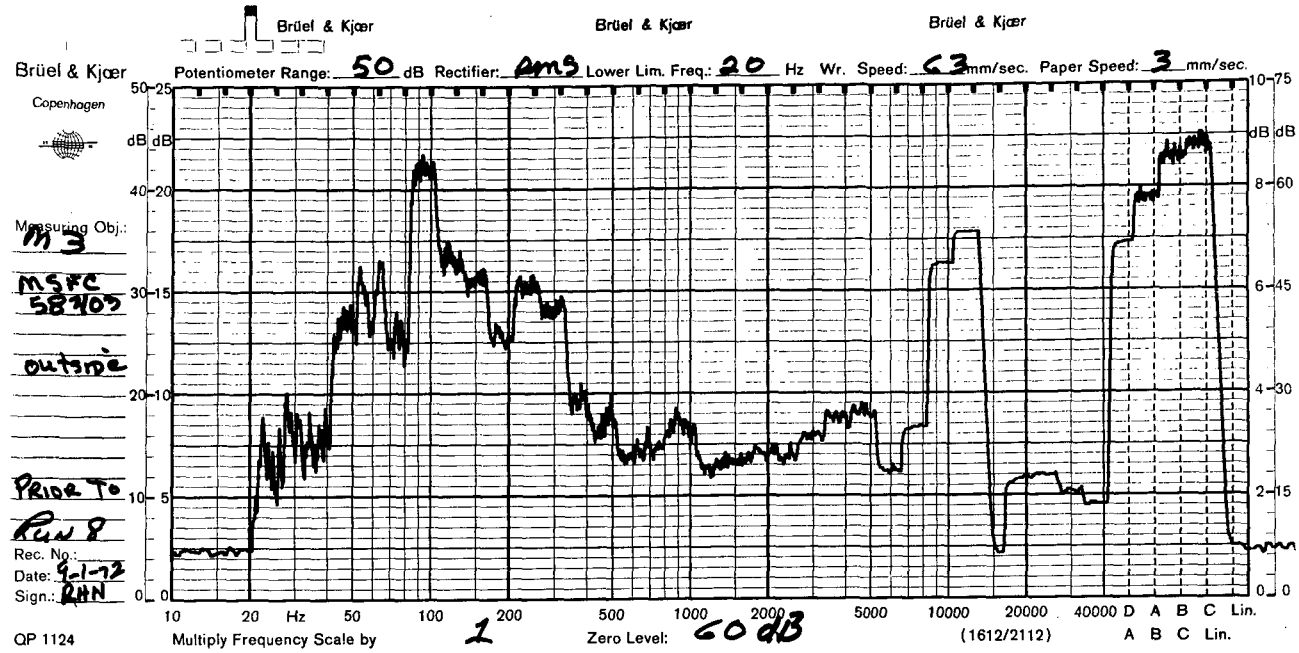

(a) Microphone M3 Prior to Test Run

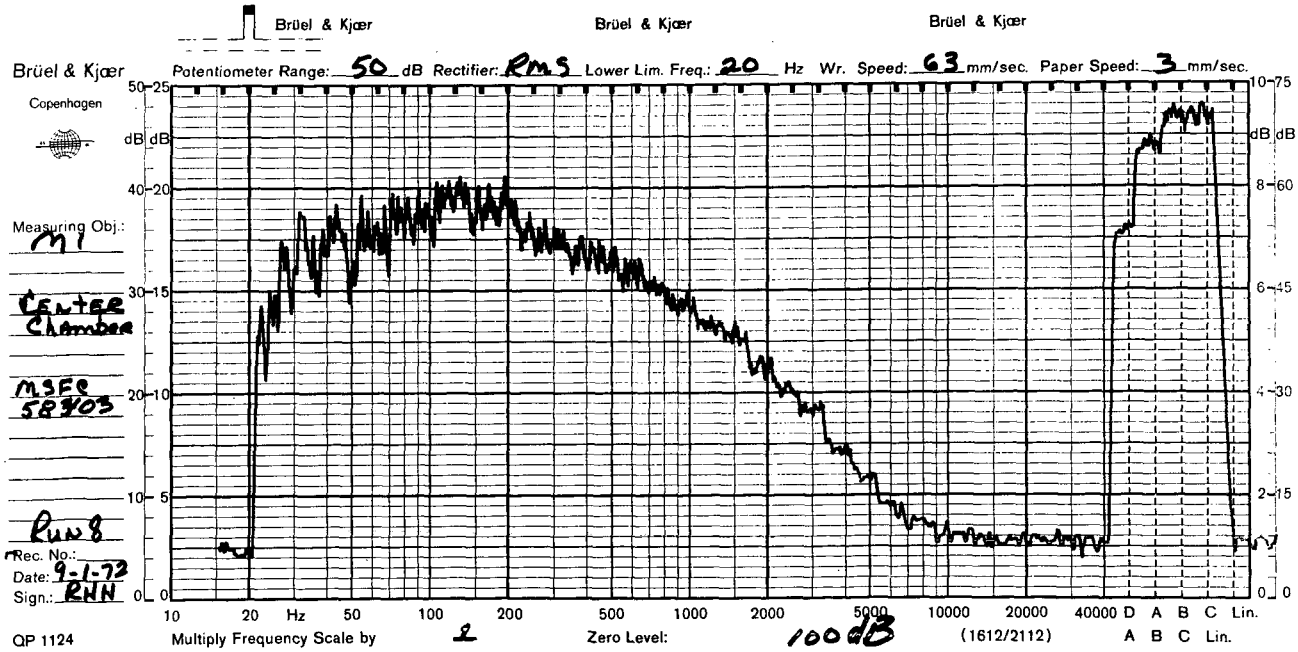

(b) Microphone M1 During Test Run

Figure A-9. Sound Pressure Levels During Acoustic Test Run Number 8

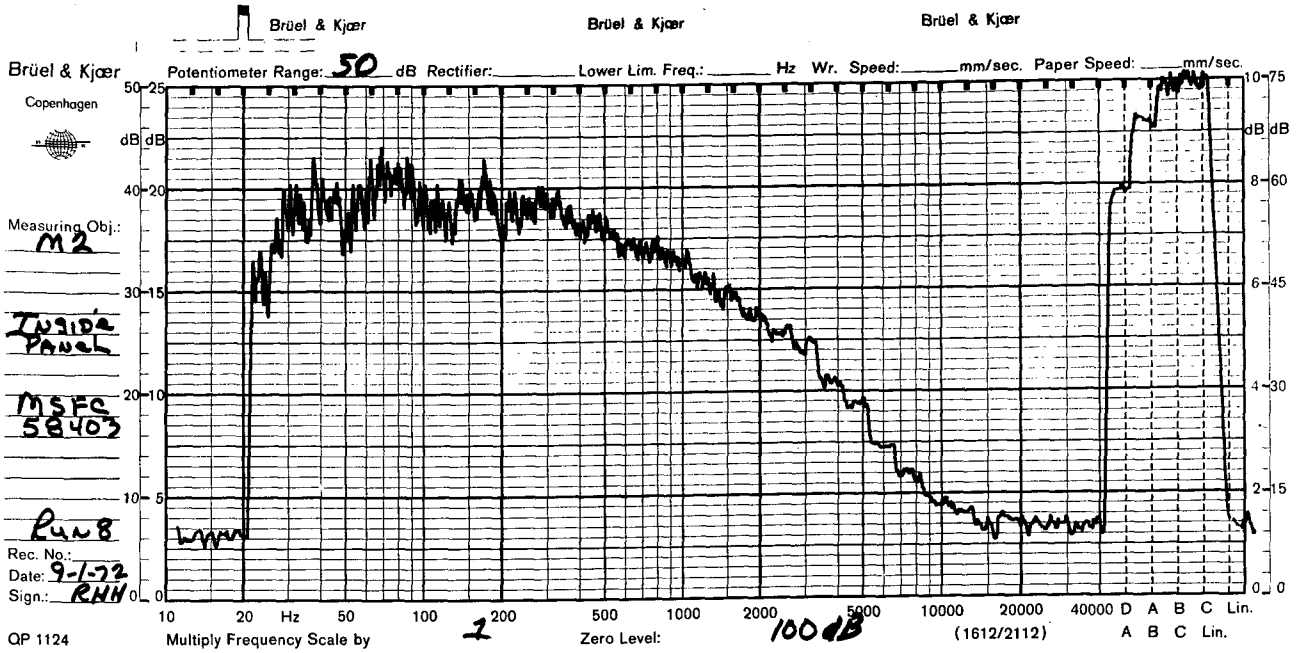

(c) Microphone M2 During Test Run

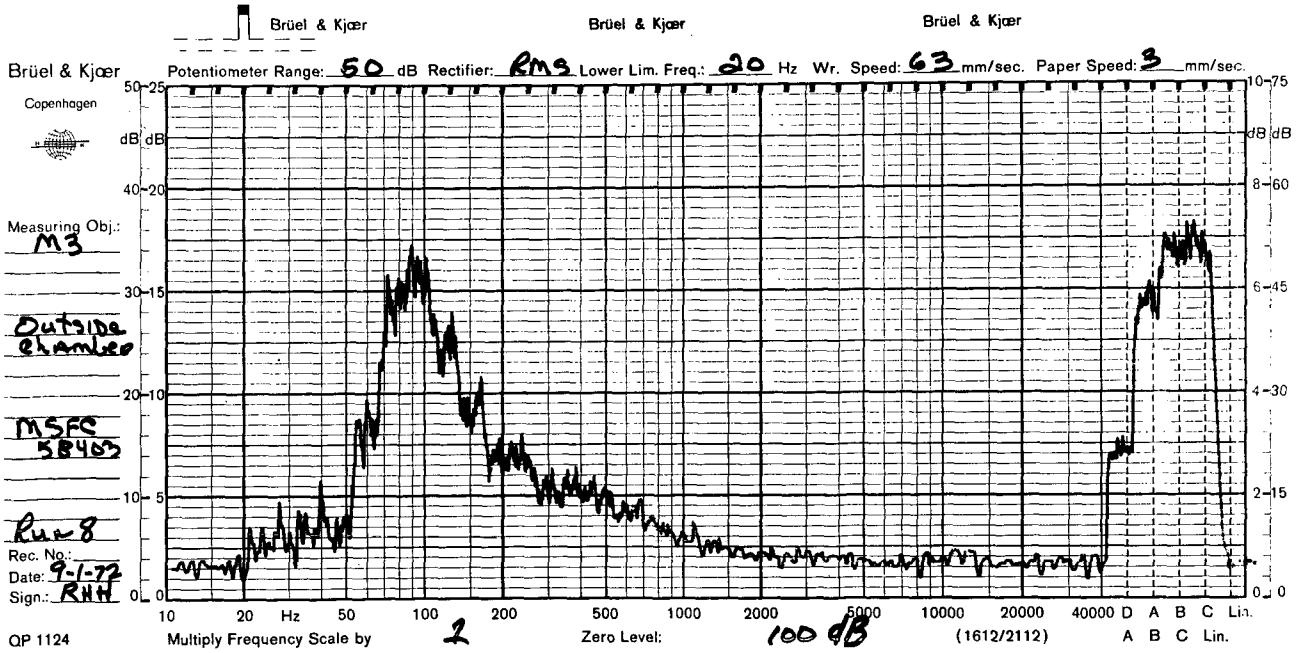

(d) Microphone M3 During Test Run

Figure A-9. (Concluded)

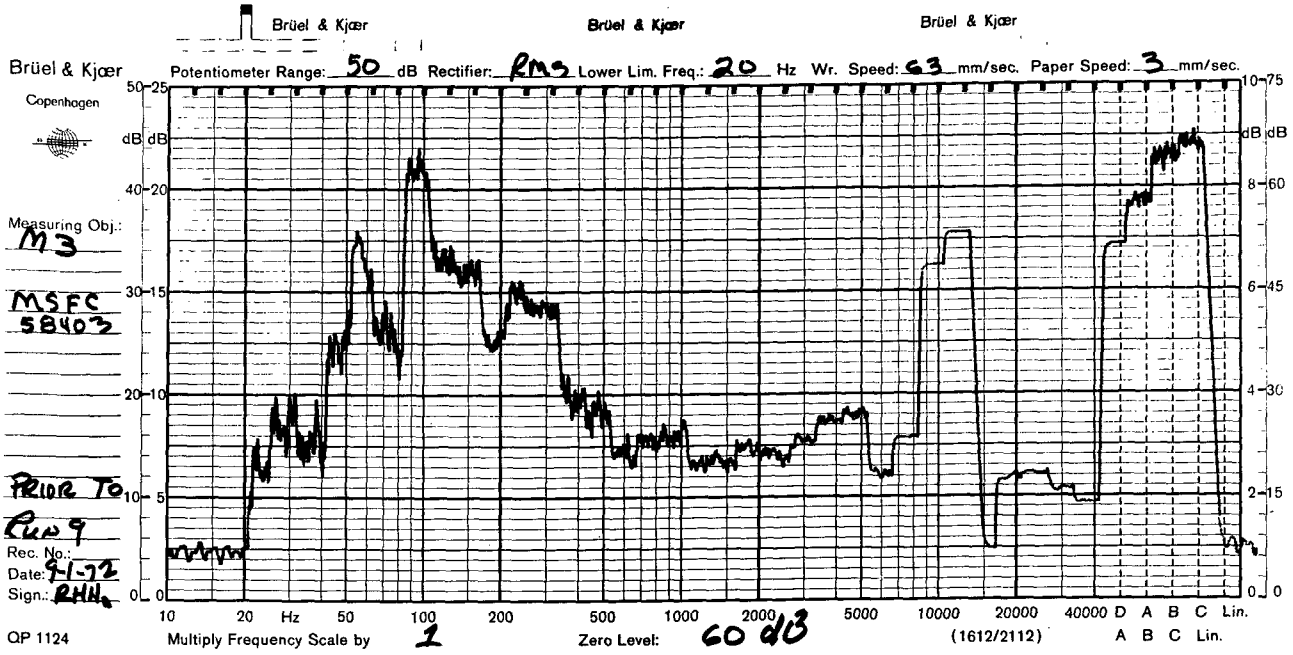

(a) Microphone M3 Prior to Test Run

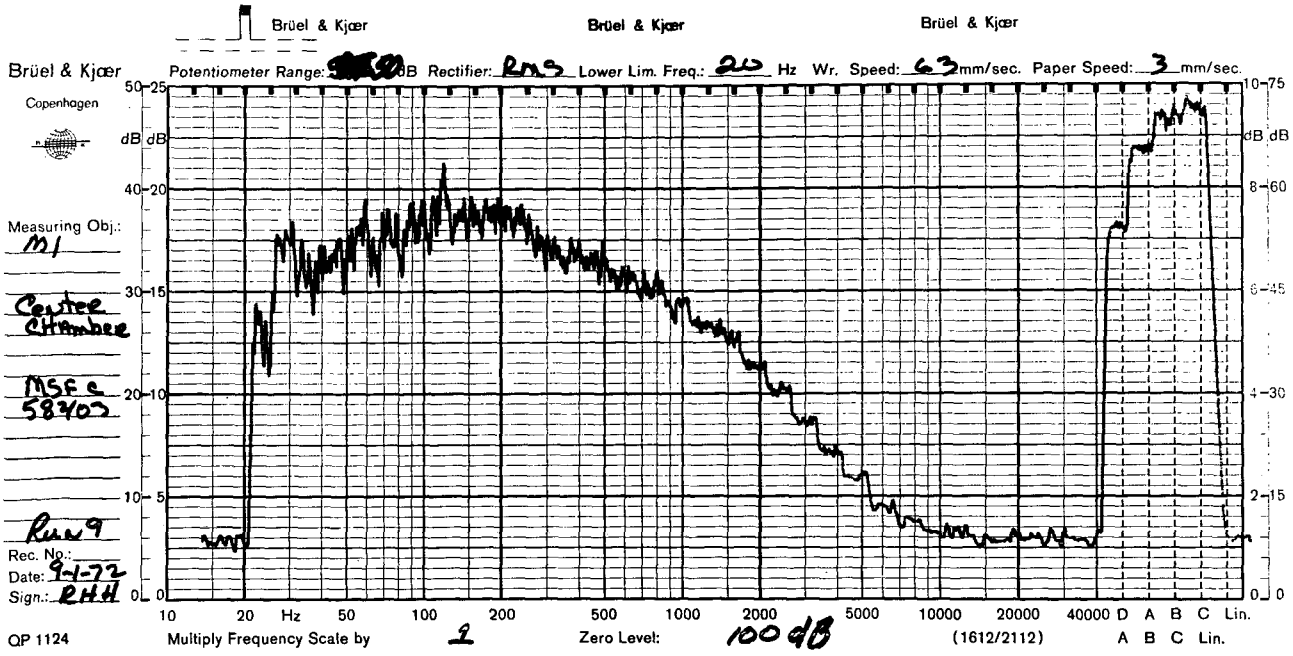

(b) Microphone M1 During Test Run

Figure A-10. Sound Pressure Levels During Acoustic Test Run Number 9

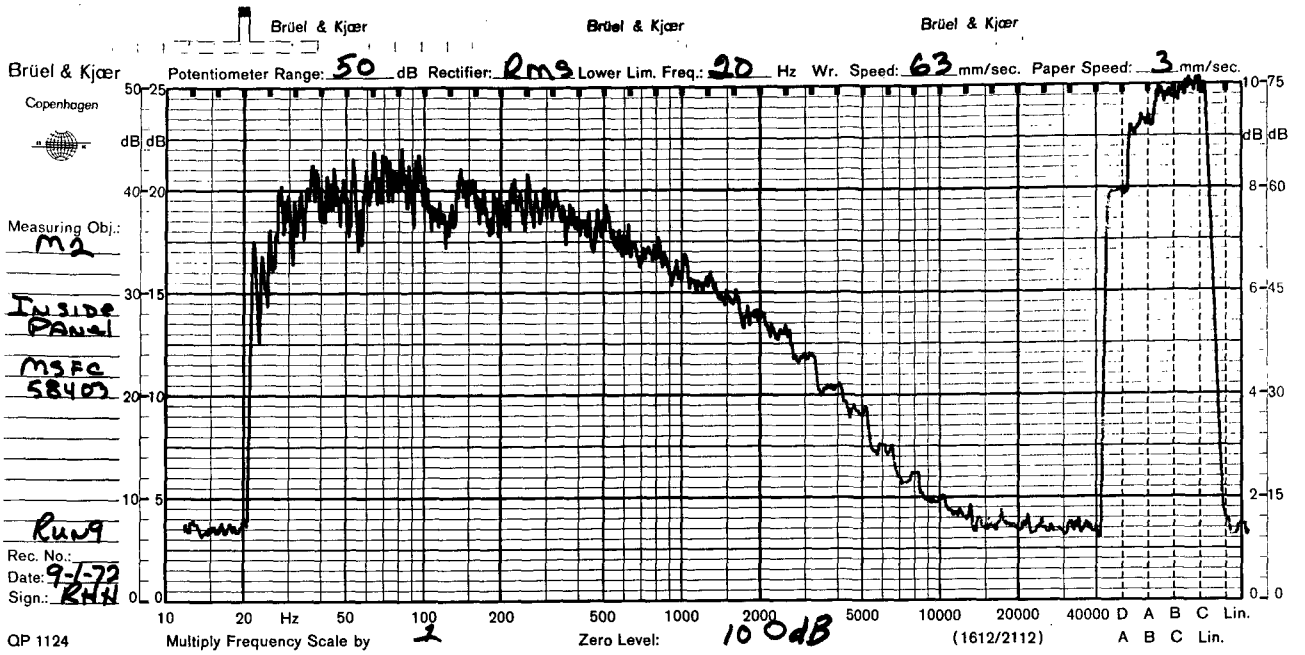

(c) Microphone M2 During Test Run

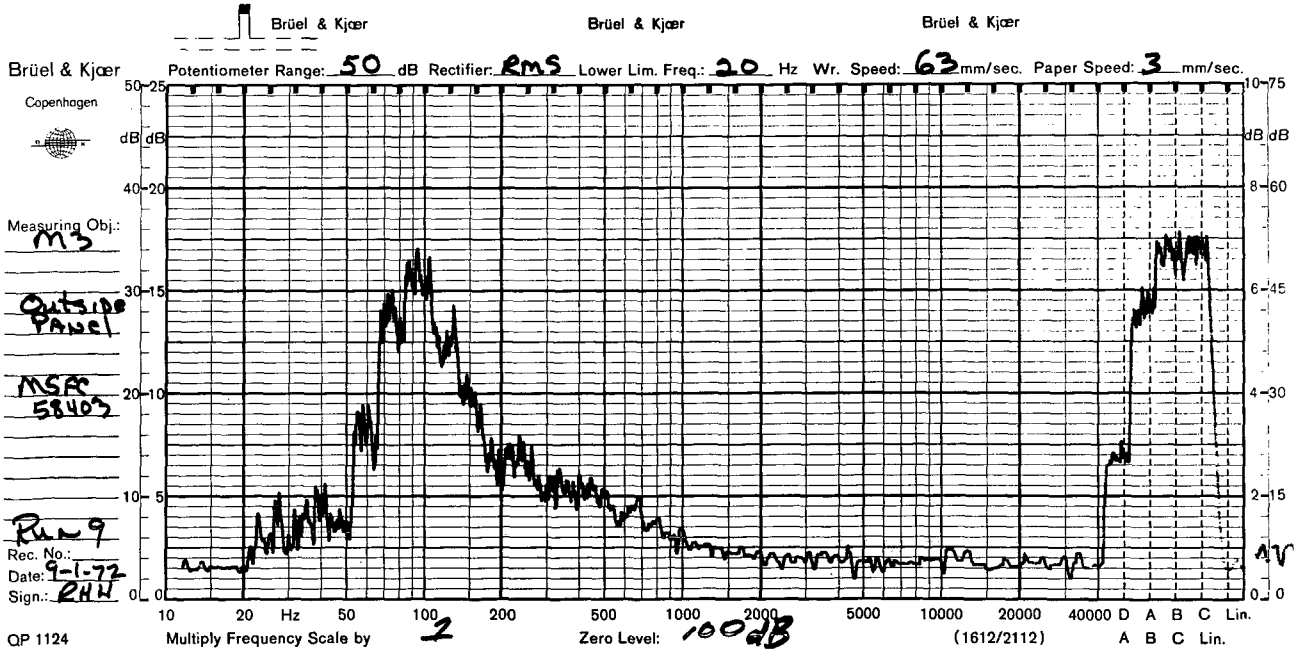

(d) Microphone M3 During Test Run

Figure A-10. (Concluded)

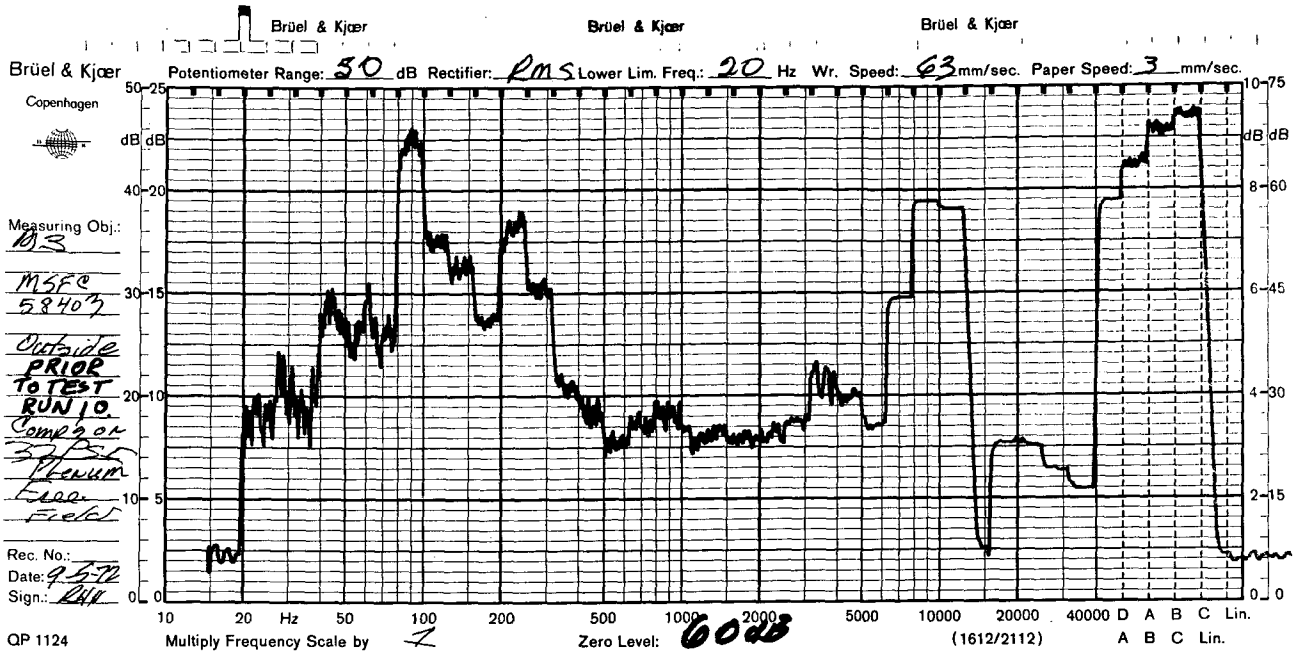

(a) Microphone M3 Prior to Test Run

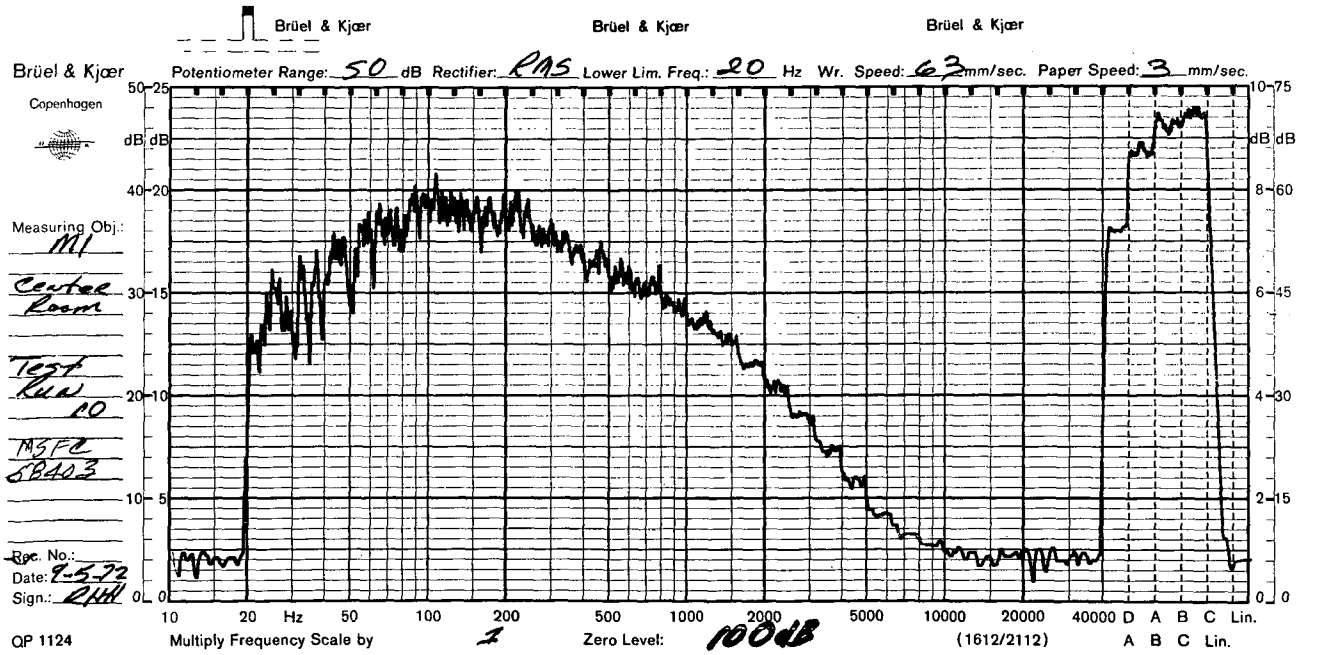

(b) Microphone M1 During Test Run

Figure A-11. Sound Pressure Levels During Acoustic Test Run Number 10

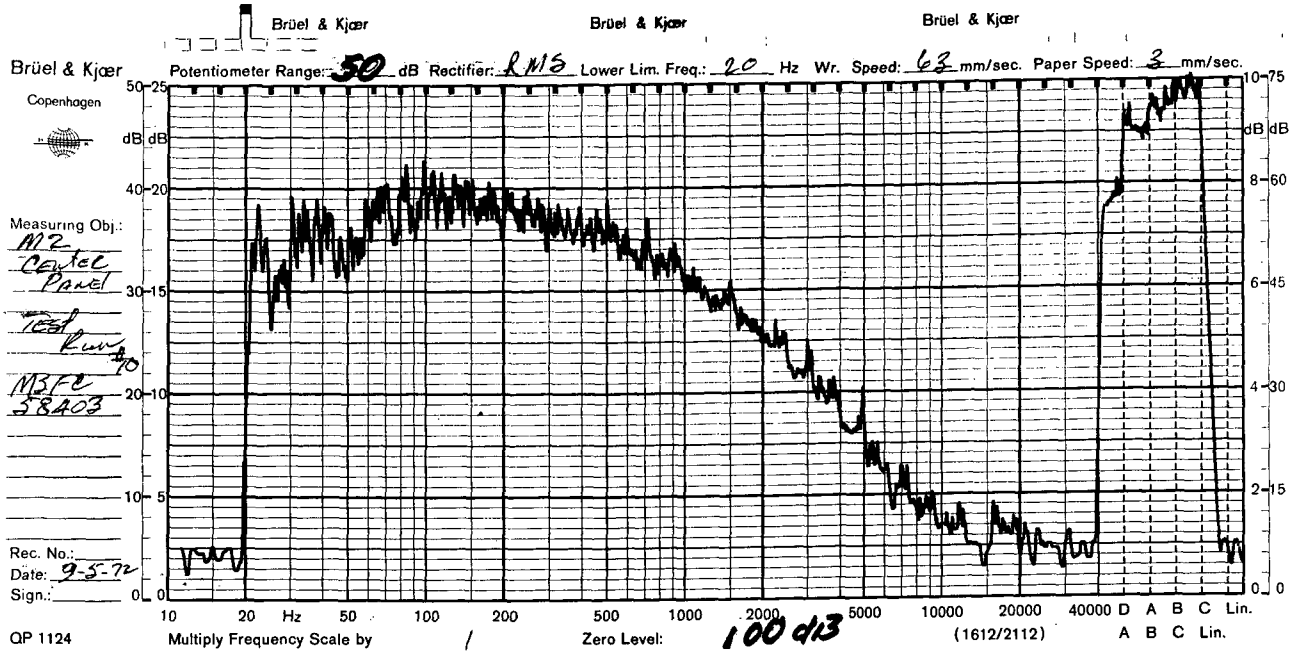

(c) Microphone M2 During Test Run

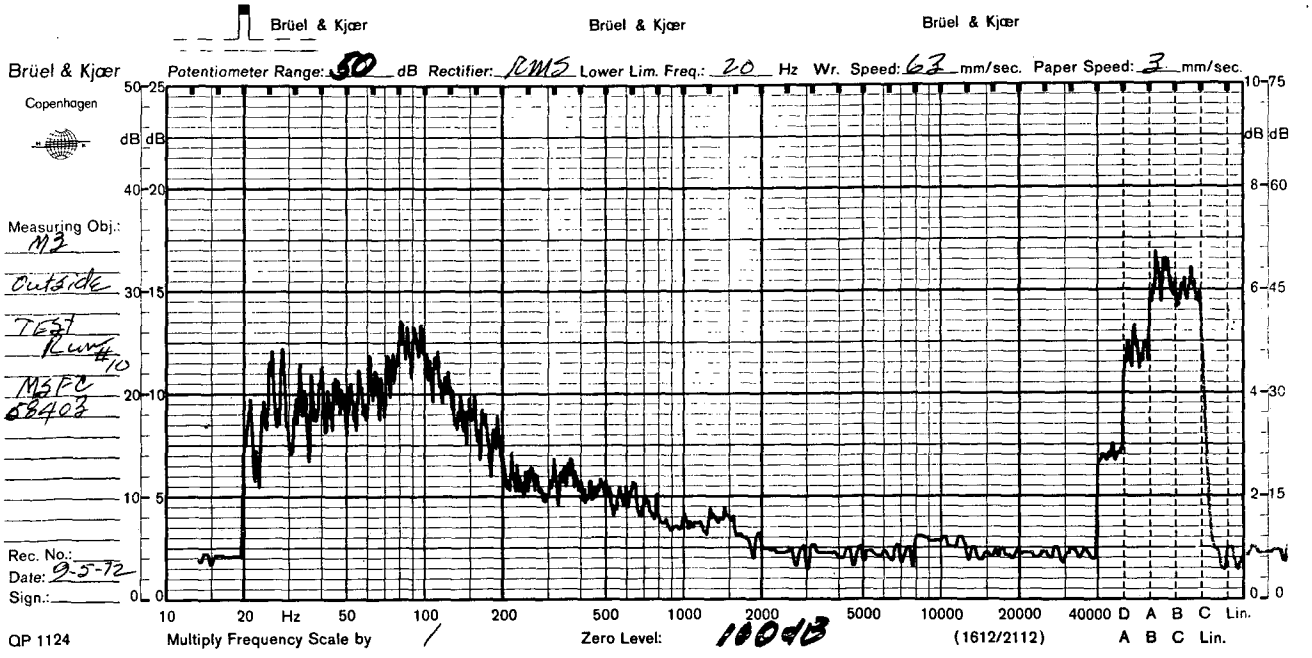

(d) Microphone M3 During Test Run

Figure A-11. (Concluded)

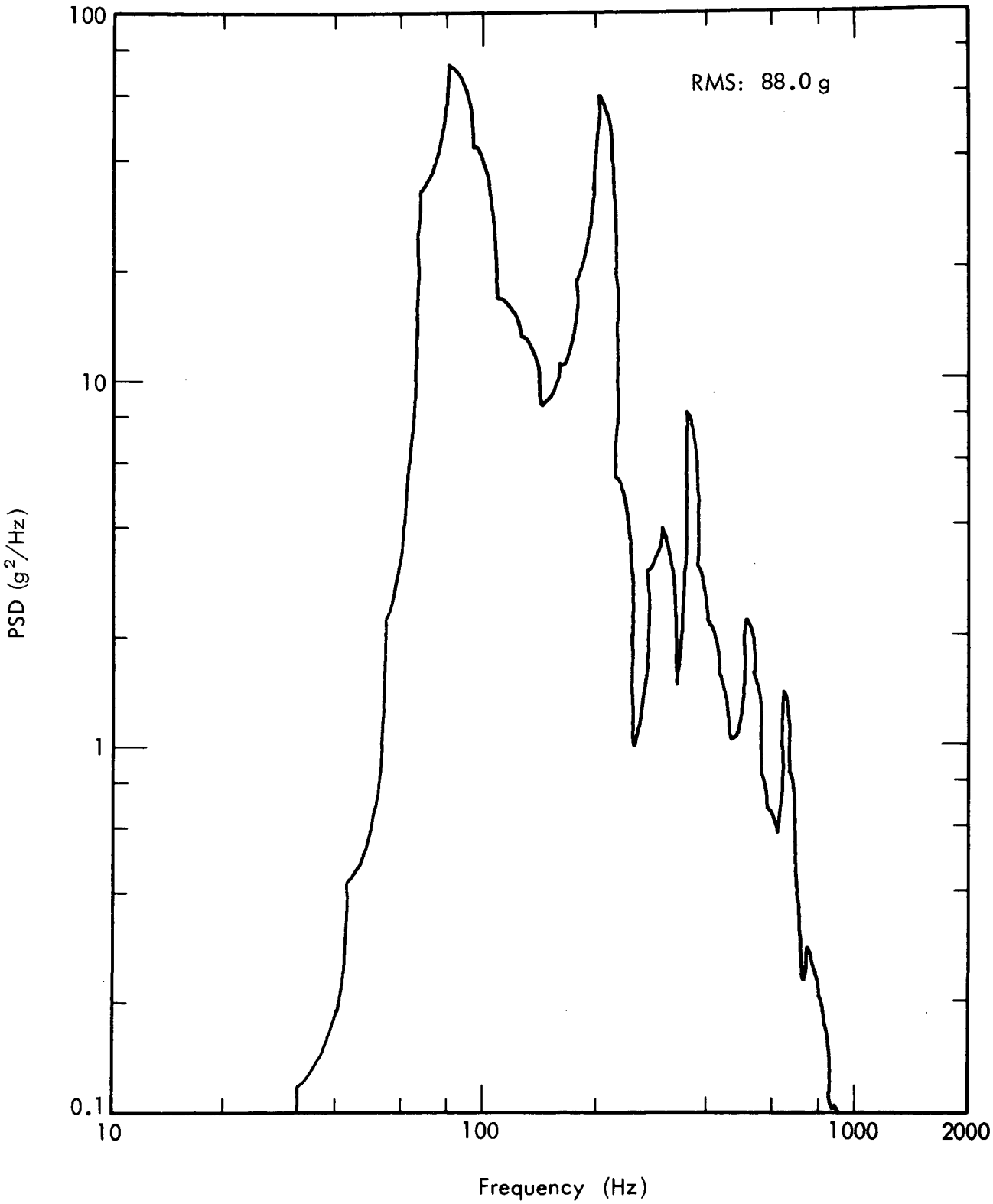

Figure A-12. PSD of Accelerometer A1 — Run 9

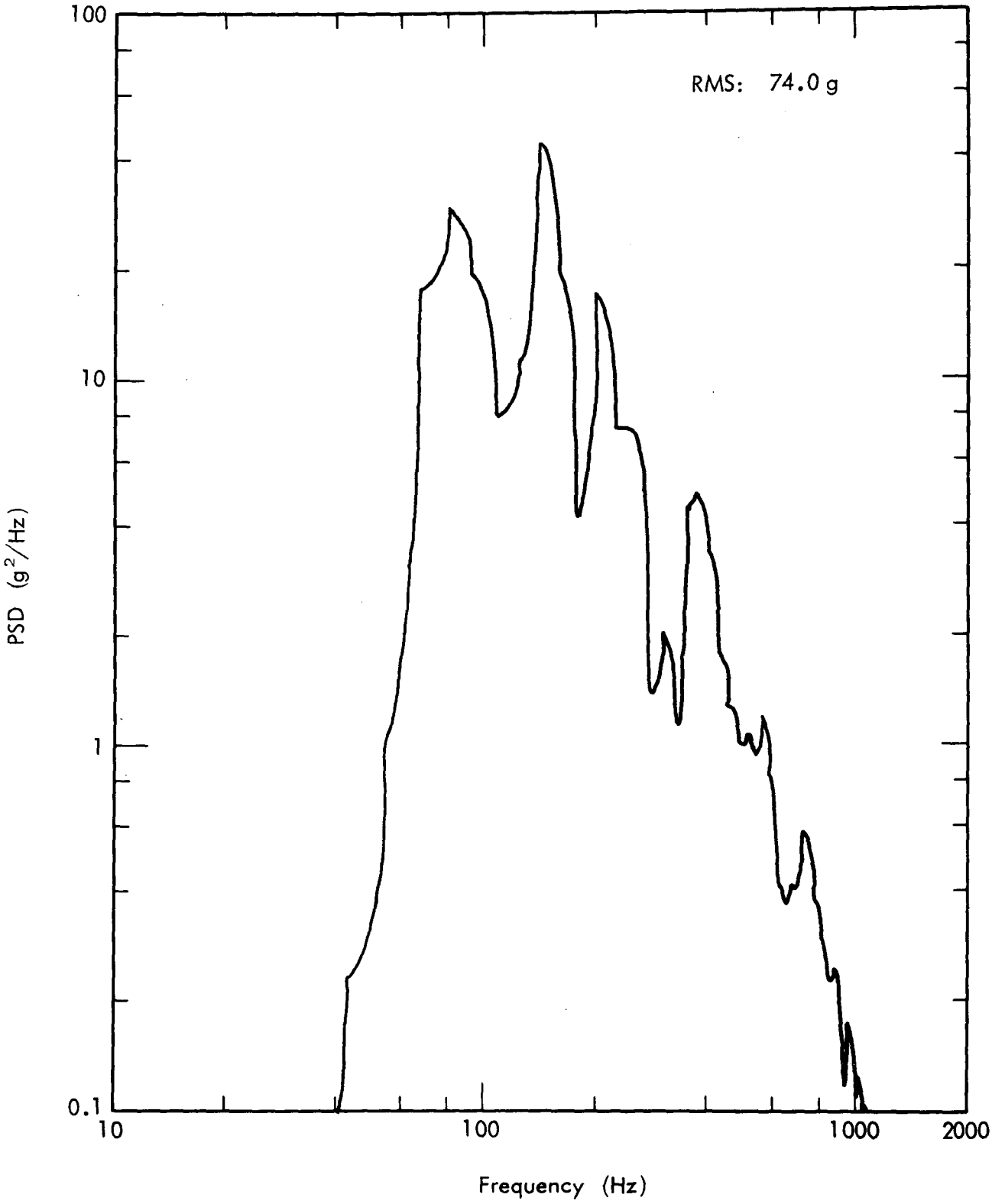

Figure A-13. PSD of Accelerometer A2 — Run 9

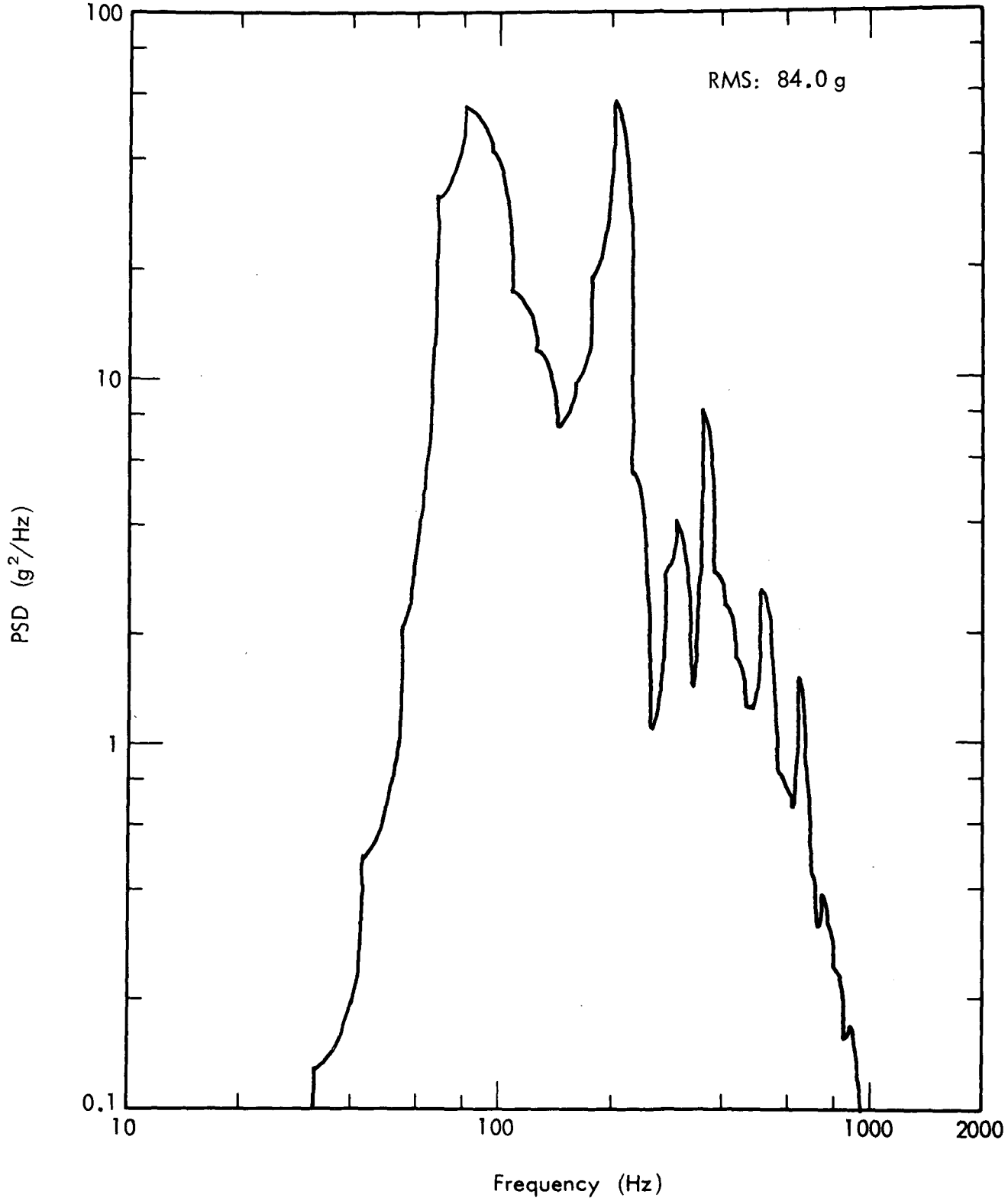

Figure A-14. PSD of Accelerometer A3 — Run 9

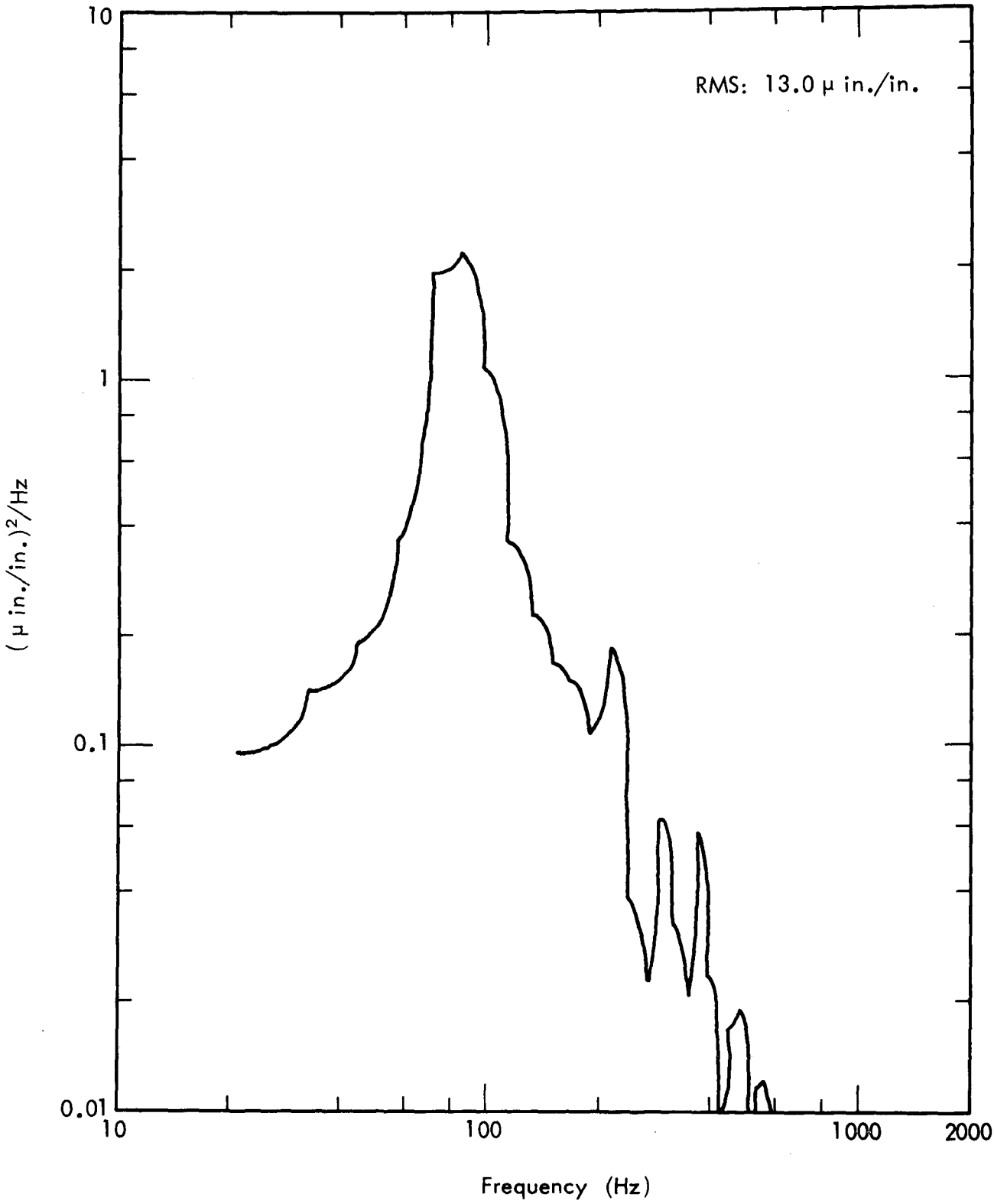

Figure A-15. PSD of Strain Gage SG1—Run 9

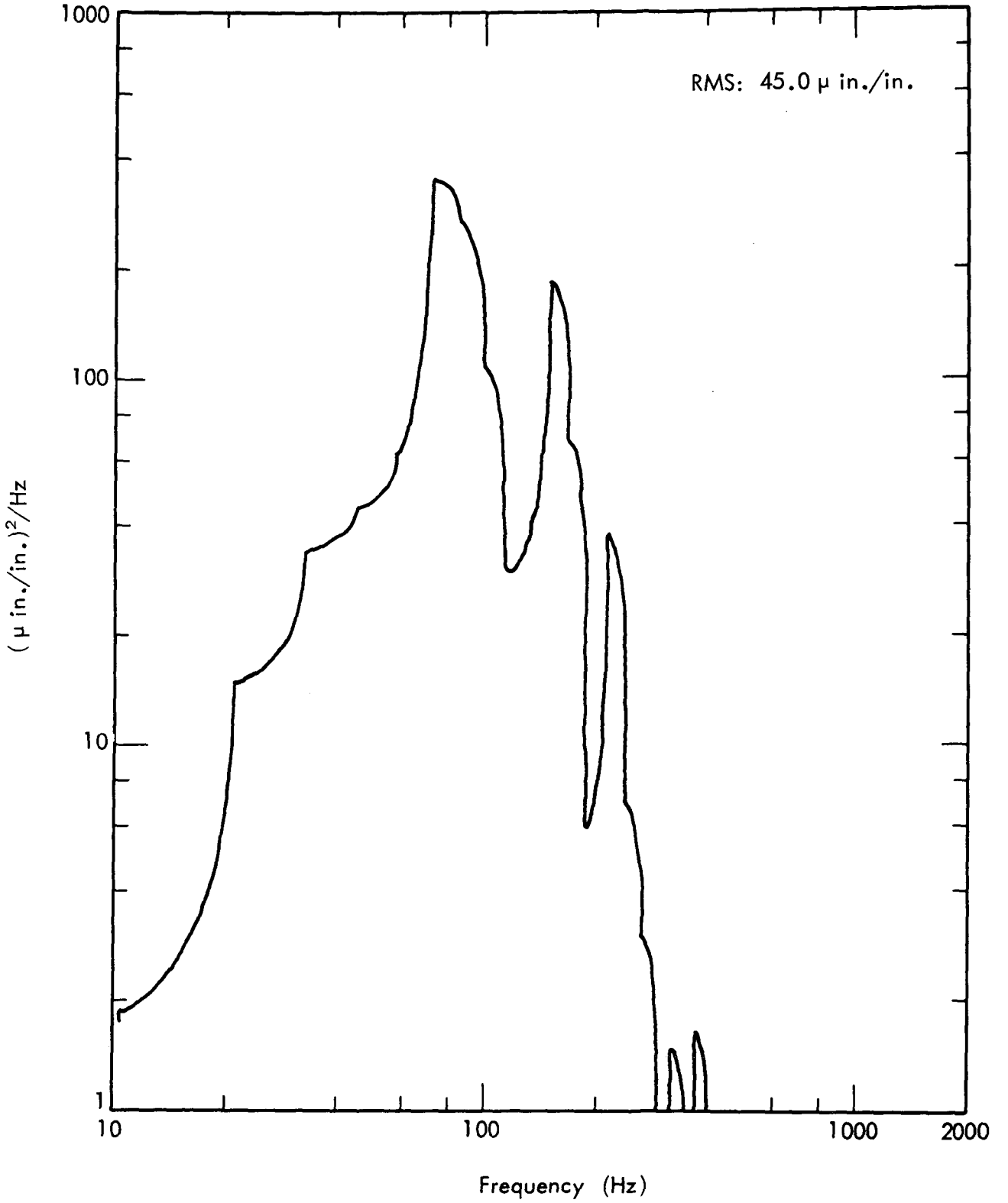

Figure A-16. PSD of Strain Gage SG2 — Run 9

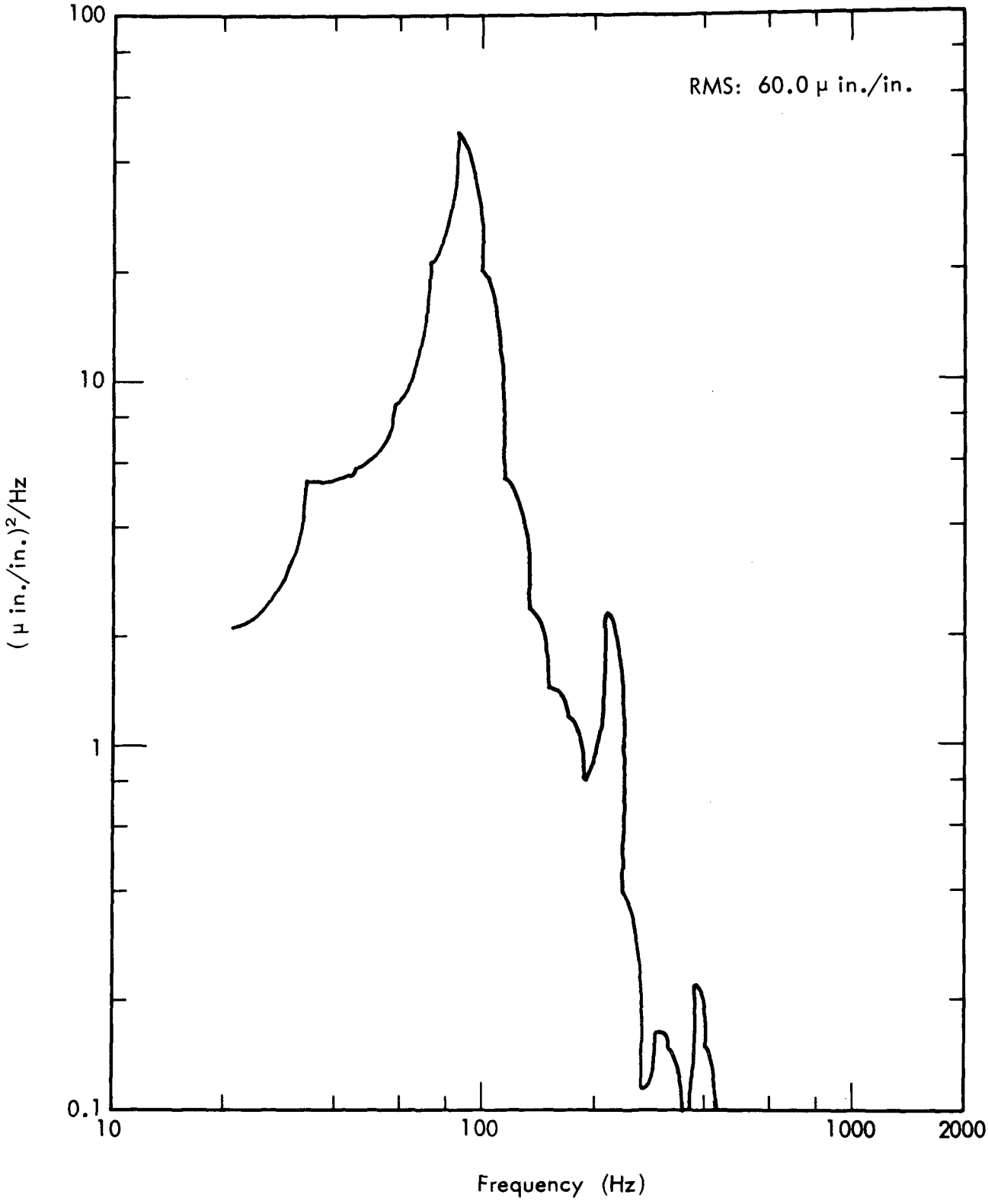

Figure A-17. PSD of Strain Gage SG3 — Run 9

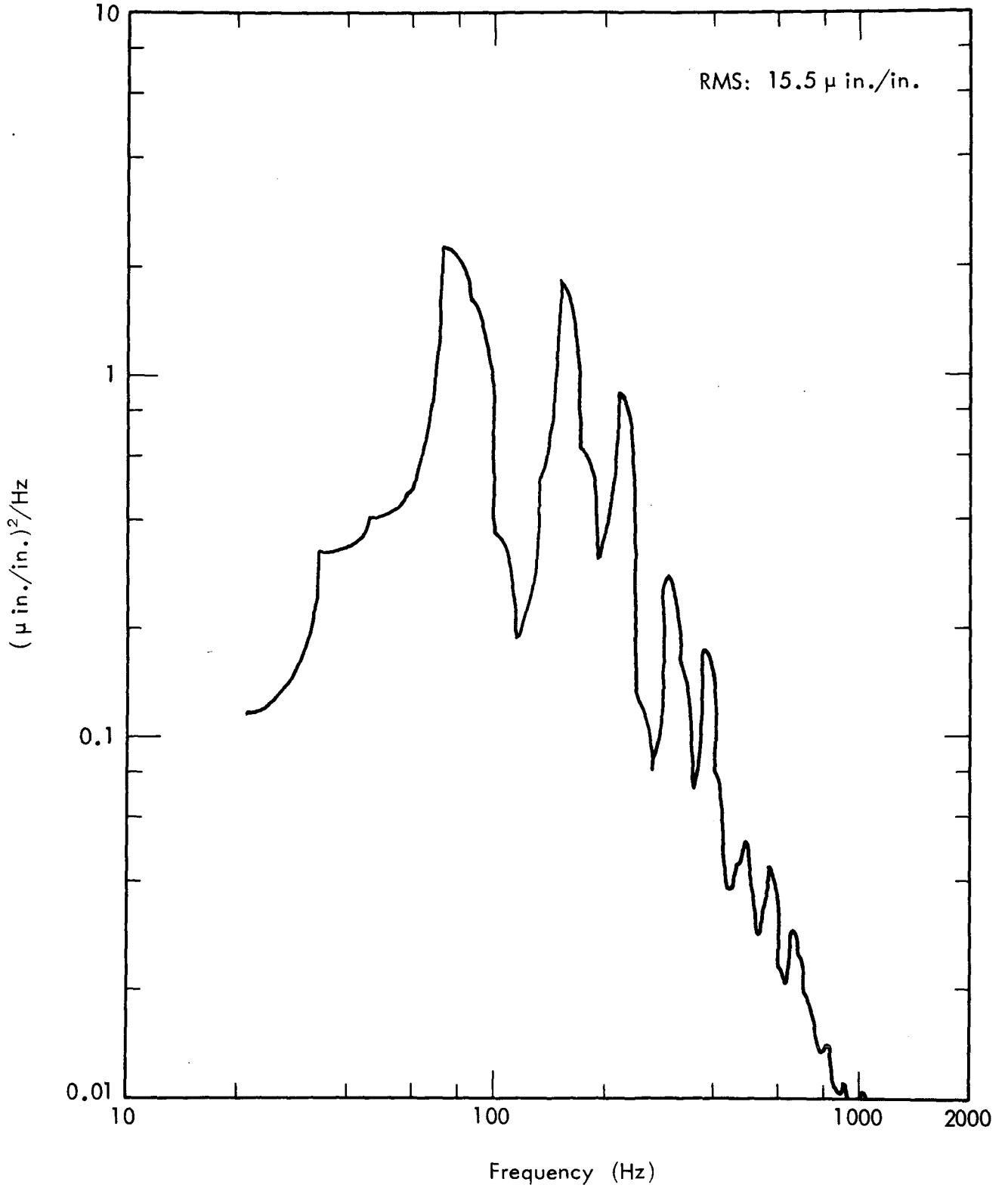

Figure A-18. PSD of Strain Gage SG4 — Run 9

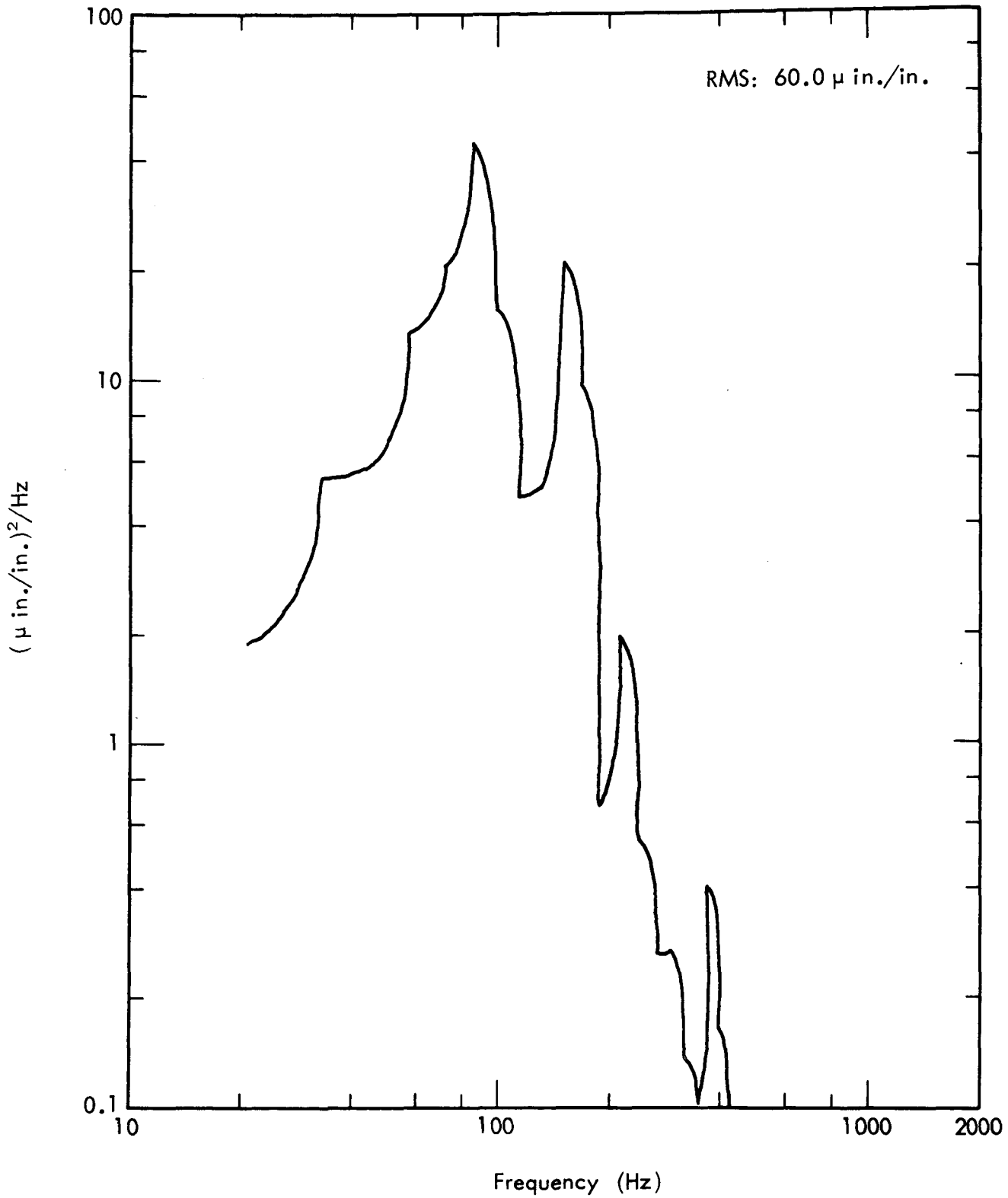

Figure A-19. PSD of Strain Gage SG5 — Run 9

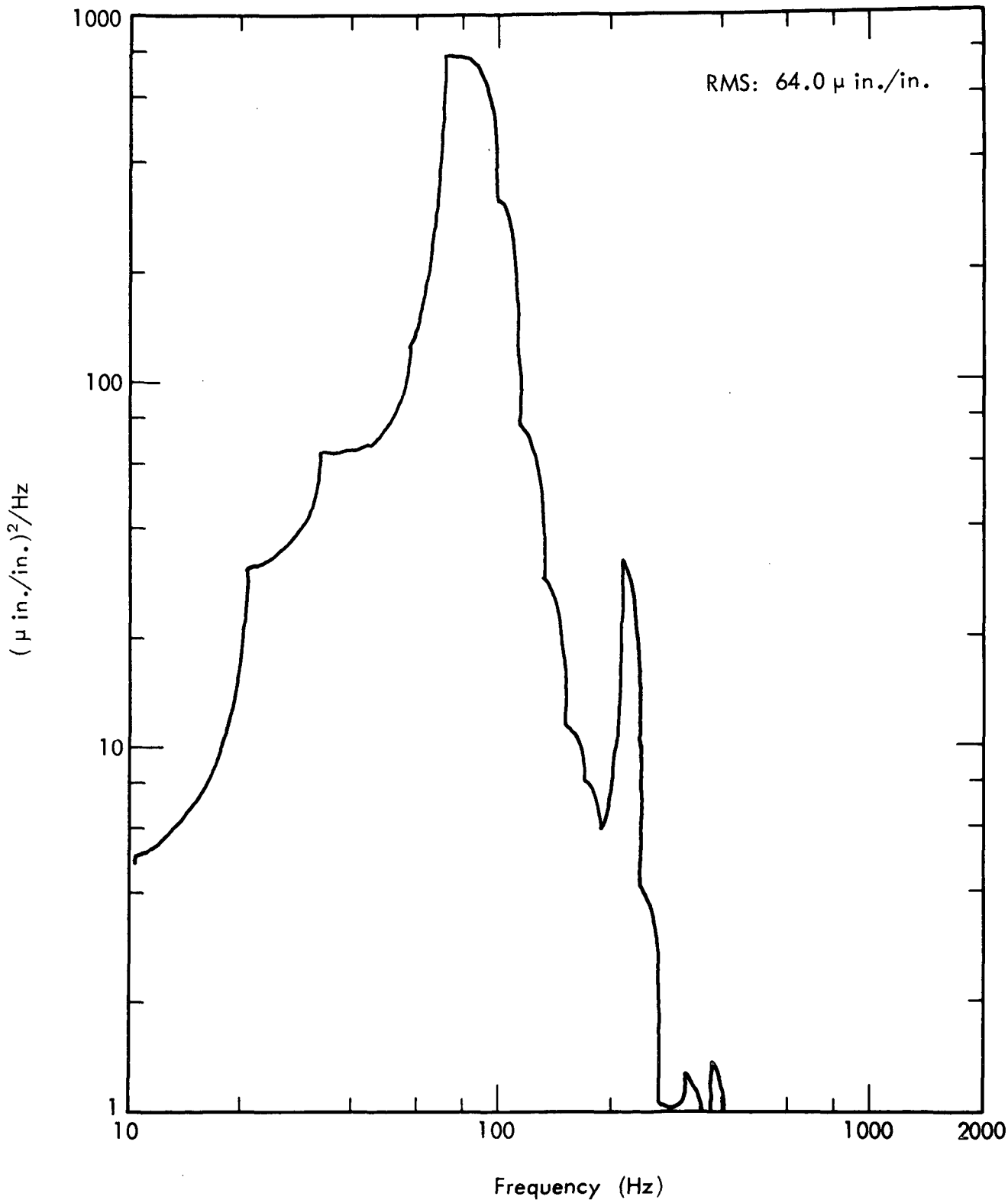

Figure A-20. PSD of Strain Gage SG6 — Run 9

APPENDIX B

PREDICTION OF ACOUSTIC FATIGUE LIFE

1.0 DISCUSSION OF APPROACHES

The fatigue life, L_f, of an acoustically excited structure depends upon the proximity of the induced stress, S_s, to the fatigue strength, S_f, of the structural material located in critical, fatigue-prone locations. In the case of structures excited by constant-amplitude sinusoidal pressure fluctuations, the fatigue life can be determined from the conventional S-N diagram. For structures excited by random loads more sophisticated definitions are required for the fatigue strength S_f. As a result of current studies, the relationship of the acoustical fatigue life, L_f, under random excitation may be expressed as follows:

$$L_f = f\left\{ \frac{1}{P_r}, S_f, \frac{1}{S_0}, \frac{1}{\sqrt{f_0}}, \sqrt{\delta} \right\} \qquad (1)$$

where

P_r = power spectral density of random (acoustic) loads, sound pressure levels per unit bandwidth,

S_0 = stress response produced by unit static loading

f_0 = fundamental resonant frequency of structural system, and

δ = damping coefficient of structural system per cycle of sinusoidal vibration

Equation (1) shows that the acoustical fatigue of a structure can be specified in terms of the properties of the structural material and other parameters shown. Since the fatigue process is often highly nonlinear and is an imprecise response of the structure, the application of linear criteria such as Miner's Rule is often unrealistic. Therefore, an analytical expression of the above relation is almost impossible and impractical owing to the unavailability of a reliable fatigue damage theory. Nevertheless, the practical solution to this gap in dynamic stress analysis is reliance on siren tests. The siren life test performed on a specimen panel is offered to obviate the need for the stress response information and to complete the analytical approach to engineering estimates. The method and techniques are essentially those developed by

Belcher, Van Dyke, and Eshleman, * which were used successfully in the design and development of the acoustical fatigue prediction method.

This empirical prediction method or so-called sine-random equivalence technique is derived from the problem of a simple linear single-degree-of-freedom system and is briefly discussed below.

It has been shown theoretically and experimentally that the random resonance stress response, S_r, of single-degree-of-freedom under a random force input, P_r, is:

$$S_r = \sqrt{\frac{\pi}{4}} \sqrt{\frac{f_0}{\delta}} \; S_0 \; P_r \tag{2}$$

Similarly, for sinusoidal excitation the expression reduces to:

$$S_s = \frac{1}{2\delta} \; S_0 \; P_s \tag{3}$$

where P_s is the root-mean-square (rms) sinusoidal excitation pressure. Elimination of S_0 yields:

$$\frac{S_r}{S_s} = \sqrt{\pi \delta f_0} \; \frac{P_r}{P_s} \tag{4}$$

Panel structures, especially of skin-stringer construction, often exhibit a tendency to respond significantly to excitations at frequencies other than the fundamental mode frequency under random excitation, and the stress response also exhibits nonlinearity at relatively low stress levels. These two factors are both important in fatigue damage considerations and, therefore, when added to equation (4) yield the following:

---

* Belcher, P.M., J.D. Van Dyke, Jr., and A.L. Eshleman, "Development of Aircraft Structure to Withstand Acoustic Loads," Aero-Space Engineering, Vol. 18, No. 6, June 1959.

$$\frac{S_r}{S_s} = \sqrt{\pi \delta f_0}\ \lambda \gamma\ \frac{P_r}{P_s} \tag{5}$$

where γ is the multi-mode correction factor and is defined as the ratio of the total rms stress response to the modal stress response. The number λ is a correction factor introduced to account for nonlinearity in the stress response of the structure relative to increasing sound pressure level. This correction factor is simply the ratio of slopes at the two different stress levels.

Equation (5) shows that stresses induced in structures can be directly related to the sound pressure levels which excite their surface panels. By relating the resulting stresses to fatigue life and comparing cycles to failure, the expected fatigue life under random loading can then be determined from the "random" fatigue curve, $\emptyset\,(N_r)$.

$$\frac{S_r}{S_s} = \frac{\emptyset(N_r)}{\emptyset(N_s)} \tag{6}$$

The success of the above method depends upon the theoretical development of the random fatigue curve. The typical development is as follows:

1) Assume that the distribution of the amplitudes of stress peaks is closely described by the Rayleigh probability distribution,

$$p(x) = x\, e^{-\frac{x^2}{2}} \tag{7}$$

where $p(x)$ = fraction of the total number of cycles of stress level x

x = ratio of peak stress to rms stress of the random stress response.

2) Utilizing cumulative damage methods, in this case Miner's hypothesis of cumulative damage theory, we have;

$$\text{Cumulative Damage, } 1 = \int_0^{S_{max}} \frac{d\,n(S)}{N(S)} \tag{8}$$

where $n(S)$ = number of cycles at stress S, and

$N(S)$ = number of cycles of stress S that would cause failure.

The fatigue life, expressing the total number of occurrences to failure, for a given rms value of random stress peak can be calculated as follows;

$$\text{Random Cylces, } N_r = \left(\int_0^{x_{max}} \frac{p(x)\,dx}{N(x)} \right)^{-1} \tag{9}$$

where $N(x)$ is evaluated from the standard S-N curve at each stress level and which is equal to x times the rms stress chosen.

It is noted that in recent years various approaches, which attempt to account for the variation in the mean and alternating stress and/or for nonlinearity in damage accumulation, have been used for constructing the random fatigue curve. It is apparent that each of the methods contains some desirable improvement over the above simplified expression. However, considering the inaccuracies encountered in fatigue life evaluation, the complexity, and the data requirement of these methods, the Miner's linear rule is still the choice at this time and is appropriate for design predictions.

A detailed description of the above method in the prediction of acoustical fatigue life for a hypothetical problem is presented in the following section.

2.0 EXAMPLE PROBLEM SOLUTION

The procedure, derived in the preceding section, can be reduced to a step-by-step process as shown in Figure B-1 for conceptual understanding. These steps assume that the acoustic environment has been completely described by the following data:

- Sound Pressure-frequency spectrum. (See Figure B-2)
- Standard S-N curve of the structural material for fully reversed loading. (See Figure B-3)

In addition to the above data, it is also assumed that a siren test has been performed on a specimen which accurately simulated the structural panel. The data assumed extracted from the siren test are:

- Number of cycles (or time) to failure at specified sound pressure levels and frequencies.
- Plots of stress versus frequency response curves. (See Figure B-4)
- Plots of stress-load curves for each excitation mode, if necessary. (See Figure B-5)

The stress versus frequency curve provides a means of calculating the damping of the structure. (Other methods such as the decay rate method may be used for determining the damping coefficient.) The stress-load curve is necessary for computation of the nonlinearity correction factor.

2.1 Construction of Random S-N Curve

With the appropriate S-N curve for the test specimen at the point of failure, the random S-N curve can be constructed as follows:

Select an arbitrary value of the random rms stress, $\sqrt{S_r^2}$. The solution then consists of solving for the total number of random cycles corresponding to the random rms stress, by using Miner's rule of cumulative damage. Values of x, relative stress, are chosen at discrete

intervals. At these values of x, P(x), the relative number of cycles, is read from the Rayleigh curve. N_x, the allowable number of cycles at each stress level, is obtained from the S-N curve at each stress level and which is equal to x times the rms stress chosen. Relative damage or damage density is then the ratio of two values $P(x)/N_x$. The $P(x)/N_x$ versus x is called the damage density curve and reveals the peak damage stress level, S_{PD}. Mathematically stated, the $\left.\frac{n_x}{N_x}\right|_{x=S_{PD}}$ term is the largest term in the summation:

$$\text{Damage, } 1 = \sum \frac{n_x}{N_x}$$

This means, as seen in examining the Rayleigh distribution curve, that a very small number, compared to the total, of high stress peaks do most of the significant damage. If all intervals of x, from zero to maximum, were included, the sum of $P(x)/N_x$ would be the integral of the area under the damage density curve. The reciprocal of the integral $\frac{1}{\int_0^\infty \frac{P(x)\,dx}{N_x}}$ is the desired number, the total random cycles, at all stress levels about the chosen rms stress which the specimen could endure. By repeating the calculation for a series of rms stress values, the curve of rms versus cycles, N_r, can be plotted. The curve of peak damage stress, S_{PD}, can also be plotted. Figure B-3 shows the calculated random S-N curve and the curve of peak damage stress along with the original fatigue test data for a 6Al-4V titanium material. The peak damage stress, which usually varies from 2 to 4 times the value of the rms stress, will be used in the calculation of a correction factor for nonlinear stress response. It is necessary to make this correction because the stress response of the siren test is likely to be of different magnitude than the peak damage stress.

The calculation of the random S-N curve can be performed entirely by a digital computer if desired.

2.2 Interpretation of Siren Testing

A hypothetical test is presented here to illustrate use of the techniques advanced before.

Assume that the frequency scans were conducted at a sound pressure level (SPL) of 145 dB for several strain gages having representative locations, and the specimen frequency responses appeared as shown in Figure B-4. In Figure B-4 the fundamental frequency was determined as approximately 655 Hz. The damping coefficient corresponding to this resonant frequency is determined by measurement of the bandwidth at the half-power point from the frequency response curve.

$$\delta_0 = \frac{\Delta f_0}{2 f_0} = \frac{6}{2 \times 655} = 0.0046 \qquad (10)$$

Similarly, for second mode we obtain:

$$\delta_1 = \frac{\Delta f_1}{2 f_1} = 0.0015$$

where $f_1 = 695$ Hz is the resonant frequency corresponding to the second mode showing significant response. The multi-mode correction factor then is:

$$\gamma_0 = \sqrt{\sum_{i=1}^{n} S_{si}^2} \Big/ S_{s0} = \left(\sum_{i=1}^{n} \delta_i f_i S_{si}^2 \right)^{\frac{1}{2}} \Big/ \sqrt{\delta_0 f_0 S_{s0}} \qquad (11)$$

$$= 1.15$$

for P_s constant as it is in the frequency response curve, and where i refers to the structural mode of response.

In the above equation, the relative stress at each mode is taken from a stress-frequency response curve such as shown in Figure B-4. Actually, the stress values used here should be taken from the curve for sound pressure level that would cause failure. However, with the approximately linear response, values from the frequency response curve at 145 dB serve as well.

It is recommended to perform "Step-tests" wherein a specimen is tested for some nominal time period at increased SPL increments until failure occurs. The test results are then equated to an equivalent time-to-failure and SPL by the cumulative damage method for comparative purposes and analysis. This technique permits the acquisition of as much data as possible from a limited number of specimens. Assume that the specimen was step-tested for 15-minute periods in the fundamental mode with the SPL increased 3 dB per level, and that stress levels were recorded during each run in order to provide data for constructing stress-load curves for computation of the nonlinearity factors. Assume that failures developed after 3 minutes of testing at 154 dB. The hypothetical test results are tabulated as follows:

Time (Min)	SPL (dB)	Relative Stress (psi)
15	148	13,200
15	151	15,900
3	154	21,700

Now since

$$\text{Cumulative Damage, } 1 = \sum \frac{n_x}{N_x} = \frac{n_{148}}{N_{148}} + \frac{n_{151}}{N_{151}} + \frac{n_{154}}{N_{154}}$$

at failure, it is necessary only to find values of N_x which satisfy the above equation. By trial and error, a value of $N_{154} = n_{154}$ was found. This means that only the exposure at 154 dB contributed to the failure. Clearly this is a trivial case; not all are. The stress corresponding to $N_{154} = 1.2 \times 10^5$ cycles (3 minutes of frequency 655 Hz) is $S_{154} = 0.707 \times 87,500 = 61,800$ psi (rms value) from the S-N curve for the mode.

Based on the testing results, the stress-load curve can also be plotted and is shown in Figure B-5. The nonlinearity correction factor is determined by the equation:

$$\lambda_0 = \frac{\alpha_{PD}}{\alpha_s} = \left(\frac{S_{PD}}{P_{PD}}\right) \Big/ \left(\frac{S_s}{P_s}\right) = 0.95 \qquad (12)$$

in which $\left(\frac{a}{b}\right)$ denotes the slope at the point (a, b).

where S_s = 87,500 psi (Obtained from the original S-N curve at the test life)

P_s = 0.145 psi (Sound pressure level of the siren test)

S_{PD} = 100,000 psi (Estimated from the peak-damage curve for a conservative prediction)

P_{PD} = 0.176 psi (Calculated from a point on the stress-load curve whose relative stress is $(100,000/87,500)\,P_s$)

2.3 Sine-Random Equivalence

From Figure B-2, the one-third octave SPL at frequency 655 Hz is approximately 152 dB. The corresponding spectrum level (by definition, SPL in unit bandwidth), found by subtracting the correction dB value, is approximately:

$$P_r = 152 - 21 = 131 \text{ dB}$$

By using Equation (5), the random rms stress S_r can then be calculated.

$$S_r = \sqrt{\pi \delta_0 f_0}\ \lambda_0 \gamma_0 \left(\frac{P_r}{P_s}\right) S_s$$

$$= 23,000 \text{ psi}$$

The expected fatigue cycles, N_r, determined from the random S-N curve, as shown in Figure B-3, is

$$N_r = 5 \times 10^7 \text{ cycles at } 655 \text{ Hz}$$

which represents an expected life of 22 hours under the specified random loading condition.

3.0 CONCLUSIONS

The combination of the acoustic environment, its duration, the response of the structure, and basic material fatigue data can be brought together in a manner to permit analytical solution. The solution is in the main, dependent on the same assumptions as those used in solving conventional fatigue problems. The difficulty involved in the acoustical fatigue lies in the imprecise knowledge of the stress magnitudes being imposed at the point of failure. Logically, these data could be collected in tests of simulated structure with either discrete frequency sirens or with broadband sound sources. However, a random test cannot be empirically related to basic S-N curves, thus, a valuable source of fatigue data would be unavailable to help solve the problem. It is not economically feasible to test sufficient numbers of specimens to recreate basic fatigue data in random source form. Therefore, for design and development work, siren testing with constant sinusoidal sound pressure levels appears to be more practical. The sine-random equivalence procedure described herein provides a method which considers all important response factors in the prediction of acoustical fatigue life.

STEP 1 - CONSTRUCT RANDOM S-N CURVE

Determine:

S_s From S-N Curve at N_s

$\sqrt{S_r^2}$ From Random S-N Curve at N_r

$$N_r = \left(\int_0^{x_{max}} \frac{p(x)\,dx}{N(x)} \right)^{-1}$$

STEP 2 - INTERPRET SIREN TEST DATA

Estimate:

Damping Factor, $\delta = \Delta f / 2f_i$

Multi-Mode Factor, $\gamma = \sqrt{\sum_i S_i^2} \Big/ S_i$

Nonlinearity Factor, $\lambda = \alpha_{PD} / \alpha_s$

STEP 3 - SINE-RANDOM EQUIVALENCE

Compute:

Equivalence Response Stress, S_r

$$S_r = \sqrt{\pi \delta f}\ \lambda \gamma \left(\frac{P_r}{P_s} \right) S_s$$

Comparison Random S-N Curve, N_r

Figure B-1. Steps in Sine-Random Equivalence Prediction

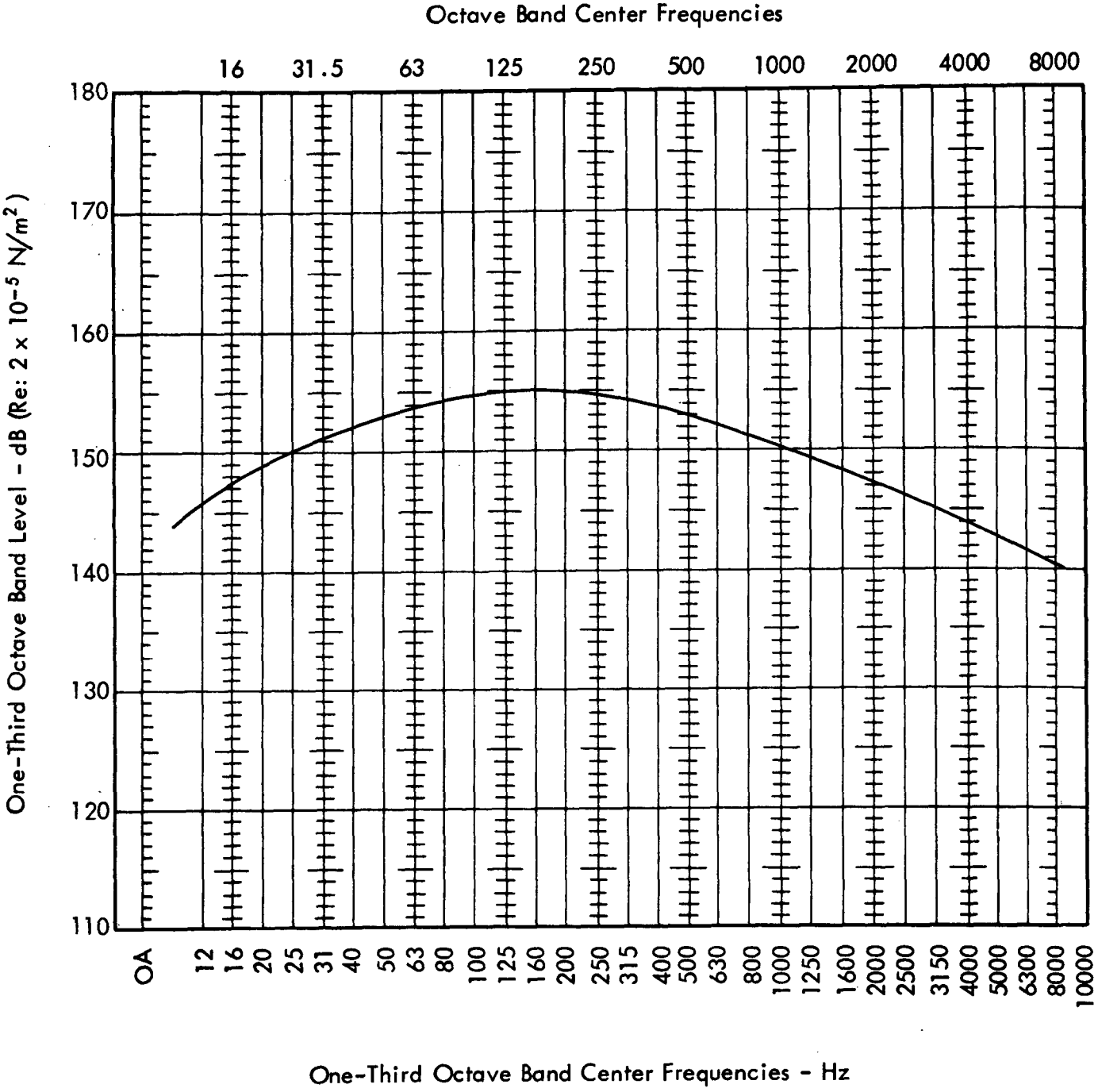

Figure B-2. Sound Pressure-Frequency Spectrum (For Example Problem)

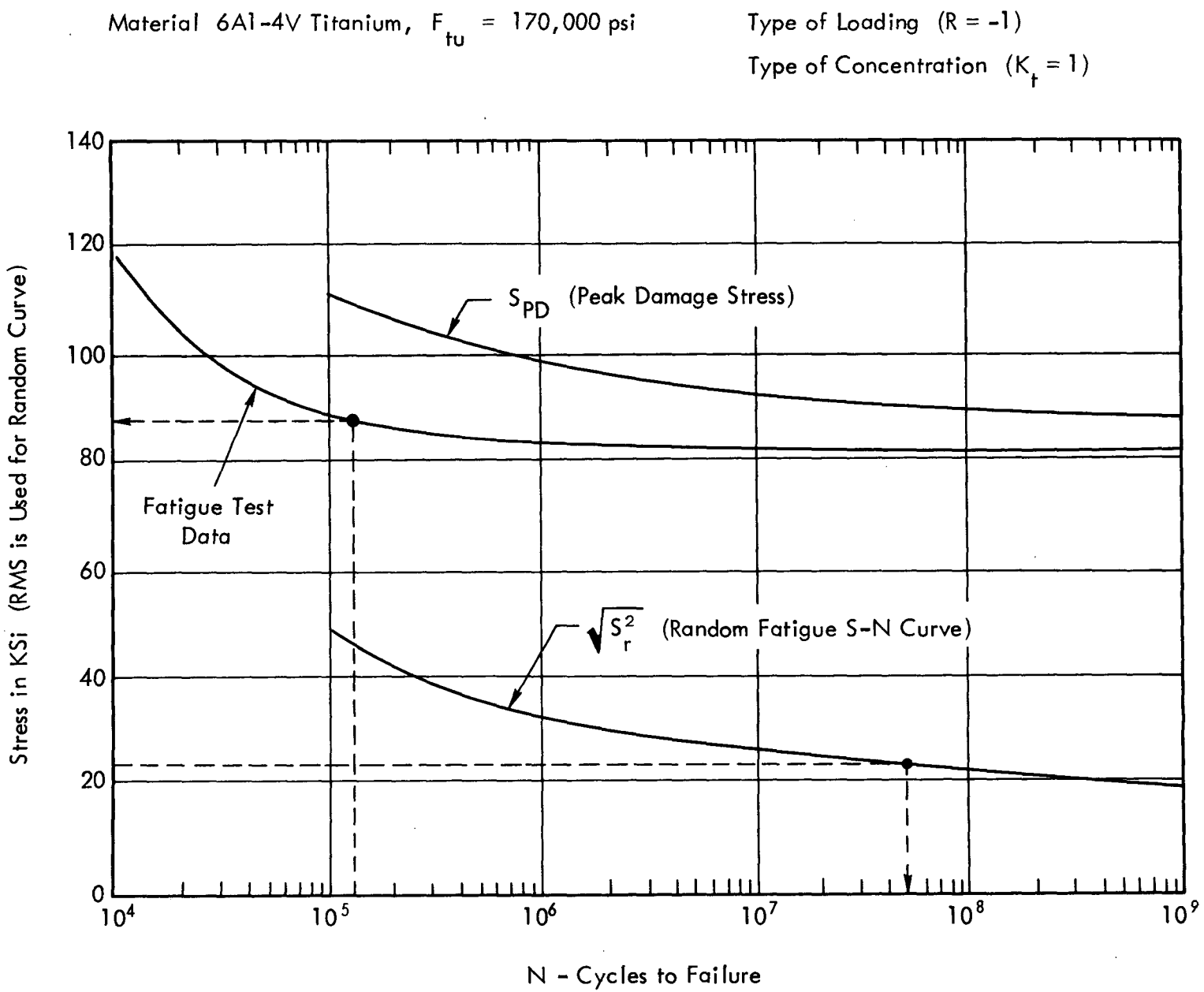

Figure B-3. Calculated Random S-N and Peak Damage Curves

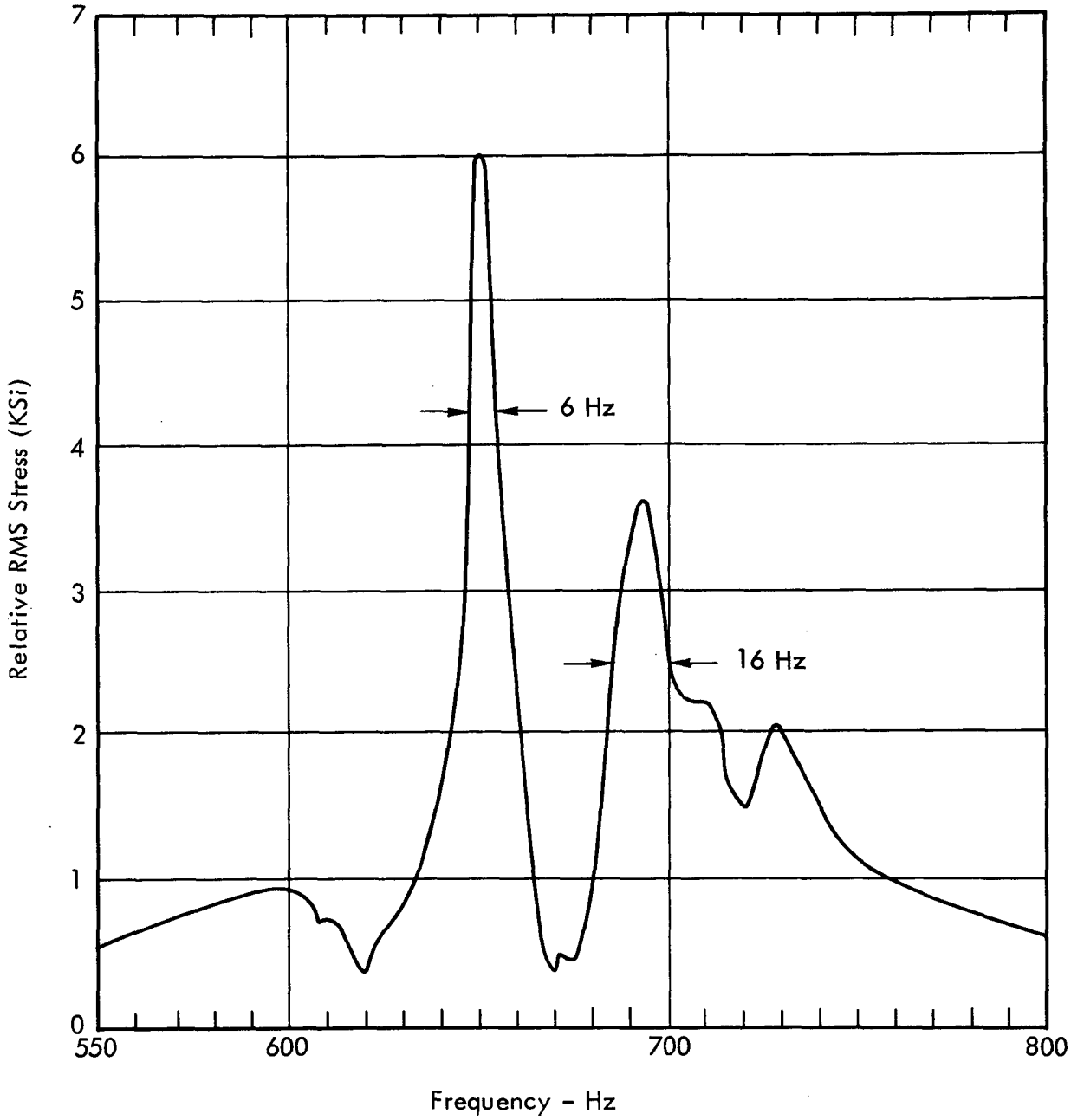

Figure B-4. Stress-Frequency Response Curve at SPL = 145 dB
(For Example Problem)

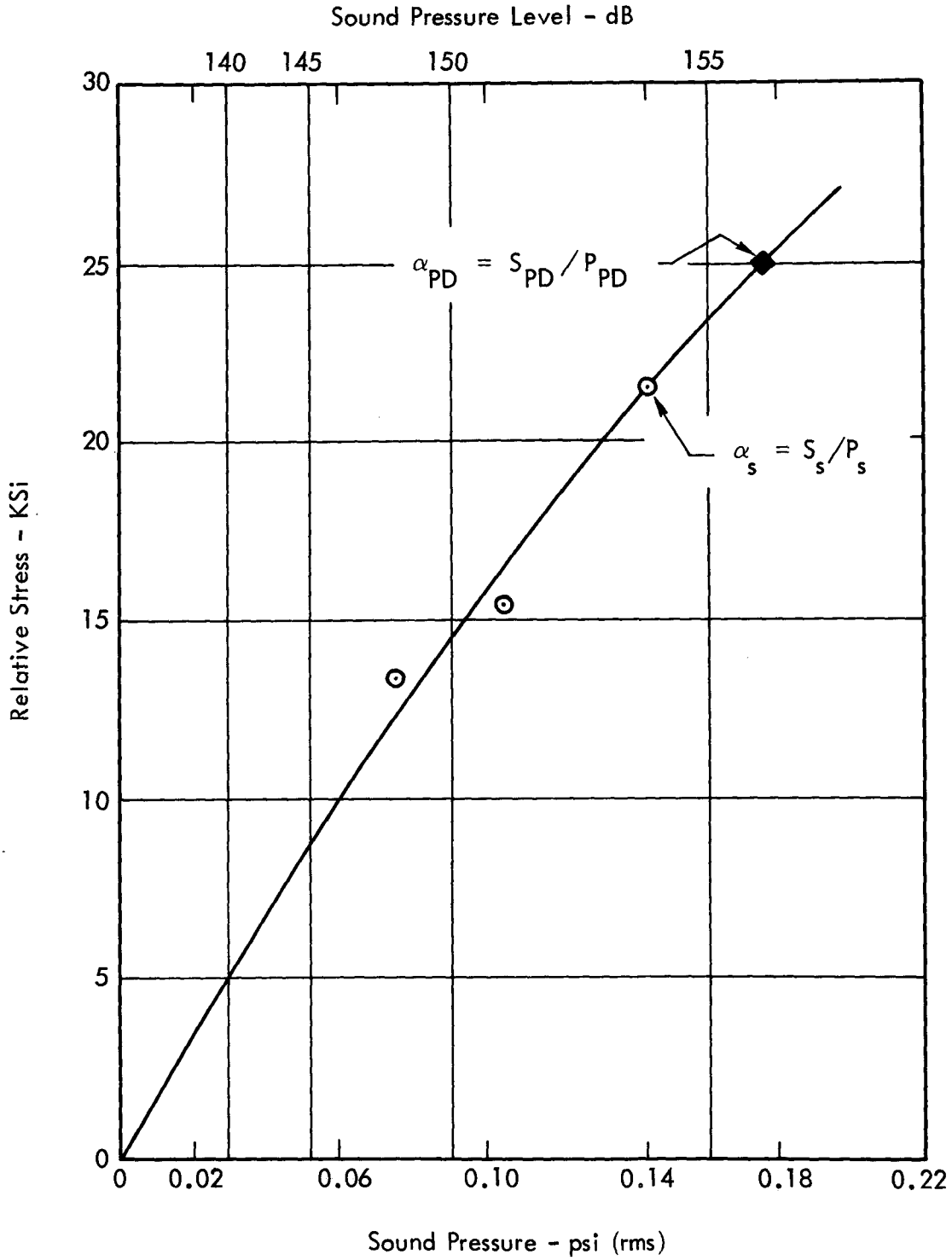

Figure B-5. Stress-Load Curve (For Example Problem)